

Distribution Agreement

In presenting this thesis or dissertation as a partial fulfillment of the requirements for an advanced degree from Emory University, I hereby grant to Emory University and its agents the non-exclusive license to archive, make accessible, and display my thesis or dissertation in whole or in part in all forms of media, now or hereafter known, including display on the world-wide web. I understand that I may select some access restrictions as part of the online submission of this thesis or dissertation. I retain all ownership rights to the copyright of the thesis or dissertation. I also retain the right to use in future works (such as articles or books) all or part of this thesis or dissertation.

Signature:

Briana Brown Rackley

Date

An integrative approach to investigate treatment-resistant lung adenocarcinoma

By

Briana Brown Rackley
Doctor of Philosophy

Graduate Division of Biological and Biomedical Sciences
Cancer Biology

Melissa Gilbert-Ross, Ph.D.
Advisor

Adam Marcus, Ph.D.
Committee Member

Kenneth Moberg, Ph.D.
Committee Member

Renee Read, Ph.D.
Committee Member

Wei Zhou, Ph.D.
Committee Member

Accepted:

Lisa A. Tedesco, Ph.D.
Dean of the James T. Laney School of Graduate Studies

Date

An integrative approach to investigate treatment-resistant lung adenocarcinoma

By

Briana Brown Rackley
B.S., Georgia Institute of Technology 2012

Advisor:
Melissa Gilbert-Ross, Ph.D.

An abstract of
A dissertation submitted to the Faculty of the
James T. Laney School of Graduate Studies of Emory University
in partial fulfillment of the requirements for the degree of
Doctor of Philosophy
in
Graduate Division of Biological and Biomedical Sciences
Cancer Biology
2020

An integrative approach to investigate treatment-resistant lung adenocarcinoma

By

Briana Brown Rackley

Lung cancer is the leading cause of cancer-related deaths, killing 135,720 people per year. Co-mutation of the oncogene *KRAS* and the tumor suppressor *LKB1* has been shown to increase disease severity, promote metastasis, and decrease survival. The impact of these co-mutations on patient outcomes has been well studied, but how these two mutations work together to promote tumorigenesis is unknown. The work in this dissertation uses *in vivo* models and patient data to demonstrate that synergy between KRAS and LKB1 is driven by autonomous growth, proliferation, and co-activation of downstream targets. Additionally, tumorigenesis is dependent upon high levels of oncogenic KRAS. Using *Drosophila melanogaster*, we determined that knockdown of *Lkb1* works with Ras^{V12} to override organ size control. This increase in organ size was driven by autonomous proliferation and offset by autonomous cell death. Additionally, Ras^{V12} and *Lkb1* knockdown work together to promote filamentous actin disorganization and basement membrane degradation. To further elucidate the mechanisms by which oncogenic KRAS and loss of LKB1 promote tumor progression and impede treatment response, we sought to understand how levels of oncogenic Ras contribute to *Lkb1*-null tumor progression and uncover novel signaling pathway components that may be targetable therapeutically. Comparison of high Ras^{V12} expression (Ras^{Hi}) to low/moderate Ras^{V12} expression (Ras^{Lo}) shows that Ras^{Hi} is required for complete neoplastic transformation of *Lkb1*-null tissues. The effects of Ras^{Hi} extend beyond tumor initiation, as Ras^{Hi} levels drive tumor progression and metastasis via breakdown of basement membrane and collagen structures resulting in dissemination into secondary sites. We show that phenotypes observed using *Drosophila* are also observed in human patients, as co-mutation of high levels of KRAS and loss of LKB1 were shown to decrease overall patient survival compared to low level KRAS expression. Finally, we determined that tumor severity is likely driven by unprecedented co-activation of AMPK and mTOR signaling, promoting cell autophagic mechanisms and unrestricted growth. Indirect inhibition of AMPK via the CaMKII inhibitor KN-93 was shown to partially rescue observed phenotypes, offering potential avenues for continued exploration. Follow-up studies in this area will help in providing opportunities for better treatment of this subset of patients.

An integrative approach to investigate treatment-resistant lung adenocarcinoma

By

Briana Brown Rackley
B.S., Georgia Institute of Technology 2012

Advisor:
Melissa Gilbert-Ross, Ph.D.

A dissertation submitted to the Faculty of the
James T. Laney School of Graduate Studies of Emory University
in partial fulfillment of the requirements for the degree of
Doctor of Philosophy
in
Graduate Division of Biological and Biomedical Sciences
Cancer Biology
2020

Acknowledgements

But by the grace of GOD! I am extremely grateful for all the support of my family and friends throughout this process. While I cannot thank everyone individually, I must personally acknowledge those whom I could not have done this without.

First, I would like to thank my advisor, Melissa Gilbert-Ross, for taking a chance on me after switching labs my second year. Your knowledge is incredible, and I am thankful I could learn so much from you. Beyond that, you have been nothing short of supportive with my journey beyond science, into motherhood. While this process has been hard, I genuinely thank you for being there to help and support along the way. While I may be your first graduate student, I know I won't be the last, and I know you will inspire countless young scientists.

I would also like to thank my thesis committee, Adam Marcus, Ken Moberg, Renee Read, and Wei Zhou, for being so knowledgeable and so kind over the last several years. I remember being so afraid to have my first committee meeting, but I have enjoyed our meetings and time together, as they have been invaluable to both my project and my future goals. Being accountable for my progress has helped me to think critically and has made me a better scientist.

To my ride or die lab mates, Chang-Soo and Evan, thank you for always being a source of support. Whether it has been lending an ear to vent to, or helping me with countless experiments, I could not have asked for better colleagues. I also wouldn't have finished without either of you! I pray for nothing but continued success for you both, and hope to always stay in touch.

To my Cancer Biology cohort, especially Alex and Fadi, thank you for your friendship. We come from such diverse backgrounds, but I couldn't have asked for a better group to power through this program with. Thank you for study sessions, inspiration, lunches, and such enthusiasm for science. Through your passion, I was always reminded of the bigger picture: why we do what we do, and the patients we do it for.

To my friends, especially my bridesmaids and forever CB sisters Jamie, Rachel, and Ale, thank you for reminding me that there is more to life than graduate school. Thank you for weekend brunches, girl time, and love. I am blessed to have genuine friendships with people that want nothing but the best for me and that celebrate every success with me as if it were their own. You all have helped brighten some of the darkest days and for that I am eternally grateful.

I would also like to thank my family. To my parents, thank you for instilling in me the faith that I can do anything through Christ who gives me strength, and thank you for reminding me of that fact countless times throughout this journey. Thank you for watching Eli to give Will and I a break, and thank you for always being there. To the Rackley's, thank you for welcoming me into the family and listening to me talk about school and science (and acting interested!). You all have provided me with such support and comfort over the last several years.

To my son, Elijah, you won't remember any of this time, but thank you for reminding mommy that my life is so much more than school and thank you for always being the bright spot at the end of even the worst days.

To my husband, where do I begin?? I could not and would not have done this without you. You have blessed my life more than I can imagine or put into words. Your constant support through all the breakdowns, bad moods, long nights, and early mornings have never gone unnoticed or unappreciated. Knowing that I could focus on experiments, presentation slides, or writing because Eli and our home were taken care of is HUGE. I love you soooo very much and I know we are both so glad we made it through!

Last, but not least, I would like to thank my inspiration for pursuing this degree. To my grandmother, Dovie, thank you for being such an incredible fighter and for showing me what perseverance looks like. I started this journey because we lost you, and I'm finishing this journey because I know you're watching over me. To Pops, Grizzle, and G-daddy, I miss you so much. I wish you could see me now, but I know you're smiling down on me and I hope I've made you all proud.

Table of Contents

Chapter 1. Introduction	Pages 1-38
1.1 Lung cancer	
1.1.1 Lung cancer overview	2-3
1.1.2 Lung cancer subtypes	4
1.1.3 Common lung cancer mutations	5-6
1.1.4 Current treatments	7-10
1.1.5 Racial and ethnic disparities	10-12
1.2 KRAS background	
1.2.1 RAS superfamily	13
1.2.2 KRAS in cancer	14-15
1.2.3 KRAS prognosis and treatment in lung cancer	16-17
1.2.4 mTOR activation in KRAS-mutant lung cancer	17-18
1.3 LKB1 background	
1.3.1 LKB1 in disease development	18-20
1.3.2 LKB1 as a master regulator	21-22
1.3.3 Regulation and function of AMPK	23
1.3.4 KRAS and LKB1 in lung cancer	24-26
1.4 Cancer cell metastasis	
1.4.1 Metastasis overview	27-28
1.4.2 Metastatic heterogeneity	29-30
1.4.3 Metastasis in lung cancer	30-31
1.5 <i>Drosophila melanogaster</i>	
1.5.1 <i>Drosophila melanogaster</i> as a model organism	31-32
1.5.2 <i>Drosophila melanogaster</i> biology	32
1.5.3 <i>Drosophila melanogaster</i> genetics	32-35
1.5.4 Understanding organ size control using <i>Drosophila</i>	36-37
1.5.5 <i>Drosophila melanogaster</i> as a model for human cancer	37
1.6 Rationale and scope of dissertation	37-38
Chapter 2. Oncogenic Ras cooperates with knockdown of the tumor suppressor <i>Lkb1</i> by RNAi to override organ size limits in <i>Drosophila</i> wing tissue	39-64
2.1 Introduction	41-43
2.2 Methods	44-47
2.3 Results	48-58
2.4 Discussion	59-61

Chapter 3. The levels of oncogenic Ras control clonal growth dynamics to transform Lkb1-mutant tissue *in vivo* **65-106**

3.1	Introduction	67-69
3.2	Methods	70-79
3.3	Results	80-99
3.4	Discussion	100-102

Chapter 4. Summary and Future Directions **107-124**

4.1	Discussion of dissertation	108-109
4.2	Oncogenic Ras ^{V12} drives Lkb1-mutant tissue overgrowth	109-112
4.3	High levels of oncogenic Ras ^{V12} are required for neoplastic transformation and metastatic spread	112-117

References **118-131**

List of Figures

Figure 1.1. Leading sites of estimated new cancer deaths – 2020.	Page 3
Figure 1.2. Oncogenic driver mutations in early stage lung adenocarcinoma.	Page 6
Figure 1.3. Racial disparities in cancer survival rates.	Page 12
Figure 1.4. KRAS mutations by cancer type.	Page 15
Figure 1.5. LKB1 mutations by cancer type.	Page 20
Figure 1.6. LKB1 functions in biological processes.	Page 22
Figure 1.7. Co-mutation of KRAS and LKB1 drives decreased progression-free survival.	Page 26
Figure 1.8. Overview of metastatic progression.	Page 28
Figure 1.9. Understanding <i>Drosophila</i> biology and genetics.	Page 35
Figure 2.1. Ras ^{V12} /Lkb1 ^{RNAi} mutations override 3 rd instar wing imaginal disc size control.	Page 50
Figure 2.2. Co-mutant Ras ^{V12} /Lkb1 ^{RNAi} overrides 3 rd instar eye imaginal disc size control.	Page 52
Figure 2.3. Expression of co-mutant Ras ^{V12} /Lkb1 ^{RNAi} drives autonomous cell proliferation and autonomous cell death.	Page 55
Figure 2.4. Ras ^{V12} promotes basement membrane degradation of Lkb1-mutant tissue.	Page 58
Figure S2.1. Co-mutation of Ras ^{V12} with loss of Lkb1 function causes adult wing overgrowth.	Page 62
Figure S2.2. Ras ^{V12} /Lkb1 ^{RNAi} rescue 3 rd instar wing imaginal disc cell size.	Page 63
Figure S2.3. Co-mutant Ras ^{V12} /Lkb1 ^{RNAi} drives F-actin filament disorganization.	Page 64
Figure 3.1. Clonal loss of Lkb1 in vivo results in autonomous cell death.	Page 82

Figure 3.2. Oncogenic Ras ^{Hi} promotes the malignant transformation of Lkb1 mutant tissue.	Page 85
Figure 3.3. SiMView light sheet microscopy allows visualization of local and distant collagen IV degradation by tumor cells over time.	Page 89
Figure 3.4. Ras ^{Hi} /Lkb1 ^{-/-} mutant cells exhibit single and multi-cell dynamics during cell migration in vivo.	Page 91
Figure 3.5. Oncogenic Ras ^{Hi} promotes co-activation of AMPK and mTOR in Lkb1-mutant malignant tumors in vivo.	Page 94
Figure 3.6. High level oncogenic KRAS drives decreased patient survival and is associated with AMPK activation in LKB1 mutant patients.	Page 98
Figure S3.1. Blocking cell death with P35 in Lkb1 mutant clones does not phenocopy Ras ^{Lo} / Lkb1 ^{-/-} .	Page 103
Figure S3.2. High level oncogenic Ras promotes proliferation and S-phase progression of Lkb1-mutant tissue.	Page 104
Figure S3.3. Acidic vesicle accumulation in Ras ^{Hi} /Lkb1 ^{-/-} tissue.	Page 105
Figure S3.4. High level KRAS does not result in survival differences in TP53 mutant lung cancer patients.	Page 106

Chapter 1. Introduction

1.1 Lung cancer

1.1.1 Lung cancer overview

Lung cancer is the leading cause of cancer-related deaths, killing more people than breast and prostate cancer combined (1). An estimated 606,520 Americans will die from cancer in 2020, with one-quarter of those deaths (135,720) attributable to lung cancer (Figure 1.1) (1). In part, the high mortality rates observed with lung cancer are due to metastatic progression. Lung carcinomas are most often detected after metastatic dissemination to distant organs (57%) and these tumors are categorized as stage IV. This is important because metastatic progression is an important predictor of mortality. Across solid tumors, 90% of cancer-related deaths are due to metastatic disease and this statistic has not changed much in the last 10 years (2). The 5-year survival rate for lung cancer patients after metastatic progression is 5% (SEER Cancer Statistics Review (CSR) 1975-2016) (1). Unfortunately, only 16% of lung tumors are diagnosed at a localized stage. Furthermore, when detected at earlier stages, vascular invasion is still often observed, resulting in increased incidence of recurrence, as well as decreased overall patient survival (3). When diagnosed early on, prior to any metastatic invasion, the 5-year survival rate jumps to 57% (1). Thankfully, elucidating mechanisms that drive metastasis is an area of intense research, not only in the context of lung cancer, and will be invaluable in better understanding how to treat patients.

Estimated Deaths

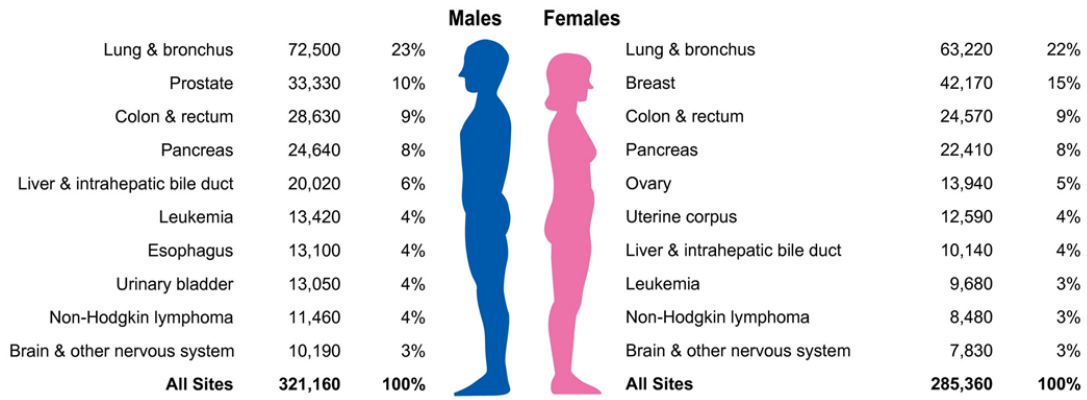


Figure 1.1. Leading sites of estimated new cancer deaths – 2020. Adapted from American Cancer Society (ACS), Cancer Statistics 2020 (1). Lung cancer is estimated to be the leading cause of cancer related deaths in 2020 with 135,720 estimated deaths combined in males and females. This figure highlights the importance of continued lung cancer research to improve patient prognosis and treatment outcomes.

1.1.2 Lung cancer subtypes

Lung cancer is categorized into two main histological subtypes, small cell lung carcinoma (15%) and non-small cell lung carcinoma (85%). From there, non-small cell lung carcinomas are further subcategorized into adenocarcinoma, squamous cell carcinoma, and large cell carcinoma (4). Most non-small cell lung cancers are lung adenocarcinomas. Extensive efforts to better understand the molecular makeup of each subtype has led to the identification of novel molecular characteristics of lung cancer and how each subtype differs at the DNA, RNA, and protein levels. This identification of deemed “driver mutations” has been an extensive area of study and is especially important for better understanding tumor development and progression/metastasis. For example, it is known that different types of lung cancers prefer different metastatic sites. Small cell lung carcinomas preferentially metastasize to the liver and brain. However, it was recently determined that there are also preferential metastatic sites among different oncogenic drivers. Brain metastases are increasingly observed with epidermal growth factor receptor (EGFR) mutations and ALK rearrangements (3). In the past, tobacco use was noted to be the most prominent risk factor for lung cancer, with exposure accounting for up to 90% of lung cancer cases in the United States (Centers for Disease Control and Prevention). However, the incidence of lung cancer in never smokers is rising (5-7). While squamous cell carcinomas are commonly associated with cigarette smoking, adenocarcinomas are becoming more and more prevalent in never smokers (8). The increasing incidence of lung cancer in never smokers highlights the importance of better understanding the driving forces in cancer formation to improve incidence rates as well as treatment efficacy.

1.1.3 Common lung cancer mutations

The Cancer Genome Atlas (TCGA) has allowed for extensive opportunities to increase knowledge of tumor mutational landscapes with the hope of developing better targeted therapies that not only incorporate a patient's histological subtype but are also dependent on each patient's molecular subtype (9-11). Lung cancer, mostly lung adenocarcinoma, has been comprehensively studied, and several key oncogenic driver mutations that initiate and maintain tumorigenesis have been identified allowing for further study and understanding. Prevalent oncogenic drivers associated with lung adenocarcinoma include activating mutations in KRAS, EGFR, ALK, HER2 (ERBB2), PIK3CA, AKT, BRAF, MAP2K, and NRAS (Figure 1.2) (11, 12). Interestingly, tumors harboring mutations in one prevalent oncogene rarely co-occur with mutations in another, except for PIK3CA which has been shown to co-occur with mutations in KRAS and EGFR. Conversely, oncogenic mutations frequently co-occur with inactivating or loss of heterozygosity mutations in genes known as tumor suppressors. Prevalent tumor suppressor genes in lung adenocarcinoma include *TP53*, *STK11 (LKB1)*, *CDKN2A*, and *KEAP1* (9, 13). While the heterogeneity of mutations within each tumor can add to the complexity of treatment, another complicating factor involves the fact that the clear majority of non-small cell lung cancer patients (~27%) do not have mutations in known oncogenic drivers (14). This makes development and implementation of effective treatment strategies challenging, and highlights the importance of continued research into new and diverse treatment strategies.

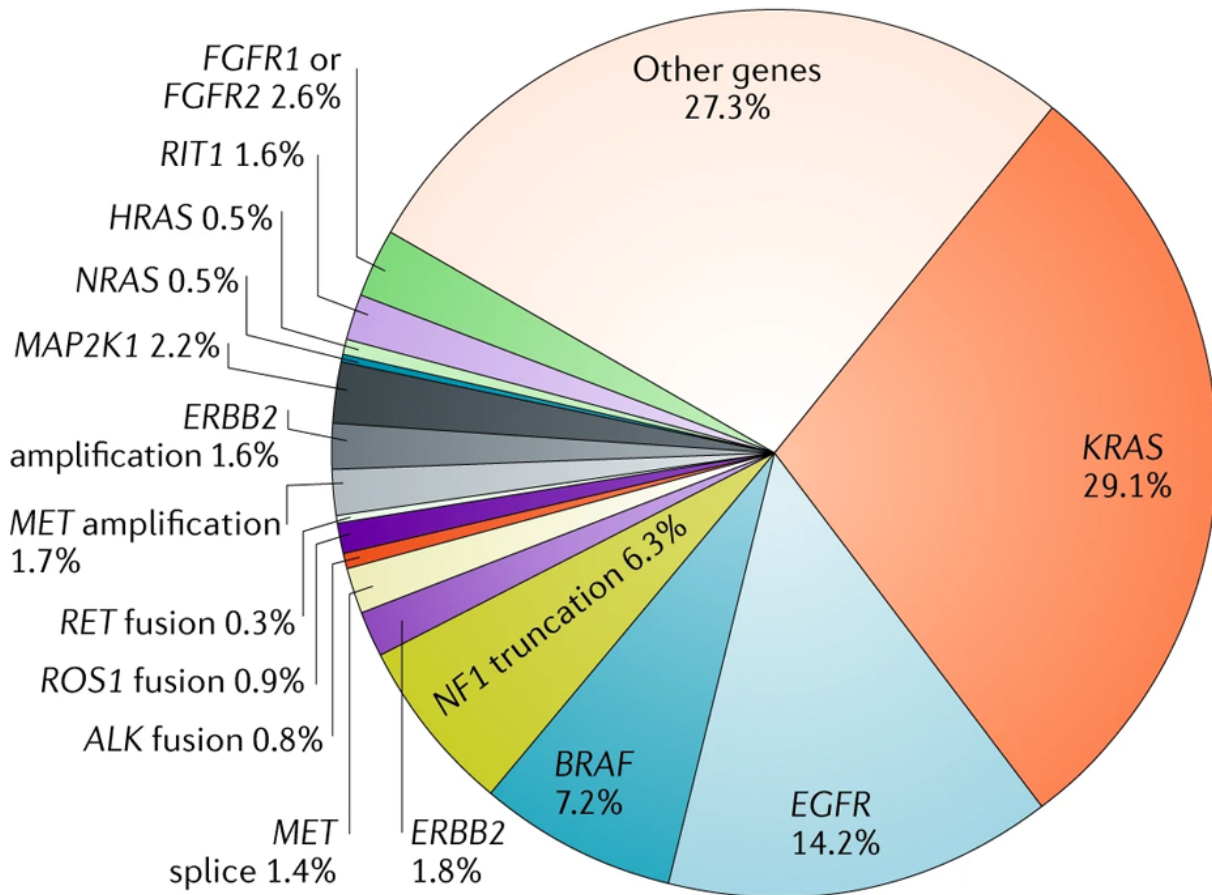


Figure 1.2. Oncogenic driver mutations in early stage lung adenocarcinoma. Adapted from (14). Activating mutations in KRAS, EGFR, NF1, and others are commonly observed in lung adenocarcinoma. Often, activating, oncogenic mutations are mutually exclusive, but these mutations do frequently co-occur with secondary inactivating mutations in tumor suppressor genes. Several studies seek to target these oncogenic mutations for better treatment of patients.

1.1.4 Current treatments

Treatment of lung cancers first involves diagnosis, followed by staging and determination of histological subtype. However, due to relatively few treatment options, and heterogeneity between histological subtypes, treatments over the last several decades have involved surgical resection to remove primary tumors and accessible metastases if possible, and/or systemic treatment using cytotoxic, platinum-based doublet chemotherapeutic agents (15-17). Chemotherapeutic treatment can be either neoadjuvant or adjuvant, and radiation therapy may also be recommended to shrink tumors prior to surgical resection (18). Unfortunately, treatment with platinum-based doublet chemotherapy has resulted in little objective efficacy based on low response rates and no major improvements to overall survival (19). Fortunately, progress with identification of molecular subtypes that may contribute to dismal treatment response rates has opened doors for development of targeted therapeutics to improve clinical responsiveness to treatment. The genetic background of a tumor can help with understanding responsiveness to different treatment modalities. For example, after identifying EGFR as a prominent oncogenic driver mutation, tyrosine kinase inhibitors (TKIs), such as gefitinib and erlotinib were developed for more targeted therapy. Unfortunately, while initial trials showed significantly improved progression free survival compared to standard of care chemotherapy, no overall survival benefit was achieved and resistance to therapy developed, warranting sequential treatment (19-22) and uncovering a continued need for better understanding of secondary mutations that may contribute to resistance and limited treatment responses. Since the initial development of first generation TKIs, subsequent generations of therapeutics such as AZD3759, Osimertinib, and pyrotinib have been developed, specifically targeting resistance mechanisms, such as secondary mutations and deletions, that often develop (23-27). While trials are ongoing, results are promising. Similarly to TKIs used for

treatment of EGFR-mutant lung cancers, TKIs used for treatment of ALK-mutant lung cancers showed initial benefit followed by disease progression within twelve months (28). Similar resistance mechanisms were observed in these patients, leading to development of subsequent generations of ALK specific TKIs that aim to avoid resistance due to mutations and rearrangements (29-31). Treatment options also exist for patients with known mutations in ROS1, BRAF, and MEK (32).

Unfortunately, not all known and common oncogenic drivers are currently treatable with approved targeted therapeutics. While significant progress has been made with better understanding the mechanisms by which KRAS mutations work to promote tumor development and metastasis, until recently, KRAS-mutant lung cancers were considered not only undruggable, but also resistant to chemotherapies, EGFR TKIs, and monoclonal antibody treatments (33). Efforts at targeting KRAS therapeutically have involved targeting signaling components downstream of KRAS, targeting KRAS directly, such as by inhibiting its interaction with GTP or using small molecules (34-37). Aiding in the difficulty of treating these subsets of patients, is the variation in KRAS mutation frequency. Depending on the study, approximately 40% of KRAS mutations are G12C missense mutations, 20% are G12V missense mutations, and 15% are G12D missense mutations (38). Promisingly, the first KRAS-specific inhibitor (AMG-510) was introduced in 2019. This inhibitor specifically targets the KRAS G12C cysteine-mutant residue. While further trials are needed, this optimized inhibitor has shown promising preclinical results for treatment of this previously non-targetable oncogene (39).

Until 2013, patients with no known oncogenic driver mutations were limited to standard of care chemotherapy for treatment. Since then, immunotherapy in the form of checkpoint inhibitors that target the interaction between PD1 and its ligand PD-L1 have been used as both first- and second-line treatments for oncogene mutant tumors that are non-targetable due to either lack of identifiable driver mutation, or known, currently untreatable, driver mutations (32). Nivolumab was the first anti-PD1 targeted drug approved for treatment of recurrent non-small cell lung cancer. Since then, pembrolizumab, atezolizumab, avelumab, and durvalumab have all been developed (19). While long-term clinical benefit has also been observed with immunotherapy treatment, some patients still eventually develop resistance and even hyper-progression of disease after treatment (32). Beyond checkpoint inhibitors, adoptive immunity (CAR-T therapy) has emerged as a promising field. Adoptive immunity involves hijacking effector T cells and modifying their antigen receptors to specifically target tumor cells directly, regardless of tumor type. While checkpoint therapies are most effective on specific tumor types, adoptive immunotherapies may offer efficacy among a broader range of tumors once a targetable surface antigen is established. Thus far, treatment of hematological malignancies with CD19-positive surface antigens have shown the most efficacy while solid tumors are presenting more of a challenge due to a lack of targetable surface antigen, as well as issues with the immunosuppressive microenvironment of solid tumors (19, 40, 41). Finally, bispecific antibody therapy or targeting of oncogenes involves simultaneous inactivation of more than one pathways driving tumor proliferation and growth (42, 43). Preliminary results are promising, but more research is needed to better understand clinical applicability. Overall, while significant progress has been made to better treat lung cancer patients, only limited treatment options exist and continued understanding of mutation types along with improved prevention of secondary resistance mechanisms will be essential for anticancer treatment. Additionally,

continued understanding with the ultimate goal of improving treatment responses should extend beyond understanding mutations but also to understanding/eliminating health disparities among ethnic groups.

1.1.5 Racial and ethnic disparities

Over the years, other areas of persistent research with regards to multiple cancer types include efforts to better understand racial and ethnic disparities that drive decreased patient response to treatment, higher incidence rates, and higher mortality rates. Compared to any other racial or ethnic group, African Americans suffer disproportionately higher cancer death rates and lower survival rates (44). After adjusting for sex, age, and stage at diagnosis, the relative risk of death after a cancer diagnosis is 33% higher in African American patients than in Caucasian patients, presumably due to increasing death rates driven by colorectal, prostate, and importantly lung cancers (Figure 1.3) (1, 44). It is believed that socioeconomic status is the most prevalent driver of this inequality, but other factors such as comorbidities, implicit bias, barriers to trust and communication, and lack of representation in clinical trials may also play a role. In 2019, approximately 202,260 new cancer cases and 73,030 cancer deaths were expected to occur among African Americans. Lung cancer is the second leading cause of cancer in African Americans and the leading cause of cancer related deaths. In 2019 alone, 25,390 new lung cancer cases were expected to be diagnosed along with 16,550 deaths in African Americans. Interestingly, when lung cancer mutations of interest, like KRAS and LKB1, are stratified by race, African American patients suffer from starkly different mutation types than Caucasian patients, aiding in both the complexity and difficulty in narrowing treatment disparities (Figure 1.3). While lung cancer incidence rates are approximately 15% higher in African American compared to Caucasian males,

these rates have been steadily declining since the peak in the mid-1980s. Additionally promising, is the fact that the overall Caucasian-African American racial disparity has narrowed, particularly in men. Even still, lung cancer death rates among black men are still the highest of any racial or ethnic group and five-year survival rates are lower in African Americans for every stage of diagnosis except distant metastases, again most likely due to socioeconomic status affecting stage at initial diagnosis and comorbidities that likely contribute to survival (45). These barriers to treatment result in African American patients being less likely than Caucasian patients to receive curative-intent surgery, even despite socioeconomic status. To conclude, while major steps have been made to narrow the gap between incidence, treatment, and survival rates between various racial and ethnic groups, African Americans continue to suffer from a disproportionate cancer burden, and future work should continue progress toward eliminating any gaps in prevention, detection, treatment, and overall survival outcomes between groups.

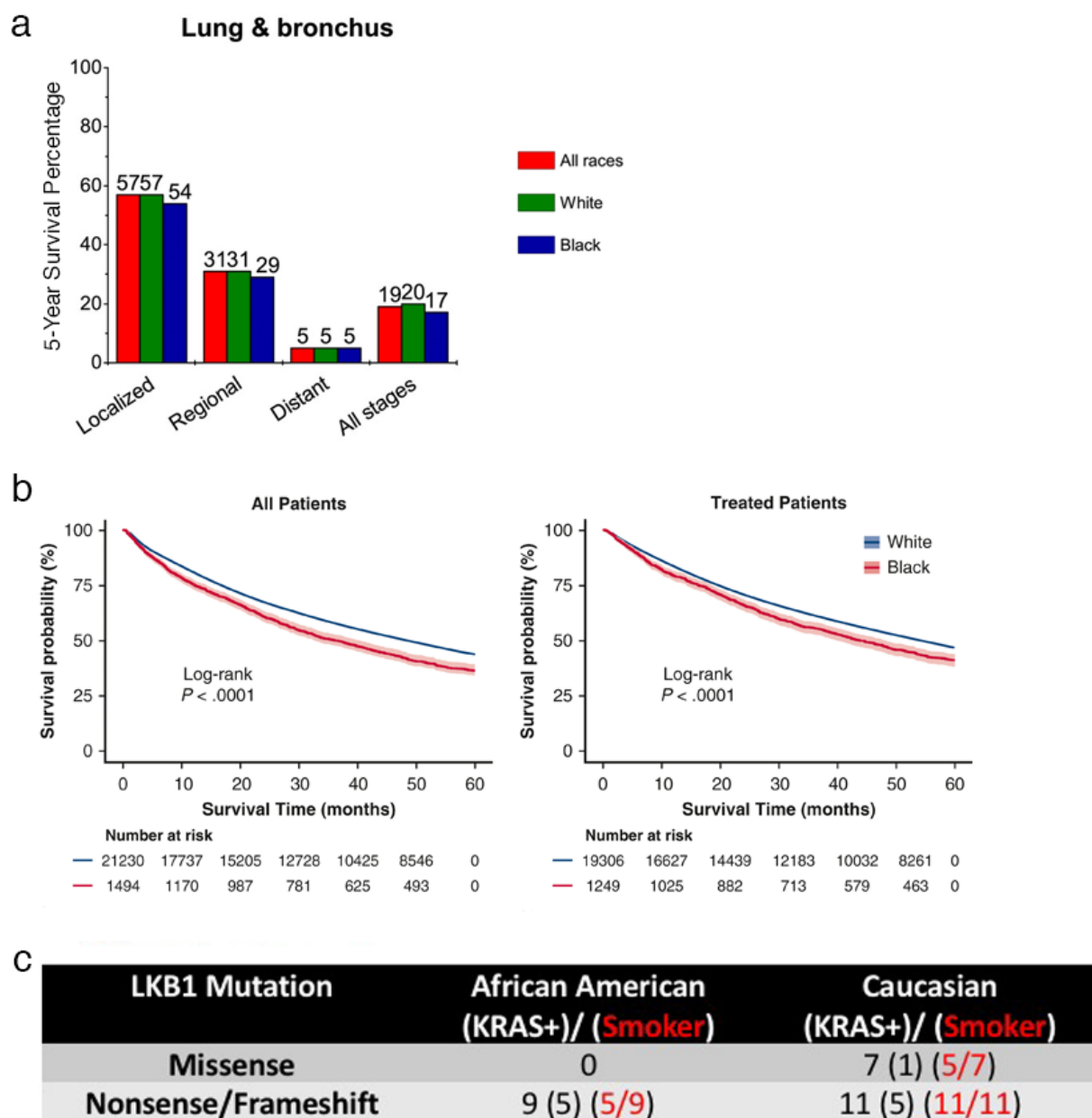


Figure 1.3. Racial disparities in cancer survival rates. Adapted from (1) and (45). Although disparities are improving between racial groups, African American patients still suffer from disproportionately lower five-year survival rates of any ethnic group (a). In lung cancer specifically, African-American patients suffer from significantly poorer survival, even after treatment (b). When Winship Cancer Institute patient samples are stratified by race and mutation type, African American patients suffer from distinctly different LKB1 mutation types than Caucasian patients (c).

1.2 KRAS background

1.2.1 RAS superfamily

RAS is one of the most well-known and well-studied oncogenes with gain of function mutations occurring in approximately 30% of all human cancers (46). Members of the RAS superfamily of guanosine triphosphate (GTP) binding proteins are further subdivided based on structure, sequence and function, with the five main families including RAS, RHO, RAN, RAB, and ARF GTPases. The RAS family specifically can also be divided into subfamilies, but each family shares a common G domain that is essential for GTPase and nucleotide exchange activity. This G domain includes the GTP-binding pocket necessary for activation. RAS is the most commonly studied of the RAS subfamilies, and in humans, three *RAS* genes encode highly homologous RAS proteins. These proteins include HRAS, NRAS, and KRAS. Kirsten Rat Sarcoma viral oncogene (KRAS) is the most commonly mutated RAS isoform and exists as two splice variants, 4A and 4B, with KRAS4B being the dominant form in humans. The KRAS protein also contains a hypervariable region that guides post-translational modifications and plasma membrane modeling. KRAS switches from an active (GTP-bound) and inactive form (guanosine diphosphate (GDP)-bound), using guanine nucleotide exchange factors (GEFs) to catalyze the exchange of GDP for GTP and GTPase-activating proteins (GAPs) to hydrolyze GTP to GDP (47, 48). KRAS is predominantly inactive unless stimulated by growth factors. When active, KRAS promotes the activation of various downstream signaling pathways including mitogen-activated protein kinase (MAPK) pathway, phosphoinositide 3-kinase (PI3K) pathway, and Ral-GEFs pathway (46). Once activated, these pathways carry out a chain of downstream phosphorylation reactions to propagate signal growth. Understandably, mutations in these pathways can result in dysregulation of growth signals and ultimately disease.

1.2.2 KRAS in cancer

KRAS is the most frequently mutated RAS isoform in human cancer, constituting approximately 86% of RAS mutations. KRAS mutations are most commonly observed in pancreatic cancers (90%), colorectal cancers (~40%), and non-small cell lung cancers (~20) (Figure 1.4) (46). Mutations are most frequently found at codons 12, 13, and 61, but have been noted to occur less frequently at codons 63, 117, 119, and 146 (49). While the mechanisms vary between codons, ultimately mutations at each either interfere with GAP binding and GAP-stimulated GTP hydrolysis, or help to stabilize transition states and diminish GTPase activity allowing for an accumulation of KRAS in its active state. Disparities surrounding the prognostic value of KRAS status add to the complexity of these mutations. For example, while some studies suggest that mutations in KRAS are correlated with poorer progression free survival and/or overall survival, other studies show no significant differences in the prognostic value of KRAS mutation status (50, 51). Various studies have also shown different amino acid substitutions at each codon vary the transformation capability of KRAS as well as responses to treatment modalities (52). For example, the KRAS G12V substitution has been associated with a worse prognosis than KRAS G12C substitution in colorectal cancer (53). This variability highlights the importance of better understanding the functional effects of specific permutations. Additional areas of study include better understanding how wild-type KRAS works to antagonize oncogenic KRAS, and if that is a potential exploitable area for better treatment of patients, as well as how mutations in KRAS remodel the tumor microenvironment to promote and maintain tumor formation (54, 55).

1.2.3 KRAS prognosis and treatment in lung cancer

In addition to being the most commonly mutated RAS isoform, KRAS is also the most frequent oncogenic aberration in non-small cell lung cancer. Mutations are found in 6.7% to 40% of smokers, and 2.9% to 11.4% of never/light smokers (56). It has been established that two different groups of KRAS mutations exist in non-small cell lung cancer: KRAS-dependent and KRAS-independent based on their dependence on mutant KRAS to maintain viability. These groupings provide information related to metastatic potential, as KRAS-dependent tumors are associated with a well-differentiated epithelial phenotype, and KRAS-independent tumors are associated with a more epithelial-to-mesenchymal (EMT) phenotype (57, 58). KRAS mutations in lung cancer commonly co-occur with secondary mutations in tumor suppressor genes. Most commonly, secondary mutations occur in P53, LKB1, or KEAP1, and each secondary mutation effects distinct tumorigenic pathways that must be considered when determining treatment course (59-63). For example, secondary mutations in LKB1 show a worse prognosis than patients with TP53 mutations and these patients show resistance to checkpoint inhibitor therapies (59, 64). Patients with co-mutation of TP53 and KRAS suffer from poor overall survival and decreased response to chemotherapeutics (65). In lung adenocarcinomas, KRAS is most often mutated at G12. As previously mentioned, approximately 40% of cases involve codon 12 cysteine-for-glycine (G12C) substitutions, 20% of cases involve codon 12 valine-for-glycine (G12V) substitutions, and 15% of cases involve codon 12 aspartic acid-for-glycine (G12D) substitutions (38, 66, 67). Although both substitutions have been associated with shorter progression free survival, patients harboring G12C mutations have been shown to suffer from significantly shorter overall survival compared to other KRAS mutations (68, 69). Patients harboring G12C mutations are also more likely to suffer from bone metastases while patients with G12V mutations are more likely to suffer from

pleuropericardial metastases (70, 71). Finally, while responses to specific agents differs, patients with G12C, G12V, and G12D substitutions suffer from resistance and reduced responses to treatment with standard of care chemotherapies. Together, while evidence shows KRAS mutations are significant in determining lung cancer patient prognosis, significant gaps remain related to roles and effects of secondary mutations, as well as individual amino acid substitutions, and how best to use such information in improving patient treatment and responses.

1.2.4 mTOR activation in KRAS-mutant lung cancer

Mammalian target of rapamycin (mTOR) is a serine/threonine protein kinase involved in the PI3-related kinase family that forms a catalytic subunit comprised of mTORC1 and mTORC2. While mTORC1 is defined by Rictor and is primarily involved in translation, metabolism, and protein turnover necessary for cell growth, mTORC2 is defined by Raptor and is primarily involved in cell proliferation and survival (72). In cancer, mTORC1 phosphorylation of eukaryotic initiation factor 4E binding protein (4EBP1) and ribosomal protein S6 kinase (S6K) are hypothesized to be most critical for tumor development, while mTORC2 is implicated in cancer due to its activation of Akt. Unfortunately, because mTORC1 acts to regulate mTORC2 via a negative feedback loop, mTOR inhibitors used for treatment of cancer have been less successful in the clinic than originally anticipated. As previously discussed, despite progress in identifying druggable targets to improve treatment approaches, the development of drug resistance is still an area of concern. Recently, research has shown that alterations in Rictor are present in both early and advanced stage KRAS-mutant lung adenocarcinomas, and that Rictor expression is correlated with poorer overall survival (73). Additionally, research has shown that mTOR pathway is hyper-activated in KRAS-mutant cancers secondary to treatment, typically chemotherapy (74). KRAS drives oncogenic

transformation by activating its downstream signaling network (Mek/Erk) that subsequently promotes activation of mTOR. This activation of mTOR is essential for KRAS-mutant lung cancer cells to resist treatment modalities. Together, these data highlight the importance of mTOR activation in for KRAS-mutant tumor development and progression, and suggest that combinatorial targeting of KRAS and mTOR may be beneficial for KRAS-mutant lung cancer patients.

1.3 LKB1 background

1.3.1 LKB1 in disease development

Liver Kinase B1 (LKB1) is a serine/threonine kinase originally identified as responsible for regulation of Peutz-Jeghers Syndrome (PJS), a rare, autosomal dominant disorder characterized by the development of benign gastrointestinal hamartomatous polyps (75). Germline mutations in *STK11 (LKB1)* are documented in potentially more than 80% of patients, depending on the screening method, and are considered the major cause of PJS (76, 77). Additionally, somatic mutations in the unaffected allele are often observed, resulting in bi-allelic inactivation. While early complications include intussusception due to multiple polyps, in patients with PJS, mutations in LKB1 increase the risk of developing both benign and malignant tumors over a lifetime to over 80% (78). Most commonly, cancers form in the gastrointestinal tract, but in women, the likelihood of breast cancer incidence is increased to 32% by age 60 (79). The established link between LKB1 and tumor formation led to the suggestion and further study of LKB1 as a tumor suppressor. In addition to malignancies associated with PJS, mutations in LKB1 have been most commonly associated with lung cancer, cervical cancer, and melanoma (Figure 1.5) (80-83). In lung cancer

LKB1 mutations seem to be exclusively found in non-small cell lung cancers. In lung adenocarcinoma, *LKB1* mutations are predominately truncating mutations that result in partial or complete loss of functional domains (9). While discrepancies in mutation frequency remain, it is believed that LKB1 is inactivated in up to 39% of non-small cell lung cancer patients (84). Future studies should continue to consider those mutations that occur most frequently in patients, which functional domains they occur in, and what effects those mutations have on patient outcomes.

1.3.2 LKB1 as a master regulator

LKB1 is a master upstream serine/threonine kinase that plays a role in several biological processes, including signal transduction, cell polarity, cell motility, cell metabolism, and cell growth. LKB1 controls these processes through activation of several downstream pathways, including twelve AMP-activated Protein Kinase (AMPK)-related protein kinases. Most notably, LKB1 regulates AMPK, microtubule affinity regulating kinase (MARK), salt-inducible kinase (SIK), sucrose non-fermenting protein-related kinase (SNRK), brain selective kinase (BRSK), maternal embryonic leucine-zipper kinase (MELK), and AMPK-related protein kinase 5 (NUAK/ARK5) (Figure 1.6) (85-88). LKB1 is activated in response to stress, where it then exits the nucleus and forms a complex with scaffolding proteins STRAD and MO25 to effect downstream functions (89). Most commonly, LKB1 activates AMPK to regulate cell growth and metabolism through suppression of notable pathways such as mTOR via TSC1/2 (90). LKB1 has also been shown to regulate cell polarity via cdc42, cell motility, and cell adhesion via inhibition of focal adhesion kinase (FAK) (91-93). Given these roles, it was logical that additional studies looked further into how LKB1 is involved in tumor cell metastasis. Evidence suggests that loss of LKB1 and SIK1 signaling promotes an epithelial-mesenchymal transition (EMT) phenotype. Additional data suggests that LKB1 acts to inhibit metastasis-promoting genes, such as NEDD9 and VEGFC (94). Together, data suggest that loss of LKB1 as a tumor suppressor also contributes to tumor cell metastatic potential (95).

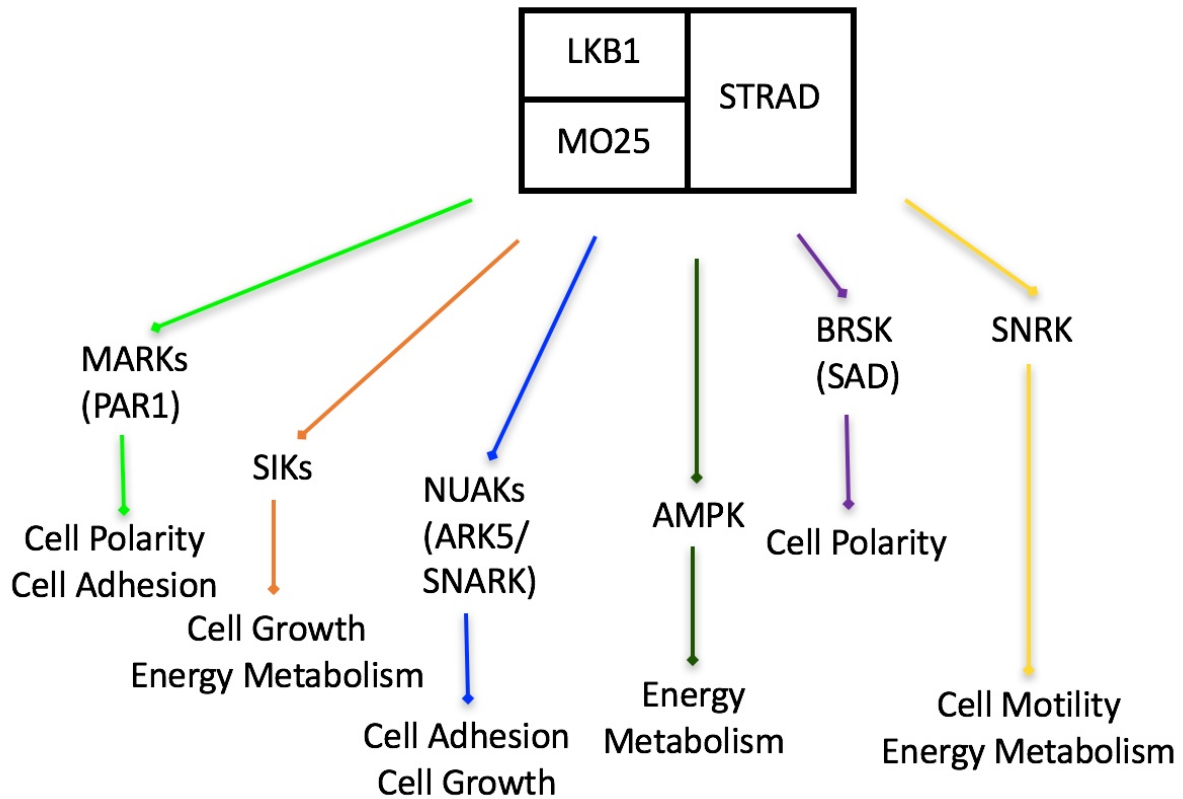


Figure 1.6. LKB1 functions in biological processes. Adapted from (96). LKB1 forms a complex with STRAD and MO25 to phosphorylate and activate 14 AMPK-related kinases, including AMPK. LKB1 plays a role in regulating cell polarity, cell adhesion, cell growth, cell metabolism, and cell survival.

1.3.3 Regulation and function of AMPK

AMPK is a serine/threonine protein kinase that acts to maintain cellular energy homeostasis. AMPK is activated in response to low intracellular ATP following stressors such as hypoxia or nutrient deprivation. AMPK regulates energy stress by inactivating anabolic processes and activating catabolic processes to generate ATP and restore energy homeostasis. Most commonly, AMPK is activated by phosphorylation at threonine 172 by LKB1 or calcium-/calmodulin-dependent kinase 2 (CAMKK2). AMPK plays a role in protein synthesis, glucose/lipid metabolism, and mitochondrial biogenesis/autophagy (catabolic processes) (97). Downstream, AMPK acts to negatively regulate mTORC1 activity (anabolic process) (98, 99). Because of this, it was originally believed that activation of AMPK would be a promising therapeutic strategy for cancer patients, as treatment of patients with the diabetes medication, metformin, resulted in significantly reduced incidence of all cancer forms (86). However, this pharmacological evidence was unable to be replicated with genetics, suggesting that AMPK may also play a tumor promoting role. Recent evidence suggests that AMPK activity in cancer is complicated, and while it is known that LKB1 is inactivated in a large proportion of lung cancer patients, data show that AMPK is frequently overexpressed in cancers, promoting tumor growth. Additionally, in murine lung cancer models, activation of AMPK was found to support tumor growth in KRAS-dependent tumors (100). Conversely, research also shows that AMPK degradation is induced in cancers. It is postulated the role of AMPK in cancer is dependent on the timing of LKB1 or AMPK modification. During early tumor development, it is proposed that inactivation of AMPK or LKB1 is important for tumor cell growth and proliferation. However, once tumors have been initiated, it is hypothesized that activation of AMPK or LKB1 would be beneficial due to promotion of metabolic adaptation that allows tumor cells to handle such dysregulated growth (101, 102).

Additionally, CAMKK2 has also been shown to promote prostate cancer progression (103). Because AMPK and upstream activator CAMKK2 have been shown to promote tumor progression in later stage disease, it is possible that targeting this protein may offer additional treatment opportunities for certain subsets of patients, especially those with known activating mutations in KRAS.

1.3.4 KRAS and LKB1 in lung cancer

LKB1 is the second most frequently mutated tumor suppressor in lung adenocarcinoma. Interestingly, LKB1 is inactivated or deleted in up to 30% of KRAS-mutant non-small cell lung cancers, potentially identifying a source contributing to KRAS-mutant tumors' poor response to therapy (Figure 1.7). In mice, loss of Lkb1 was shown to promote tumors resistant to chemotherapeutics and combination therapies with co-mutation of Kras. For example, Lkb1 inactivation in Kras-mutant tumors treated with combinatorial selumetinib and docetaxel showed primary resistance to this combination therapy compared to Kras/p53 or Kras alone (104).

Of interest for future studies is the fact that co-mutations in KRAS/P53 and co-mutations in KRAS/LKB1 result in different tumor subsets with distinct biology, immune profiles, and therapeutic vulnerabilities. Of note, cooperation between KRAS and LKB1 was first observed in pancreatic cancer, and this combination of mutations was noted to promote epigenetic modifications supportive of cancer growth (61). Lkb1 inactivation in mouse models demonstrate shorter latency to tumor formation, and promote more frequent, aggressive, metastatic spread. Although co-mutant Kras and p53 tumors were also shown to promote tumor development, the strongest mutation cooperation was observed with Kras and Lkb1 (94, 105). Inactivation of LKB1

in KRAS-mutant lung adenocarcinomas also stimulates metabolic reprogramming via perturbed nitrogen handling, a mechanism different than that observed with KRAS/P53 tumors (106). As already evidenced, KRAS/LKB1 tumors demonstrate strong resistance to standard of care therapies. Beyond that, KRAS/LKB1-mutant tumors also demonstrate resistance to more targeted therapies, such as checkpoint inhibitors. As previously mentioned, LKB1 mutations promote PD-1 inhibitor resistance in KRAS-mutant lung adenocarcinoma. Conversely, TP53 mutations show sensitivity to treatment with PD-1 inhibition (64). These discrepancies between tumor aggressiveness and treatment response highlight the importance of understanding how each combination of mutations work together to promote progression and metastasis, and open avenues for potential secondary sites for therapeutic targeting.

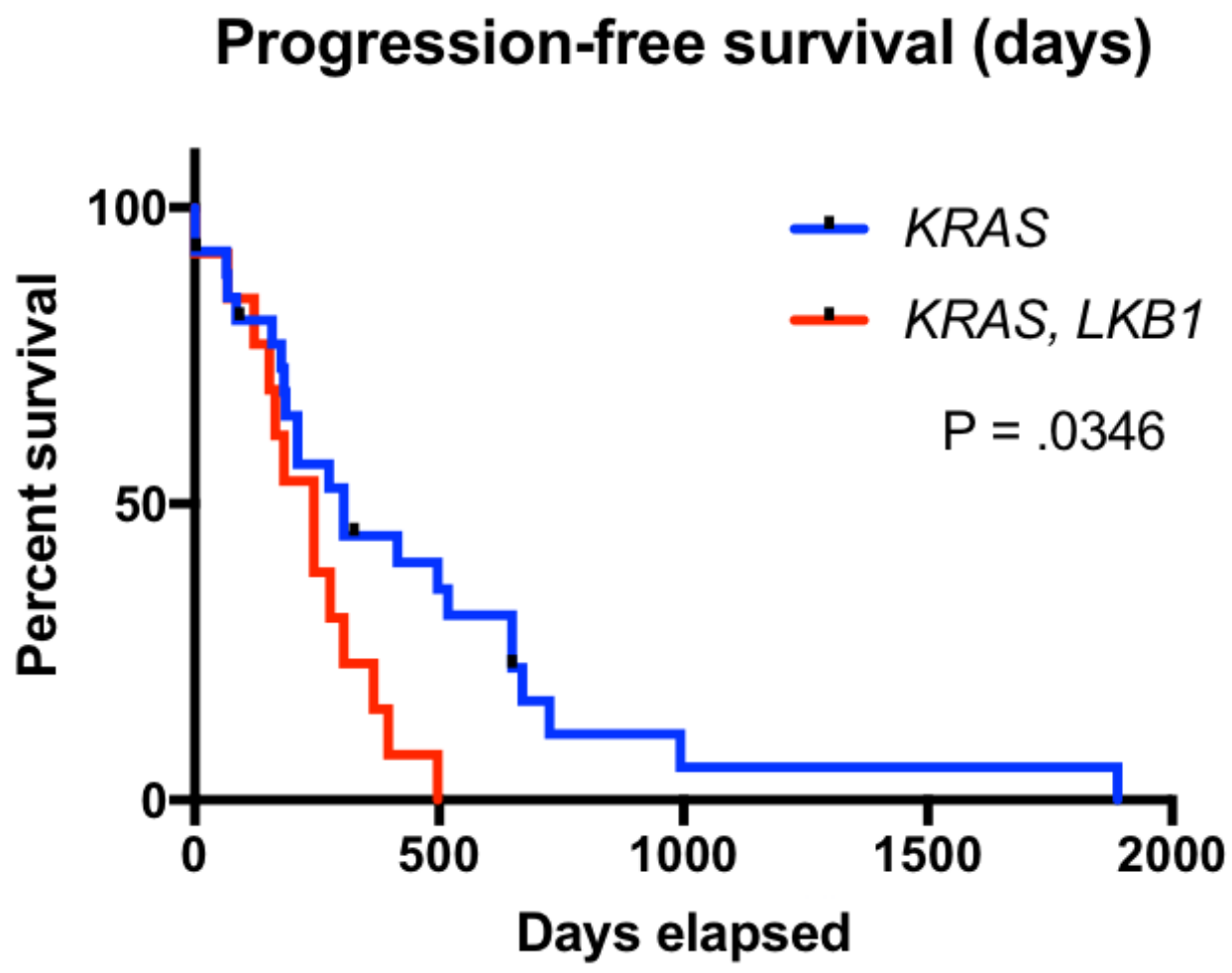


Figure 1.7. Co-mutation of KRAS and LKB1 drives decreased progression-free survival. Adapted from TCGA lung adenocarcinoma studies (9). Activating oncogenic mutations in KRAS drive significantly decreased progression-free survival in patients when combined with loss-of-function mutations in LKB1.

1.4 Cancer cell metastasis

1.4.1 Metastasis overview

Metastasis is the general term used to describe the spread of cancer cells from the primary tumor to surrounding tissues and distant organs. While metastasis is responsible for up to 90% of cancer-associated mortality, it remains a poorly understood component of cancer progression due to the limited ability of *in vitro* and *in vivo* models to accurately model a metastatic phenomenon. *In vitro* models cannot replicate all steps required for systemic metastasis, and *in vivo* models commonly utilize tail vein injections to mimic metastasis, which is not inclusive of all steps in the metastatic cascade (107). Furthermore, discrepancies exist as to the origins of metastasis. For example, it has been suggested that the metastatic cascade originates from EMT, an accumulation of stem cell mutations, or from macrophage facilitation, transformation, or fusion with neoplastic cells (108). Finally, there are also multiple mechanisms by which a cell can achieve the necessary fitness for metastatic spread. To complete the metastatic cascade, a cancer cell must first detach from the primary tumor, followed by intravasation into the circulatory and/or lymphatic systems. From there, a metastatic tumor cell must evade immune attack, extravasate out of circulation, and finally proliferate in a secondary site (Figure 1.8). Metastatic progression also involves an angiogenic component, ensuring that the microenvironment is conducive to secondary site tumor formation (108).

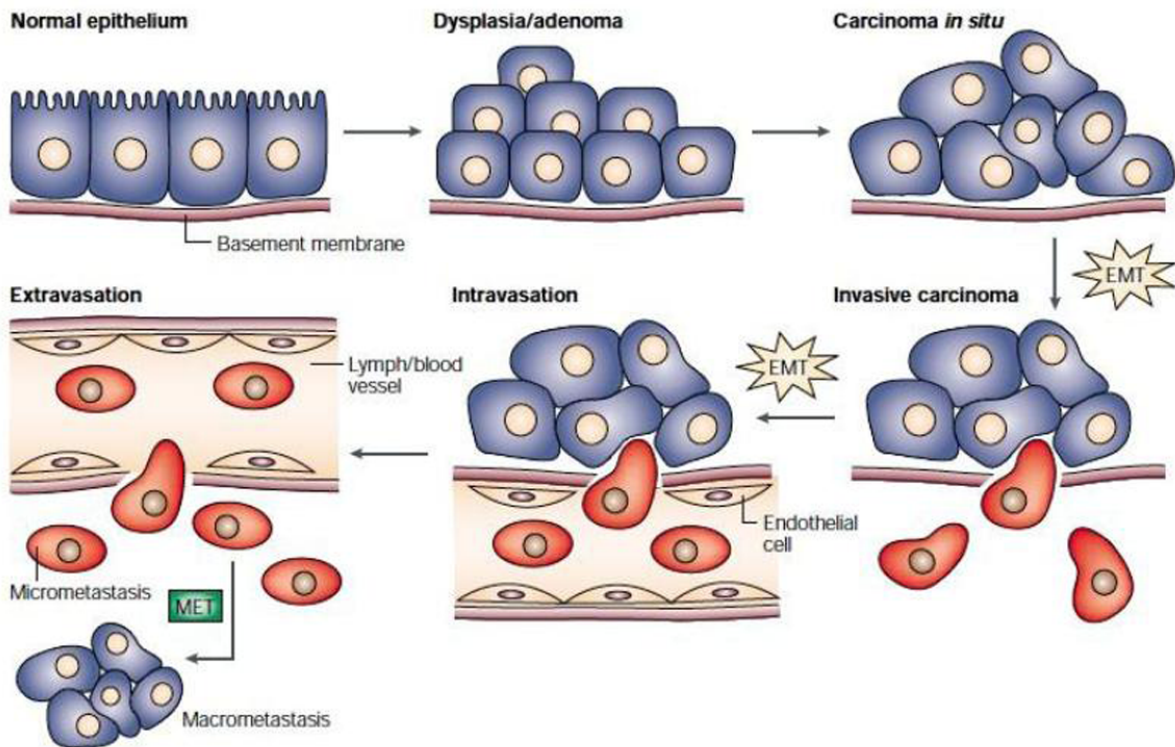


Figure 1.8. Overview of metastatic progression. Taken from (108). Metastatic progression involves several steps. Upon cellular disorganization and formation of the primary tumor, cells must first undergo EMT to break through the basement membrane and invade locally. Cells then intravasate into the lymphatic system and/or blood. After traveling through lymph/blood, cells then extravasate and can undergo mesenchymal-epithelial transition (MET) to return to a more epithelial state and form secondary tumors, or macrometastases.

1.4.2 Metastatic heterogeneity

Successful invasion of tumor cells is largely dependent on the ability of cells to migrate through the extracellular matrix (ECM). Migrating cells can employ one of two broad categories during this process: single cell migration or collective cell migration. Single cells usually utilize one of two modes for migration, amoeboid or mesenchymal (109). Amoeboid migration involves a more rounded cell comprised of weak adhesions and rapid motility. This allows cells to move through pores of the ECM, adjusting shape to fit through spaces as needed.

Conversely, mesenchymal migration is characterized by strong stress fibers, polarization, and a leading edge. Most commonly, epithelial cells undergo a series of biological alterations to transition to a more mesenchymal state and adopt a more motile, migratory phenotype. This process, as previously mentioned, is termed EMT and involves both genetic and epigenetic modifications, as well as loss of common epithelial markers like E-Cadherin and gain of mesenchymal markers like N-Cadherin. (110, 111). In addition to tumor migration and metastasis, EMT has been observed in other biological processes, such as embryogenesis (112, 113). The EMT process is transient and reversible, termed MET, allowing cells to return to an epithelial morphology once established in a secondary site (Figure 1.8) (114). Mesenchymal cells rely less on changing shape to fit through pores of the ECM, but rather work by degrading the surrounding matrix. Degradation of the ECM is achieved by matrix metalloproteases (MMPs) (115). Utilization of MMPs essentially allows mesenchymal cells to carve out tunnels as they travel, leaving a path for subsequent cells to follow. However, it is important to note that certain cell types can alternate between migration strategies as they navigate the microenvironment.

Most cancer cell metastasis is believed to occur through collective cell mechanisms (116). Collective cell migration can occur through different modes. Cells can employ cellular streaming, relying on chemoattractant gradients within the microenvironment to invade. Cells can also rely on strong cell-to-cell interactions and invade in a sheet like pattern or in clusters or tubes (117). Finally, cells can invade in what is commonly called a collective chain invasion. This form of invasion involves a leader (or tip) cell. While this cell has altered cell polarity, cells can still directly attach to the back of the cell. These secondary cells are rightfully termed follower cells and trail behind the leader cell until a secondary site is established (118, 119).

1.4.3 Metastasis in lung cancer

Lung cancer metastasis is a multifaceted process that often involves tumor cell dissemination via the lymphatic system or blood vessels (120). As previously mentioned, lung carcinomas have most often progressed to metastatic stage IV at the time of diagnosis, but vascular invasion is often observed even in lower grade tumors upon resection. In both cases, metastatic progression results in increased incidence of recurrence, as well as shortened patient survival (121). Preferentially, lung cancers metastasize to the bone (34.4%), brain (28.4%), adrenal glands (16.7%), and liver (13.4%), but interestingly, different lung cancer subtypes have different preferential sites for metastasis. For example, lung adenocarcinomas preferentially metastasize to the brain, as commonly observed with EGFR-mutant adenocarcinomas (122). In addition to preferential metastatic sites, different lung cancer subtypes also exhibit preferential migration strategies. Single cell and small cell cluster migration is commonly observed in small-cell carcinoma and undifferentiated non-small cell lung cancer, while larger cluster collective cell migration is observed in acinar adenocarcinoma and different cases of squamous cell carcinoma. Because lung

cancer is often diagnosed after metastatic progression, it is especially important to understand its progression. Emerging research will aim to better understand which subtypes, and which driving mutations promote the most aggressive metastases, and where these tumors preferentially metastasize to.

1.5 *Drosophila melanogaster*

1.5.1 *Drosophila melanogaster* as a model organism

Conservation of major signaling pathways between humans and flies has made *Drosophila melanogaster* an important and valid model system for studying cancer biology and specific genes related to tumor development and metastasis (123). Technical advantages to using *Drosophila* over vertebrate model organisms include easy and inexpensive maintenance, short life cycle, large numbers of progeny, and easy genetic manipulation due to a fully sequenced genome (124). Over the years, *Drosophila* have been used to study genetics, embryonic development, behavior, and aging. Many basic biological, physiological, and neurological properties are conserved between mammals and *Drosophila*. Importantly, 75% of human disease-related genes are believed to have a functional homolog in the fly. Compared to mammalian systems, the fly life cycle is complete within ten to twelve days. Additionally, each developmental stage of the fly life cycle (embryo, larvae, pupae, and adult) can be studied for understanding different aspects of development and growth. The embryo is often used for studying pattern formation and cell fate. Larvae, particularly third instar larvae, are used for studying developmental processes due to undifferentiated epithelium. Future adult structures are contained within the developing larvae, termed imaginal discs, making these structures of important use when studying tumor development. Similarly,

pupae are also used to study certain developmental processes. Finally, adult flies have structures like mammalian systems and carry out complex behaviors, making this developmental stage useful for studying aspects of biology such as drug development (125). Because of this, *Drosophila* offer opportunities for effective, low-maintenance therapeutic discovery for a variety of diseases and disorders.

1.5.2 *Drosophila melanogaster* biology

Drosophila melanogaster was the first major organism to have a fully sequenced genome that encodes for approximately 14,000 genes over four chromosomes (three of which carry the bulk of the genome). Upon fertilization, embryogenesis is completed in about 24 hours, followed by three larval stages. These larval stages are called first, second, and third instar, and each stage is characterized by a molting event. Each of the first two larval stages last approximately 24 hours, and the third larval stage lasts closer to two days. After completion of the third larval stage, pupation occurs and lasts four to five days. During this time, larval tissues break down and adult structures, such as legs, eyes, and wings, form from the 19 imaginal discs present in the larvae. After pupation, adult flies emerge and sexually mature within eight to twelve hours, allowing for the life cycle to begin again (Figure 1.9) (126).

1.5.3 *Drosophila melanogaster* genetics

Of the four chromosomes, the first is the sex chromosome. Sex is determined not by the presence of a Y chromosome, but rather by the dosage of X chromosomes. The remaining three chromosomes are autosomes, with the second and third chromosomes containing most information. The second and third chromosomes are often broken down by left or right arm (2L,

2R, 3L, and 3R), and the fourth chromosome is very small and not often utilized for genetic manipulation in experimentation.

In 2010, efforts to define all functional elements in the fly genome were completed. This information included transcription start and stop sites, promoters and regulatory regions, chromatin structure, and splice variants (127). Understanding functional elements of the *Drosophila* genome has allowed for experimental genetic manipulation and use of this model as a powerful genetic tool. For genetic manipulation, “virgin”, unmated females are mixed with males of desired genotypes. To accurately determine and select fly genotypes of interest, “balancer chromosomes” or phenotypic markers, are used to distinguish one arm of a chromosome from another. This allows for selection of offspring with the inherited gene of interest. Of note, these markers also contain inversions to prevent recombination. Additionally, these balancer chromosomes are often also recessive lethal to prevent loss of genes of interest.

Aiding in the value of *Drosophila* as a genetic tool, was the development of the P-element transposable element (128). Development of the P-element allowed for creation of a gene expression system that would allow expression of any gene of interest in any tissue of the fly. This expression system was termed the GAL4/UAS system (Figure 1.9). To expound, the yeast transcription factor GAL4 was cloned into a P-element vector. Additionally, a corresponding P-element vector, pUAST, containing the upstream activating sequences (UAS) that the GAL4 protein can bind to, was also created. When connected to a general promoter and cloning site, this GAL4/UAS system allows for insertion and expression of any gene of interest in a defined way (129). As examples, the *MS1096-Gal4* expression system drives expression of any gene of interest

only in the center wing pouch and the *Apterous-Gal4* expression system drives expression in the dorsal wing.

For analysis of genes essential for early development, clonal systems can be used to produce mosaics that have homozygous mutant patches of cells, termed clones, in an otherwise wild-type background. Clonal analysis relies on mitotic recombination and site-specific recombination components associated with the yeast 2 μ m plasmid, FLP recombinase, and its site specific recombination sites (FRTs) (130). In short, this system allows for a mutation of interest to be recombined onto a chromosome with an FRT site. When two flies, both heterozygous for that mutation, but both with FRT sites on chromosomes are mated, FLP-triggered mitotic recombination leads to patches of homozygous mutant cells (Figure 1.9). Of benefit, these homozygous mutant cells are often marked to distinguish them from neighboring wild-type cells. For example, use of the eyFLP expression system clonally drives GFP-labelled homozygous mutant expression throughout the developing eye imaginal discs (126). Through these techniques, *Drosophila* have proven to be a highly capable and successful model for use in clarifying mechanisms that regulate a wide variety of diseases.

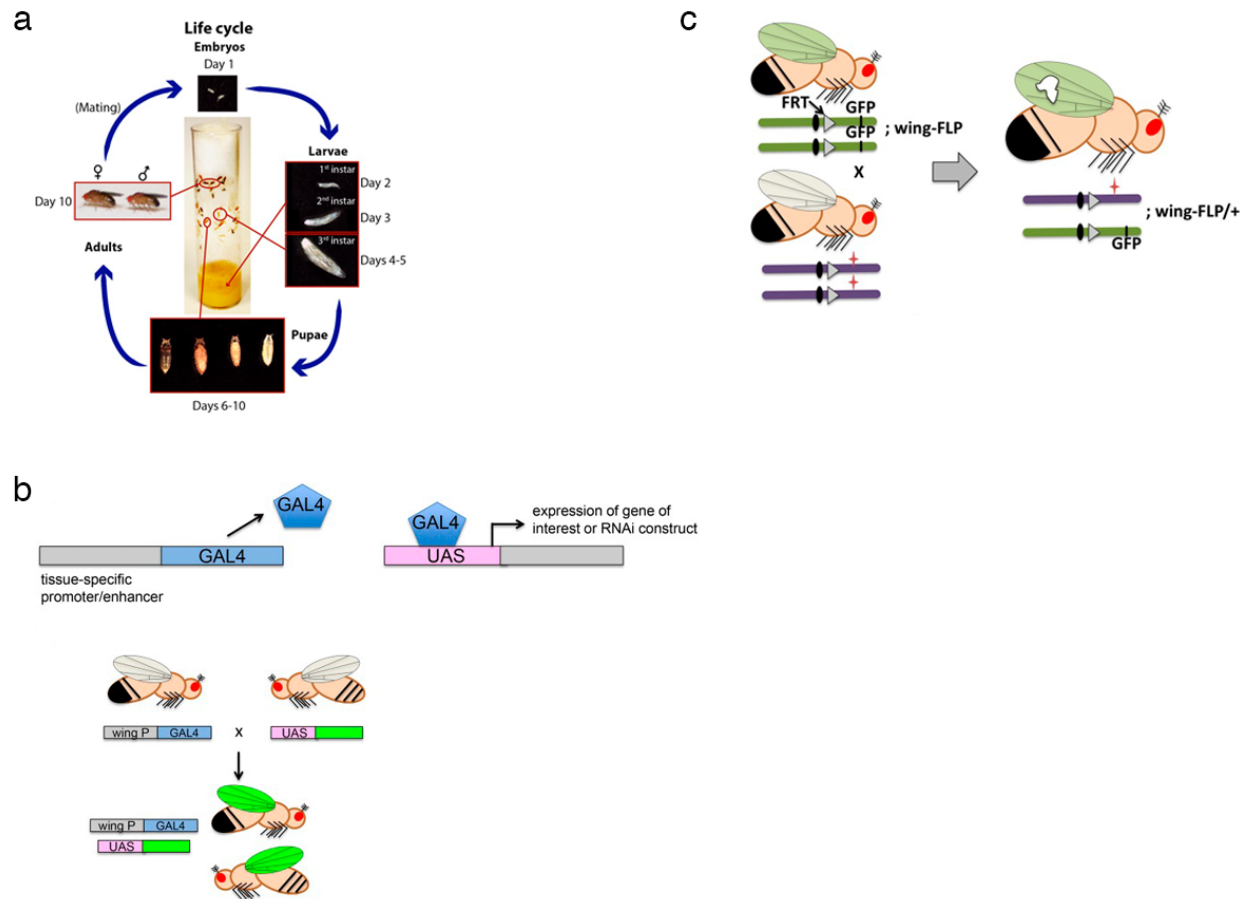


Figure 1.9. Understanding *Drosophila* biology and genetics. Adapted from (126). The *Drosophila* life cycle lasts approximately 10 days and involves an embryo stage, followed by three larval stages, pupation, and emergence into adulthood (a). What aids in *Drosophila* being a powerful genetic tool for understanding of different biological processes, are the methods by which they can be genetically manipulated. The GAL4/UAS system involves placing the yeast transcription factor GAL4 upstream of a tissue specific promoter/enhancer. When mated to a fly with an upstream activating sequence (UAS) upstream of a gene or RNAi construct of interest, the GAL4 transcription factor binds to the UAS and drives expression of the gene of interest in only the specified tissue (b). Similarly, the clonal analysis using the FLP/FRT involves mating one fly containing FRT sites and GFP-labelled cells to a second fly containing a mutation of interest (red star) along with second FRT sites. When mated, FLP-mediated mitotic recombination in the developing wing will produce patches of unmarked homozygous mutant cells (white patch) (c).

1.5.4 Understanding organ size control using *Drosophila*

Genetic studies using *Drosophila* have led to understanding important regulators of pattern formation and tissue growth, known as tumor suppressor genes. Understanding the mechanisms that regulate normal growth allows for better understanding how these mechanisms are dysregulated during diseases like cancer. Initially, *Drosophila* were used to identify 25 genes that caused tumorous growths when mutated to loss-of-function (131). Tumors were characterized by altered cell morphology, impaired differentiation, continued proliferation, and invasiveness, ultimately leading to the death of the animal. Typically, normal imaginal discs utilize mechanisms to control final size, even when externally manipulated. Through *Drosophila*, it has been determined that tissue overgrowth can occur by two mechanisms that are not mutually exclusive. Mutant cells can either grow at an increased rate, demonstrating hyperplastic growth, or can grow at a developmental time when normal tissue has stopped growing, demonstrating neoplastic growth. This is often observed when during extended larval stages which delay the pupal stage of development. Mutations that cause hyperplastic growth, such as mutations in *Hippo*, *Tsc1/2*, and *Pten*, can also result in increased cell size as well as defects in apoptosis, resulting in mutant cells that display a dramatic growth advantage over adjacent wild-type cells. However, these cells still differentiate to form adult structures and maintain a monolayer of tissue, often resulting in a phenotype marked by large outgrowths of cuticle as well as folding and protrusions of excess tissue (132). Mutations driving hyperplastic growth can also promote overgrowth in a non-autonomous manner, promoting the growth of surrounding wild-type tissue. Mutations that result in neoplastic growth lose their regular shape, no longer maintain monolayer organization, and lose proper apical/basal polarity. Neoplastic cells never stop dividing and show defects in terminal differentiation. Finally, neoplastic cells show metastatic activity, often leaving the primary tumor,

breaking down the basement membrane, and colonizing in secondary sites (133). Co-occurring mutations in Ras have been shown to promote tumor growth and neoplastic progression, as already discussed (134, 135).

1.5.5 *Drosophila melanogaster* as a model for human cancer

Over the last several years, *Drosophila* have become an important model for mimicking and understanding human cancer. The ability to conduct large scale genetic screens, as well as reduced redundancy within the genome make this model important for understanding signaling cascades, growth control, and developmental processes. Whether it be elucidating how different mutations contribute to tumorigenesis via dysregulation of growth, or by combining mutations to study tumor development in the whole animal, the capabilities of *Drosophila* in the context of cancer biology are numerous. While not all organ systems can be modeled directly, recent studies have capitalized on similarities between *Drosophila* and human glial cells to model glioblastoma in flies (136). In addition to use in modeling tumor initiation and progression, flies are a useful tool for studying how the immune system plays a role in tumor development. Finally, *Drosophila* are useful in modeling tumor metastasis into distant organs, although they are limited in their ability to directly mimic metastatic progression as observed in human disease due to differing lymphatic and circulatory systems (123). Overall, *Drosophila* prove to be a powerful and fast *in vivo* model for helping to uncover tumor development and progression.

1.6 Rationale and scope of dissertation

Together, the work presented in this dissertation aims to dissect how oncogenic KRAS cooperates with loss of LKB1 function to drive neoplastic transformation and tumor progression. While

research into these two mutations is extensive, not much progress has been made regarding the mechanism by which KRAS and LKB1 work together to drive such significant tumor growth, progression, and metastasis, ultimately leading to poorer patient outcomes. The first part of this dissertation focuses on how LKB1 and KRAS regulate growth dynamics in developing *Drosophila* wing imaginal discs. Chapter 2 first focuses on understanding and establishing a novel *Drosophila* Ras^{V12}/Lkb1 model. Following development of this model, this chapter utilizes 3D modeling software to understand how these mutations work to override growth signals.

For the second part of this dissertation, the “dosage” of KRAS required to drive oncogenic transformation was examined in detail. While extensive research has been done to show that loss of LKB1 drives poorer responses to treatment, poorer prognosis, and metastatic progression with concomitant expression of oncogenic KRAS, little is understood about the mechanisms by which this occurs and how to target these subsets of patients for better treatment responses. The work of this dissertation seeks to better understand how KRAS and LKB1 work collaboratively to drive tumor progression and metastasis using *Drosophila melanogaster* as a model organism, and aims to offer potential targets for further study in hopes of improving patient treatment outcomes. Chapter 3 aims to delve further into how levels of oncogenic KRAS contribute to LKB1-mutant tumor potential and how downstream signaling components play a role. This chapter also explores whether phenotypes observed in *Drosophila* are observed in patients and offers potential targets for future therapeutics in these subsets of patients.

**Chapter 2: Oncogenic Ras cooperates with knockdown of the tumor suppressor Lkb1 by
RNAi to override organ size limits in *Drosophila* wing tissue**

Briana Brown Rackley, Evan Kiely, Chang-Soo Seong, Manali Rupji, and Melissa Gilbert-Ross

This chapter is adapted from a manuscript published by
B Rackley, E Kiely, CS Seong, M Rupji, and M Gilbert-Ross. *Oncogenic Ras cooperates with
knockdown of the tumor suppressor Lkb1 by RNAi to override organ size limits in Drosophila
wing tissue*

microPublication Biology 2020.

doi: 10.17912/micropub.biology.000223

Abstract

KRAS is the most frequently mutated oncogene in human cancer, particularly in cancers with a high mortality rate. Improvement of sequencing data has allowed for better understanding of how secondary mutations synergize with oncogenic KRAS to drive tumor progression. Because activating mutations in KRAS frequently occur with loss-of-function mutations in the tumor suppressor Liver Kinase B1 (LKB1) and drive decreased patient survival and increased likelihood of tumor recurrence, this work sought to better understand the mechanisms by which these two mutations work together to promote tumor progression. Using the genetically tractable model organism *Drosophila melanogaster*, these data show that knockdown of Lkb1 by RNAi cooperates with activating mutations in Ras^{V12} to drive increased tissue growth in both developing and adult fly structures. 3D modelling software shows that this increased tissue size is driven by autonomous proliferation and ineffective autonomous cell death. Additionally, data show that co-mutation of Ras^{V12} with Lkb1 knockdown promotes tumor cell invasion and migration via basement membrane degradation and actin filament disorganization. Together, these data introduce mechanisms by which KRAS and LKB1 mutations work together, and offer opportunities for further study.

2.1 Introduction

Lung cancer is the leading cause of cancer-related deaths, killing more people than breast and prostate cancer combined (1). Lung adenocarcinoma has been extensively studied, and several key oncogenic driver mutations have been identified allowing for further study and understanding. These oncogenic mutations frequently co-occur with inactivating mutations in tumor suppressor genes. The heterogeneity of mutations within each tumor can add to the complexity of treatment, and makes development and implementation of effective treatment strategies challenging, highlighting the importance of continued research into new and diverse approaches to treatment.

The serine/threonine kinase LKB1 was originally determined to be responsible for regulation of Peutz-Jeghers Syndrome (PJS), a rare, autosomal dominant disorder characterized by the development of benign gastrointestinal hamartomatous polyps (75). In addition to regulating PJS, LKB1 is a master regulator in several biological processes, including signal transduction, cell polarity, cell motility, cell metabolism, and cell growth. Over time, it was discovered that in addition to malignancies associated with PJS, mutations in LKB1 have been most commonly associated with lung cancer, cervical cancer, and melanoma (Figure 1.5) (80-83). In lung cancer *LKB1* mutations seem to be exclusively found in non-small cell lung cancers, and in lung adenocarcinoma, many *LKB1* mutations are truncating mutations that result in partial or complete loss of functional domains (9). While discrepancies in mutation frequency remain, it is believed that *LKB1* is inactivated in up to 39% of non-small cell lung cancer patients (84) and is the third most commonly mutated gene behind *KRAS* and *P53*. While much is known regarding the

frequency of LKB1 mutations, how LKB1 mutations drive lung adenocarcinoma tumorigenesis remains an area of interest.

KRAS is the most frequently mutated oncogene in human cancer and is particularly prevalent in cancers with high mortality rates such as pancreatic, colorectal, and non-small cell lung cancer (137). While effective therapies for treatment of KRAS-mutant tumors have yet to be fully validated, recent clinical trials show positive progress for patients with the KRAS(G12C) mutations (39). Moreover, improvement in sequencing modalities has allowed for better understanding of how secondary mutations synergize with oncogenic KRAS to drive tumor progression. For example, sequencing efforts uncovered that activating mutations in KRAS frequently occur with loss-of-function mutations in the gene encoding LKB1, resulting in decreased patient survival, de novo resistance to targeted treatments and immunotherapies, and increased likelihood of tumor recurrence (9, 64, 138). *LKB1* is inactivated or deleted in up to 30% of KRAS-mutant non-small cell lung cancers. Previous work from genetically engineered mouse models (GEMMs) also suggests loss of *Lkb1* is sufficient to promote the progression and metastasis of nascent *Kras*-driven lung adenocarcinoma (94). Loss of *Lkb1* function was shown to promote tumors resistant to chemotherapeutics and combination therapies with co-mutation of *Kras*, potentially identifying a source contributing to KRAS-mutant tumors' poor response to therapy (Figure 1.7).

Due to this observed synergy, the model organism *Drosophila* was used to better understand how knockdown of *Lkb1* function works with activating mutations in Ras^{V12} to promote tumor formation. First, a novel co-mutant $\text{Ras}^{\text{V12}}/\text{Lkb1}^{\text{RNAi}}$ model was developed and used for all

analysis. Data show that combined mutations in Ras^{V12} with knockdown of Lkb1 work together to drive tissue overgrowth in both the developing *Drosophila* wing imaginal discs, as well as adult structures. When studied further, this data show that tissue overgrowth is predominately driven by autonomous cell proliferation to override growth signals in the developing *Drosophila* wing disc. As a proposed compensatory mechanism, these data also show co-mutation drives concomitant autonomous cell death. Additionally, combination of oncogenic Ras^{V12} with Lkb1^{RNAi} work to increase filamentous actin disorganization and expression of matrix metalloproteases (MMPs) which are important for initiation of metastatic progression. Given that LKB1 and KRAS are frequently mutated together leading to poorer patient outcomes, this work may provide insights into the mechanism by which tumors progress, offering potential new areas for study in lung cancer treatment.

2.2 Materials and Methods

***Drosophila* Stocks and Maintenance:**

Flies were grown on a molasses-based food at 25°C.

The following *Drosophila* stocks were used: $P\{UAS-Ras85D.V12\}$ ($UAS-Ras^{V12}$) and $y[1] sc[*] v[1]$; $P\{y[+t7.7] v[+t1.8]=TRiP.HMS01351\}attP2$ ($UAS-Lkb1^{RNAi}$) were provided by Bloomington *Drosophila* Stock Center. w^{1118} was a gift from K. Moberg (Emory University). $Lkb1^{4A4-2}$ was a gift from J. McDonald (Kansas State University). Fluorescently labeled mutant cells were induced in the center wing pouch of larval wing-imaginal discs using the following strain: $MS1096-Gal4, UAS-GFP$ from K. Moberg (Emory University). Fluorescently labeled mutant cells were induced in the dorsal wing of larval wing-imaginal discs using the following strain: $Apterous-Gal4, UAS-GFP$. Mitotic clones were induced in larval wing-imaginal discs using the following strain: $P\{Ubx-FLP\}, P\{tubP-GAL4\}, P\{UAS-GFP\}1, y^l w^*$; $P\{neoFRT\}82B P\{Car20y\}96E, P\{tubP-GAL80\}$. For adult eye phenotypes, the following strains were used: $w[1118]; P\{w[+mW.hs]=sevEP-GAL4.B\}7$ and $w[1118]; P\{GMR-GAL4.w[-]\}2/CyO$.

Immunostaining:

3rd instar larval wing-imaginal discs were dissected in 1X phosphate-buffered saline (PBS) and fixed in 4% paraformaldehyde for 30 minutes on ice. Discs were then washed three times for 10 minutes each in ice cold 1X PBS, permeabilized in 0.3% Triton X100/1X PBS (PBST) for 20 minutes at room temperature (RT), and washed again three times for 10 minutes each before blocking in 10% normal goat serum in 0.1% PBST for 30 minutes at RT. Discs were incubated in

primary antibodies (4°C overnight) in 10% normal goat serum (NGS)/0.1% PBST. The following day, discs were washed three times for five minutes each in 0.1% PBST before incubating in secondary antibodies (in the dark at RT for one hour) in 10% NGS/0.1% PBST. Finally, discs were washed three times for 10 minutes each in 1X PBS at RT and mounted using VectaShield anti-fade mounting medium. Primary antibodies and dilution: rabbit anti-cleaved *Drosophila* DCP-1 (Asp216) (Cell Signaling, 1:100), mouse anti-MMP1 (3A6B4/5H7B11/3B8D12 antibodies were mixed in equal amounts) (DSHB, 0.2µg/ml), mouse anti-Fibrillarlin (Nop1p) (Invitrogen, 1:500), and goat anti-rabbit Cy3 AffiniPure secondary antibody (Jackson ImmunoResearch 1:400). DAPI was used to stain DNA and 1µm Alexa Fluor-555 phalloidin was used to label F-actin (Life Technologies).

Scanning Electron Microscopy:

Adult flies were anesthetized using CO₂ then placed into a 1.5ml centrifuge tube containing 25% ethanol for 12 to 24 hours at RT. Next, the 25% ethanol was discarded and replaced with 1ml of 50% ethanol. Flies were incubated in 50% ethanol for an additional 12 to 24 hours at RT. 50% ethanol was next replaced with 1ml 75% ethanol and incubated for another 12 to 24 hours at RT. 75% ethanol was replaced with 100% ethanol and incubated at RT for 12 to 24 hours. After 12 to 24 hours, flies were incubated again in 100% ethanol. After second 100% ethanol incubation, ethanol was removed and replaced with 500µl of hexamethyldisilazane and incubated for one hour inside of fume hood. Hexamethyldisilazane was next removed and the centrifuge tube was dried overnight in the fume hood with the cap open. Finally, flies were prepared by removing legs and wings and arranged on a specimen mount (Ø15 x 10mm) (Ted Pella) for imaging through the Integrated Electron Microscopy Core.

BrdU Labeling:

3rd instar larval eye-imaginal discs were dissected in Grace's Insect Medium (ThermoFisher) then transferred into Grace's Insect Medium containing 0.25mg/ml BrdU (Invitrogen B23151) and incubated at 25°C for 90 minutes. Discs were then washed in Grace's Insect Medium for five minutes on ice followed by washing two times for five minutes each in 1X PBS on ice. Discs were fixed overnight (wrapped in foil) in 1% paraformaldehyde/0.05% Tween20. The following day discs were washed three times for five minutes each in 1X PBS and permeabilized for 20 minutes at RT in 0.3% PBST. To remove detergent, discs were washed five times for five minutes each in 1X PBS and DNase treated for 30 minutes at 37°C. Discs were then washed three times for 10 minutes each in 0.1% PBST and incubated overnight at 4°C in mouse anti-BrdU primary antibody (B44) (BD, 1:50). The next day, discs were washed 5 times for a total of 30 minutes with 0.1% PBST and incubated overnight in goat anti-mouse F(ab)'₂ AlexaFluor-555 secondary antibody (Cell Signaling, 1:500). Finally, discs were washed three times for 10 minutes each in 0.1% PBST and mounted in VectaShield anti-fade mounting medium.

Widefield and confocal imaging:

Brightfield adult images were taken using a Leica S6D dissecting microscope. Fluorescent images were taken on a Leica MZ10F ($\times 1$ 0.08899 NA) or Leica TCS SP8 inverted confocal microscope ($\times 10$ air HC PL Fluotar, 0.3 NA, $\times 20$ air HC PL APO, 0.75 NA, or $\times 40$ oil HC PL APO, 1.30 NA) using 0.5 μ m z-stack intervals and sequential scanning (405 nm DMOD Flexible, 488 nm argon, 514 nm argon).

Image Processing and Quantification:

IMARIS microscopy image analysis software and ImageJ/FIJI were used for all image processing and quantification. For three-dimensional image analysis, after file conversion into IMARIS, minimum and maximum intensity values were established for each channel and maintained across genotypes. Based on these values, regions of interest, termed “masks”, were created for DAPI and GFP channels. These masks were used to determine total volume, GFP-positive volume, and GFP-negative volumes. The “Spot” feature was used to correctly identify cells labeled with BrdU or stained with DCP1. Spot size was constrained to 2.5 and spot quality was restricted to greater than 7.07 for all genotypes. Autonomous BrdU incorporation and DCP-1 staining was calculated by taking the total number of “spots” occurring within the GFP-marked “mask”. Values were then graphed and statistically analyzed.

Statistical Analysis:

GraphPad Prism 8 was used to generate *P* values using ordinary one-way ANOVA with a Tukey’s multiple comparisons test. Due to the relatively small sample size, a p-value of $\leq .1$ or 10% was considered significant.

2.3 Results

Co-mutant $Ras^{V12}/Lkb1^{RNAi}$ overrides 3rd instar wing imaginal disc size control

To study the effects of LKB1 loss in KRAS mutant tumor progression, transgenic *Drosophila* lines expressing oncogenic Ras^{V12} were obtained. On its own, expression of oncogenic Ras^{V12} causes hyperplastic growth balanced by non-autonomous cell death in imaginal tissues (139). To knockdown *Lkb1*, an RNAi fly stock developed by the Transgenic RNAi Project (TRiP) was obtained and validated through the Harvard Medical School RNAi Stock Validation and Phenotypes (RSVP) resource (140, 141). Of note, the $Lkb1^{RNAi}$ stock was determined to have approximately 68% knockdown efficiency when used with the *MTD-Gal4* driver (142). Additional validation using the Updated Targets of RNAi Reagents (UP-TORR) Fly resource confirmed no off-target effects with this RNAi sequence (143). Next, a combined $Ras^{V12}/Lkb1^{RNAi}$ double mutant fly line was generated. The double mutant, along with the single transgenes w^{1118} (control), $Lkb1^{RNAi}$, and Ras^{V12} were crossed with the *MS1096-Gal4*, *UAS-GFP* wing pouch driver to drive expression of the genes of interest in the center wing pouch of 3rd instar larvae. To precisely measure effects on overall organ size, confocal microscopy was used to acquire *z*-sections through the entire wing disc, followed by 3D reconstruction and volume measurements using IMARIS software. It was determined that total wing disc volume was significantly larger in *MS1096-Gal4*; $Ras^{V12}/Lkb1^{RNAi}$ tissues compared to control and single transgenes. (Figure 2.1). To confirm the phenotype observed in developing larvae, control, Ras^{V12} , and $Ras^{V12}/Lkb1^{RNAi}$ transgenes were used to establish adult wing phenotypes. Like phenotypes observed in developing larvae, expression of oncogenic Ras^{V12} was found to drive increased wrinkles and increased wing thickness compared to controls, indicative of increased cell size or cell proliferation. This

phenotype was further exacerbated with expression of $Lkb1^{RNAi}$ in combination with overexpression of Ras^{V12} (Supplementary Figure 2.1). Because previous investigations have shown that $Lkb1$ can exert a non-autonomous role in tumor suppression (144-146), it was next investigated whether the increase in organ size was due to autonomous vs. non-autonomous effects on growth. To do this, individual volumes of GFP-positive and GFP-negative tissue across genotypes were measured. Expression of $Ras^{V12}/Lkb1^{RNAi}$ led to significant autonomous overgrowth in the GFP-positive *MS1096-Gal4* expression domain, while the GFP-negative (non-autonomous) tissue compartment remained unchanged (Figure 2.1). Interestingly, expression of Ras^{V12} alone resulted in significantly increased GFP-negative volume that was significantly rescued by co-expression with $Lkb1^{RNAi}$. Together, these data confirm that loss of $Lkb1$ function is needed to override growth signals in Ras^{V12} mutant tissues.

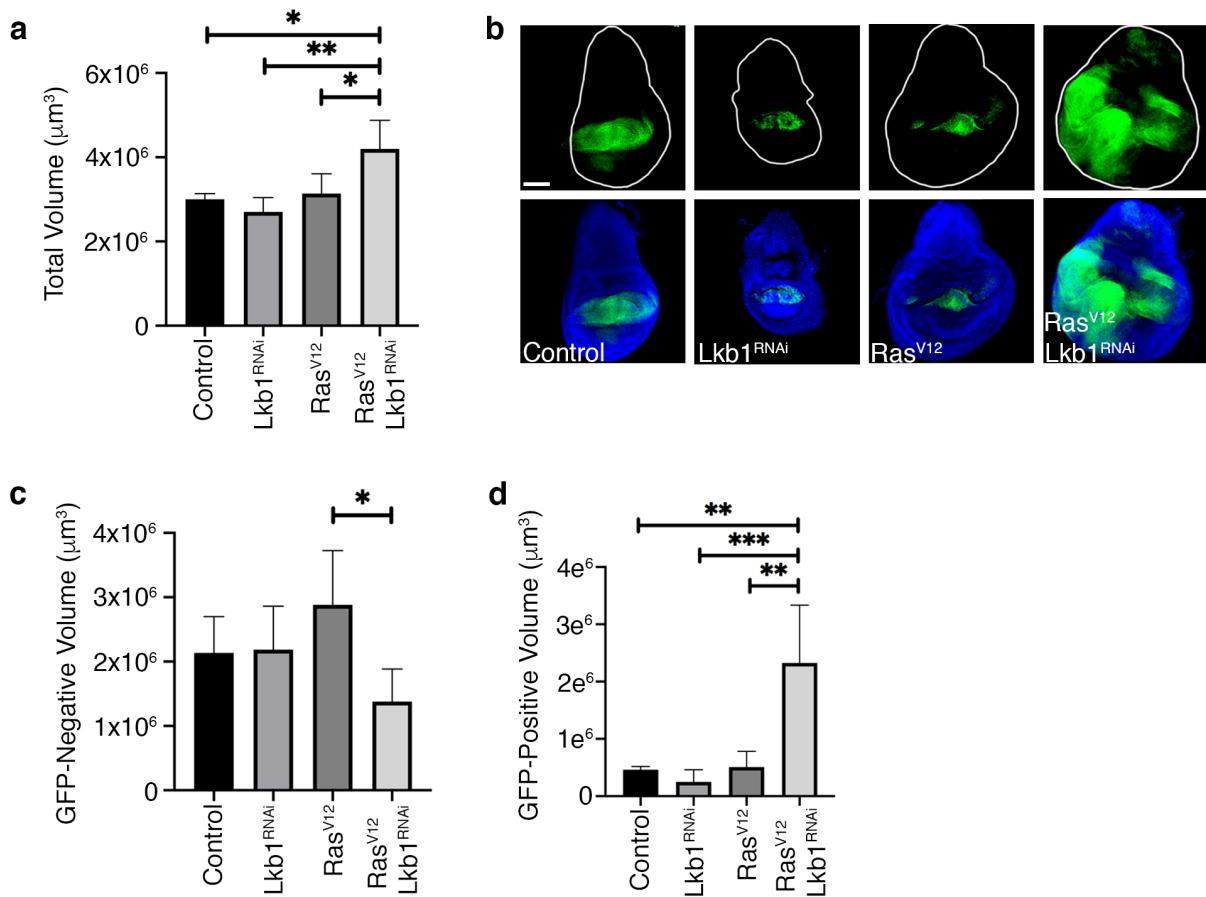


Figure 2.1. Ras^{V12}/Lkb1^{RNAi} overrides 3rd instar wing imaginal disc size control. Quantification of 3rd instar larval wing-imaginal disc total volume (a) and representative confocal images of wing imaginal discs expressing the indicated genotypes and GFP in the *MS1096-Gal4* expression domain (b). DAPI (blue) labels cell nuclei. Quantification of GFP-negative volume (non-autonomous) (c), and GFP-positive volume (autonomous) (d) from the indicated genotypes. Images are representative of 5-10 wing-imaginal discs per genotype. Scale bar, 100 μm . Control = *MS1096-Gal4*, *w¹¹¹⁸*. For graphs, bars represent mean volumes from 3-5 independent wing-imaginal discs per genotype and error bars represent standard deviation. Ordinary one-way ANOVA was conducted with significance assigned to *P* values < 0.1. (a) *p*=0.0030 (c) *p*=0.0896 (d) *p*=0.0004. *P*-values between groups were compared with post-test. **p*<0.1, ***p*<0.01, ****p*<0.001.

Co-mutant Ras^{V12}/Lkb1^{RNAi} overrides 3rd instar eye imaginal disc size control

To confirm that phenotypes observed with co-mutation of Ras^{V12} with Lkb1 knockdown were not exclusive to the developing wing imaginal discs and adult wing structures, mutations in transgenes of interest were also expressed in the adult wing and resulting phenotypes were observed. *Drosophila* contain individual ommatidia, each of which contain 22 cells. Of those 22 cells, eight (R1-R8) are photosensitive neurons called retinula (147). First, control, *Lkb1^{RNAi}*, *Ras^{V12}*, or co-mutant *Ras^{V12}/Lkb1^{RNAi}* transgenes were expressed under promotion of *Sevenless-Gal4*, the receptor tyrosine kinase responsible for development of the R7 neuron. Using scanning electron microscopy and brightfield imaging, it was determined that while expression of Ras^{V12} alone drove disorganization of proper eye morphology, combined knockdown of Lkb1 with oncogenic Ras^{V12} exacerbated this phenotype, resulting in apparent “blebbing” or eye overgrowth (Figure 2.2). Similarly, the same transgenes were expressed under the *GMR-Gal4* driver. The *GMR-GAL4* driver is believed to be expressed in cells of differentiating larval eye discs (148). As seen with *Sevenless-Gal4* driven expression, Ras^{V12} alone resulted in a slightly disrupted eye phenotype that was significantly more severe with co-mutation of Lkb1 (Figure 2.2). Together, these data confirm that phenotypes observed with co-mutation of Ras^{V12} and Lkb1 are not exclusive to the developing and adult wing disc, further confirming that loss of Lkb1 function is needed to override growth signals in Ras^{V12} mutant tissues.

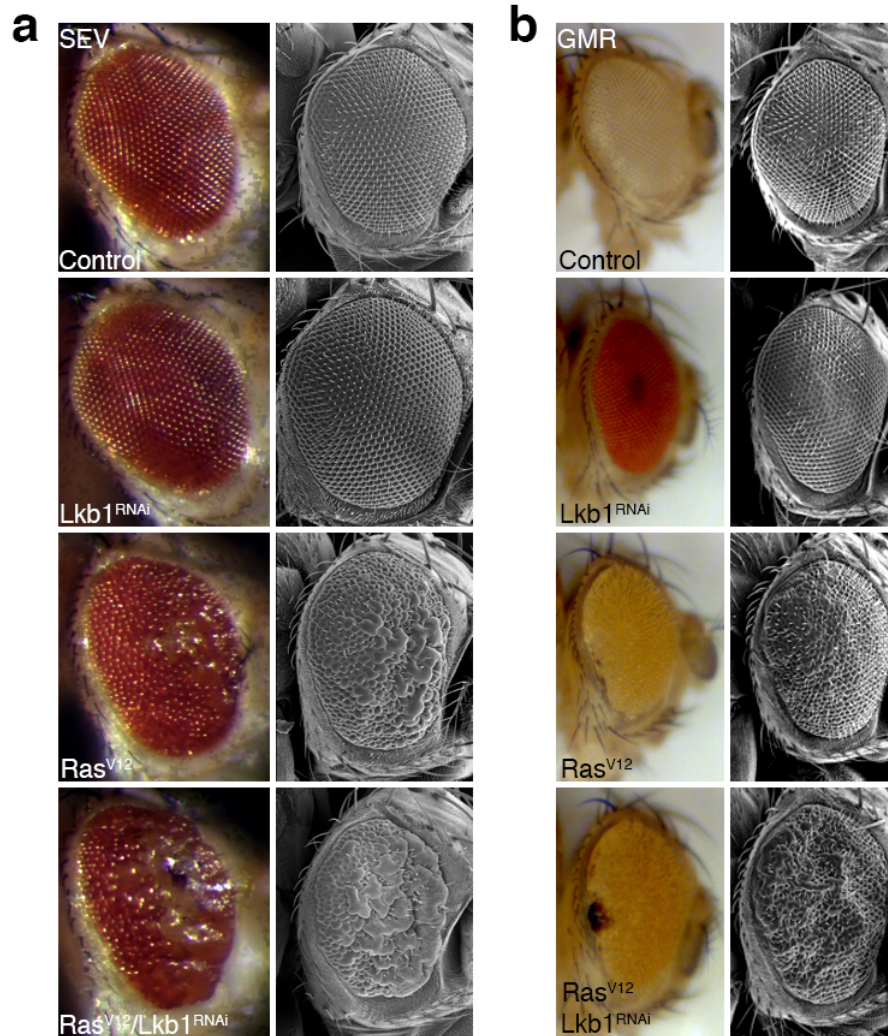


Figure 2.2. Co-mutant Ras^{V12}/Lkb1^{RNAi} overrides 3rd instar eye imaginal disc size control. Representative brightfield and scanning electron microscopy (SEM) images of adult eyes expressing the indicated genotypes in the *Sev-Gal4* expression domain (a) or *GMR-Gal4* expression domain (b). Images are representative of two adult eyes per genotype. Control = *Sev-Gal4*, *w*¹¹¹⁸ (a) or *GMR-Gal4*, *w*¹¹¹⁸ (b).

Expression of co-mutant Ras^{V12}/Lkb1^{RNAi} drives autonomous cell proliferation and death

Changes in organ size control can result from any number of combinations of cell growth, proliferation, and cell death phenotypes. To investigate the compartmental effects on cell proliferation and cell death in Ras^{V12}/Lkb1^{RNAi} tissues, the *MS1096-Gal4* driver was used to express control, *Lkb1^{RNAi}*, *Ras^{V12}*, or *Ras^{V12}/Lkb1^{RNAi}* transgenes in developing 3rd instar larval center wing pouches. First, cell proliferation was assessed by labelling tissues with BrdU. Compared to control, knockdown of Lkb1 alone resulted in a slight decrease in autonomous proliferation, but based on overall wing-disc volume, these proliferation changes had no effect on overall organ size (Figure 2.3). Conversely, expression of Ras^{V12} resulted in slightly increased autonomously proliferative cells compared to non-autonomous. This increase in autonomous proliferation was largely increased with co-expression of Ras^{V12}/Lkb1^{RNAi} and this dramatic increase in autonomous proliferation corroborates overall increased tissue volume associated with co-mutation of Ras^{V12} and Lkb1^{RNAi} (Figure 2.3). Therefore, loss of Lkb1 in the context of oncogenic Ras^{V12} in the *Drosophila* wing pouch is confirmed to exert autonomous effects that contribute to over-riding organ size control.

In addition to investigating compartmental effects on cellular proliferation, the effects of co-mutating Ras^{V12}/Lkb1^{RNAi} on cell death was also investigated using an anti-Death Caspase-1 (DCP-1) antibody. As previously mentioned, knockdown of Lkb1 alone drove predominantly non-autonomous proliferation with no significant effect on overall tissue volume. Upon driving mutant expression in the *MS1096-Gal4* expression domain and staining with DCP-1, it appears that knockdown of Lkb1 expression drives relatively equal amounts of autonomous and non-autonomous cell death (Figure 2.3). Expression of oncogenic Ras^{V12} alone resulted in almost

entirely non-autonomous proliferation (Figure 2.3), which raised the question of what is driving slightly increased overall tissue volume in Ras^{V12} tissues compared to control. To answer this question, control, Lkb1^{RNAi}, Ras^{V12}, and Ras^{V12}/Lkb1^{RNAi} tissues were stained against fibrillarin, a nucleolus marker used as a proxy for measuring cell size. It was determined that overall cell size is larger in Ras^{V12} mutants compared to all other genotypes, which might possibly explain the slight differences observed in overall tissue volume (Supplementary Figure 2.2). Finally, co-expression of Ras^{V12} with knockdown of Lkb1 led to a dramatic shift in cellular phenotypes with a large increase in autonomous cell death that ultimately rescued the non-autonomous cell death observed in cells expressing Ras^{V12} alone (Figure 2.3). To summarize, loss of Lkb1 function in the context of oncogenic Ras^{V12} in the *Drosophila* wing pouch can exert both non-autonomous and autonomous effects that override organ size control and future studies will focus on how these autonomous and non-autonomous changed effect cellular migration and invasion.

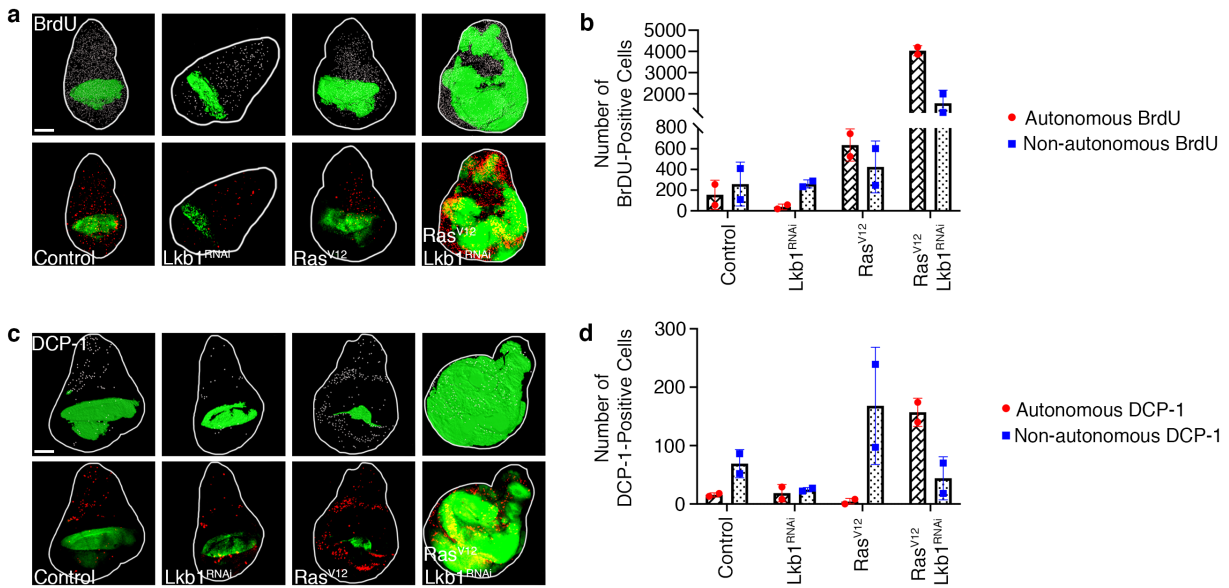


Figure 2.3. Expression of co-mutant Ras^{V12}/Lkb1^{RNAi} drives autonomous cell proliferation and autonomous cell death. Confocal images of 3rd instar larval wing-imaginal discs carrying GFP-labeled wing pouch tissue labeled with BrdU (a). Top panel is a representative image of the IMARIS spot analysis used for quantification of BrdU positive cells. Bottom panel is actual immunofluorescence image of BrdU labeling (in red). Total number of autonomous and non-autonomous BrdU labeled cells are quantified in (b). Confocal images of 3rd instar larval wing-imaginal discs carrying GFP-labeled wing pouch tissue stained with an antibody to Death Caspase 1 (DCP-1) (c). Top panel is a representative image of the IMARIS spot analysis used for quantification of DCP-1 positive cells. Bottom panel is actual immunofluorescence image of DCP-1 staining (in red). Total number of autonomous and non-autonomous DCP-1 stained cells are quantified in (d). Images are representative of 5-10 wing-imaginal discs per genotype. Scale bar, 100 μ m. Control = *MS1096-Gal4, w¹¹¹⁸*. In (b) and (d) bars represent means from two independent wing-imaginal discs per genotype and error bars represent standard deviation. Significance was not analyzed due to sample size.

Ras^{V12} promotes the invasion and metastasis of Lkb1-mutant tissue

Previous studies have determined that oncogenic Ras^{V12} plays a role in tumor progression and cell motility (149). Additionally, previous research has shown that Lkb1 regulates cell polarity as a master kinase. When combined, previous murine studies have shown that co-mutation of Kras^{V12} with loss of Lkb1 drives increased cell motility and metastasis (94). Therefore, upon understanding the role Lkb1 plays in driving Ras^{V12}-mutant tumor cell proliferation and growth dynamics, the next step involved understanding the role Ras^{V12}/Lkb1^{RNAi} co-mutations play in tumor cell migration and invasion. To study this, the *Apterous-Gal4* driver was used to express control, *Lkb1^{RNAi}*, *Ras^{V12}*, and double mutant *Lkb1^{RNAi}/Ras^{V12}* transgenes in the developing 3rd instar larval dorsal wing. Next, filamentous actin organization was measured using fluorescently labelled phalloidin. Immunofluorescence imaging revealed significant actin disorganization with co-expression of Ras^{V12} and Lkb1^{RNAi} compared to expression of oncogenic Ras^{V12} alone, or control (Figure 2.4), suggesting potential disruption to the basement membrane in co-mutant tissues that may indicate metastatic potential. MMP1 expression was next measured to further investigate basement membrane degradation. To more closely mimic tumor heterogeneity observed with human patients, the *Ubx-FLP*, *MARCM3R* driver was used to allow for clonal expression of mutations of interest in an otherwise wild-type background in the developing wing disc. Interestingly, while expression of oncogenic Ras^{V12} alone promoted increased MMP1 expression, MMP1 expression was mostly observed in surrounding wild-type tissue. Conversely, co-mutant expression of Ras^{V12} with knockdown of Lkb1 resulted in increased MMP1 expression that was predominately autonomous, indicative of basement membrane breakdown in these tissues. Of note, increased MMP1 expression was not observed with control or Lkb1^{RNAi} expression alone (Figure 2.4). In addition to investigating MMP1 expression, actin filament organization was also

examined. Phalloidin was used to stain F-actin in the dorsal wing using the *Apterous-Gal4* driver. Expression of Ras^{V12} alone promoted significant actin filament disorganization compared to control alone. Co-mutation of Ras^{V12} with knockdown of Lkb1 exacerbated this phenotype even further, supporting the conclusion that co-mutant Ras^{V12}/Lkb1^{RNAi} is necessary for actin disorganization and autonomous basement membrane degradation, ultimately promoting tumor cell migration and invasion (Supplementary Figure 2.3).

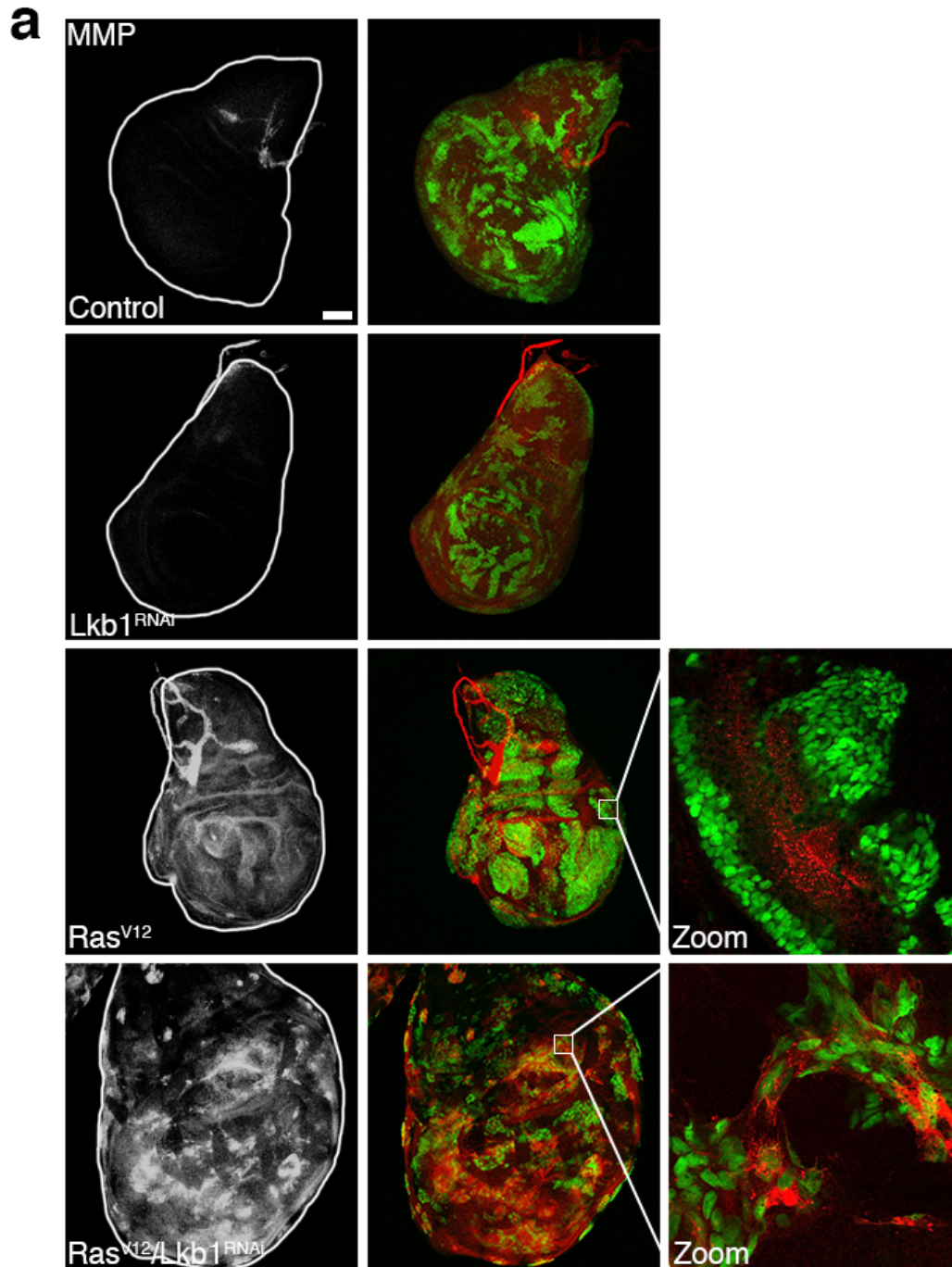


Figure 2.4. Ras^{V12} promotes basement membrane degradation of Lkb1-mutant tissue. Representative immunofluorescent images of 3rd instar larval wing imaginal discs clonally expressing the indicated genotypes in the *Ubx-FLP*, *MARCM3R* expression domain. Images are representative of ten discs per genotype. Scale bar, 100 μ m. Control = *Ubx-FLP*, *MARCM3R*, *FRT82B*.

2.4 Discussion

Mutations in Ras have been repeatedly shown to drive tumor formation and metastatic progression, especially when combined with inactivating mutations in the tumor suppressor Lkb1 (94, 105). However, the exact mechanism by which Ras^{V12} and Lkb1 work together to promote tumor severity has not been well studied. Here, the easily manipulated model organism *Drosophila melanogaster* was used to first develop an *in vivo* model to study how oncogenic Ras^{V12} works with inactivation of Lkb1 to drive this process. Together, data show that Lkb1 loss-of-function is required for growth of Ras^{V12} mutant tissues (Figure 2.1). In addition to showing that Ras^{V12} and Lkb1^{RNAi} work together to drive phenotypes in the developing wing, data also show this phenotype extends to the adult wing as well as adult eye, resulting in overgrown structures suggestive of dysregulated growth (Figure 2.2 and Supplementary Figure 2.1). Through immunofluorescence staining of nucleolus size as a measure of cell size, it was determined that the overall growth phenotype observed with co-mutation is not driven by changes in cell size (Supplementary Figure 2.2). In fact, cells were determined to be larger with expression of Ras^{V12} alone, a phenotype rescued by additional knockdown of Lkb1. Immunofluorescence staining using BrdU incorporation to study cell proliferation show that growth of co-mutant Ras^{V12}/Lkb1^{RNAi} tissues is driven by autonomous cell proliferation mechanisms (Figure 2.3). First, it was shown that in combination with expression of oncogenic Ras^{V12}, loss of Lkb1 function rescues a non-autonomous cell proliferation phenotype observed with expression of oncogenic Ras^{V12} alone. Additionally, when cell death mechanisms were studied, it was determined that knockdown of Lkb1 almost completely reverses the non-autonomous cell death observed with expression of Ras^{V12} alone. This suggests that some sort of compensatory mechanism is at play to attempt to

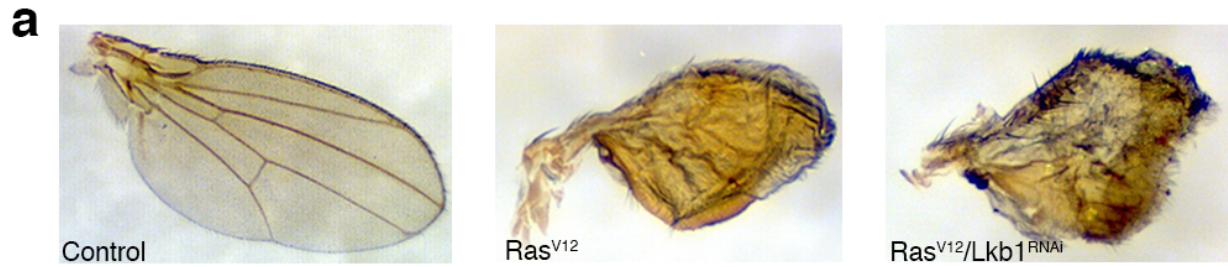
control the growth dysregulation observed with co-mutation. Based on these findings, data support that co-mutation of Ras^{V12} with knockdown of Lkb1 cooperate to promote overall growth and proliferation of *Drosophila* tissues.

Research has shown that LKB1 plays a key role in polarity regulation via cdc42, cell motility, and cell adhesion via inhibition of focal adhesion kinase (FAK) (91-93). Additionally, evidence suggests that loss of LKB1 and SIK1 signaling promotes an EMT phenotype, assisting cells in acquiring a more mesenchymal phenotype. LKB1 has also been shown to inhibit metastasis-promoting genes (94). Given these roles, it was next assumed that loss of Lkb1 function would promote Ras^{V12}-mutant tumor invasion and metastasis. As hypothesized, when stained against MMP1, combined mutations in Ras^{V12} and Lkb1 drove autonomous MMP1 expression indicative of basement membrane degradation (Figure 2.4). Interestingly, expression of Ras^{V12} alone drove non-autonomous MMP1 expression, like the non-autonomous cell death observed. Furthermore, when phalloidin was used to stain F-actin, notable filament disorganization was observed with expression of Ras^{V12} alone. This phenotype was further exacerbated by co-expression of Ras^{V12} with knockdown of Lkb1 (Supplementary Figure 2.3). Therefore, co-mutation of Ras^{V12} and Lkb1 work together to promote basement membrane breakdown and actin filament disorganization necessary for tumor cell invasion and metastasis.

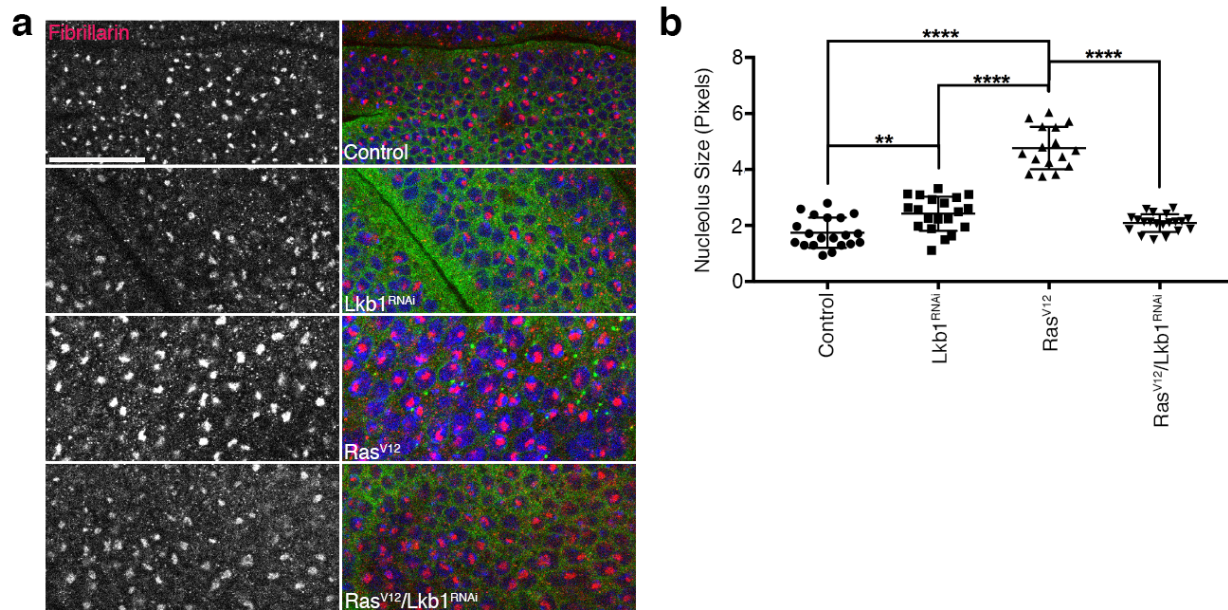
Together, these data detail the initial steps by which loss of Lkb1 function cooperate with activating mutations in Ras^{V12} to promote increased developing organ size by means of increased autonomous proliferation and insufficient compensatory cell death. This dysregulated growth extends beyond the larval stage into both adult wing and eye structures and is not influenced by

changes in cell size. Finally, data presented demonstrate increased basement membrane degradation and suggest that these mutations contribute to tumor migration and invasion.

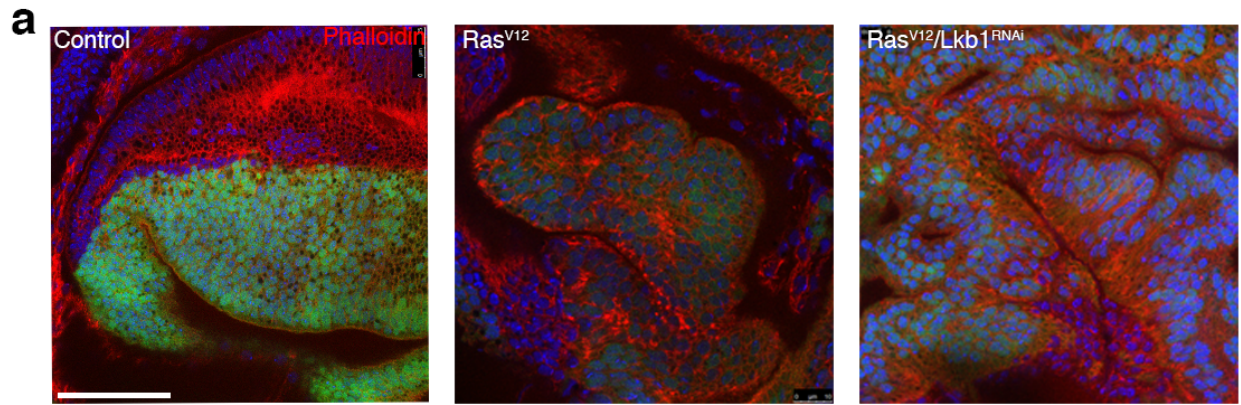
Overall, our developed *Drosophila* model is consistent with KRAS/LKB1 data observed in both patients and mice. In lung adenocarcinoma, *LKB1* is inactivated or deleted in up to 30% of KRAS-mutant non-small cell lung cancers, potentially identifying a source contributing to KRAS-mutant tumors' poor response to therapy. In mice, loss of *Lkb1* was shown to promote tumors resistant to chemotherapeutics and combination therapies with co-mutation of *Kras*. Additionally, *Lkb1* inactivation in mouse models demonstrate shorter latency to tumor formation, and promote more frequent, aggressive, metastatic spread. While work presented in this chapter only begin to demonstrate processes necessary for tumor formation, progression, and dissemination to secondary sites, they represent a strong foundation for which to continue further investigation into the mechanisms by which these mutations work together to drive cancer progression. Additionally, this model offers opportunities from which to begin investigation into pathways that can be targeted therapeutically for better treatment of patients with these subsets of mutations.

Supplemental Information

Supplemental Figure 2.1. Co-mutation of Ras^{V12} with loss of Lkb1 function causes adult wing overgrowth. Representative brightfield images of adult wings expressing the indicated genotypes in the *MS1096-Gal4* expression domain. Control = *MS1096-Gal4, w¹¹¹⁸*.



Supplementary Figure 2.2. Ras^{V12}/Lkb1^{RNAi} rescue 3rd instar wing imaginal disc cell size. Representative confocal images of 3rd instar larval wing imaginal discs expressing the indicated transgenes marked by GFP in the *MS1096-Gal4* expression domain (a). Fibrillarin (pink) marks the cell nucleolus and DAPI (blue) labels cell nuclei. Quantification of nucleolus size in pixels (b) from the indicated genotypes. Images are representative of 5-10 wing-imaginal discs per genotype. Scale bar, 25 μ m. Control = *MS1096-Gal4*, *w¹¹¹⁸*. For graphs, bars represent mean volumes from 15-20 independent wing-imaginal discs per genotype and error bars represent standard deviation. Ordinary one-way ANOVA was conducted with significance assigned to *P* values < 0.05. *P*-values between groups were compared with post-test. ***p* < 0.01, *****p* < 0.0001.



Supplementary Figure 2.3. Co-mutant $Ras^{V12}/Lkb1^{RNAi}$ drives F-actin filament disorganization. Representative confocal images of 3rd instar larval wing imaginal discs expressing the indicated transgenes marked by GFP in the *Apterous-Gal4* expression domain. Phalloidin stains actin filaments (red) and DAPI (blue) labels cell nuclei. Images are representative of 5-10 wing-imaginal discs per genotype. Scale bar, 25 μ m. Control = *Apterous-Gal4, w¹¹¹⁸*.

**Chapter 3: The levels of oncogenic Ras control clonal growth dynamics to transform Lkb1-
mutant tissue in vivo**

Briana Rackley, Chang-Soo Seong, Evan Kiely, Manali Rupji, Bhakti Dwivedi, John M. Heddleston, William Giang, Neil Anthony, Teng-Leong Chew & Melissa Gilbert-Ross

This chapter is adapted from a manuscript published by B Rackley, CS Seong, E Kiely, M Rupji,

B Dwivedi, JM Heddleston, W Giang, N Anthony, TL Chew & M Gilbert-Ross

*The levels of oncogenic Ras control clonal growth dynamics to transform Lkb1-mutant tissue in
vivo*

Communications Biology 2020 – In Revision

Abstract

The genetic and metabolic heterogeneity of RAS-driven cancers has precluded effective targeting strategies. Emerging evidence suggests that co-occurring alterations in tumor suppressor genes can add to this complexity, due to both autonomous and non-autonomous effects on tumor progression, which leads to drastic differences in therapeutic susceptibilities. To address this, rapid and genetically tractable animal models are needed that recapitulate the heterogeneity of RAS-driven cancers *in vivo*. Here, a whole animal model of Ras^{V12}-driven carcinoma was generated along with concomitant loss of the Lkb1 tumor suppressor, a genotype found in a high percentage of non-small-cell lung cancers. Data show that levels of oncogenic Ras^{V12} interact with loss of Lkb1 to ultimately determine social cell interactions and the phenotypic outcome of tumor progression. Additionally, low-level expression of oncogenic Ras^{V12} (Ras^{L0}) promotes the survival of Lkb1-mutant tissue, but results in autonomous cell cycle arrest and non-autonomous overgrowth of surrounding wild-type tissue. In contrast, high-level expression of oncogenic Ras^{V12} (Ras^{Hi}) promotes the autonomous malignant transformation of Lkb1-mutant tissue resulting in lethal malignant tumors. For the first time, molecular analysis reveals concurrent activation of the mTOR and Ampk pathways in mosaic malignant Ras^{V12}/Lkb1 tumors *in vivo*, and demonstrate the genetic and pharmacologic dependence of these tumors on CaMK-activated Ampk. To demonstrate the translational relevance of findings, LKB1-mutant human lung adenocarcinoma patients with high levels of oncogenic KRAS were shown to exhibit worse overall survival and increased AMPK activation, a phenotype not seen in KRAS patients mutant for TP53. These results suggest that high level oncogenic KRAS, possibly through copy number gains or amplifications, is a driving event in the malignant transformation of LKB1-mutant tissue, and uncovers a novel vulnerability that may be used to target this aggressive genetic subset of RAS-driven tumors.

3.1 Introduction

KRAS is the most commonly mutated oncogene in human cancer, and is frequently mutated in cancer types associated with high mortality such as non-small cell lung cancer (NSCLC). Efforts to directly target the KRAS protein have been challenging, but newly renewed efforts at targeting the KRAS G12C mutation are currently in clinical trials (137). Large-scale sequencing of lung adenocarcinoma has uncovered heterogeneity in mutant KRAS tumors due to concomitantly mutated tumor suppressor genes such as *TP53* and *LKB1*, genetic subtypes that are largely mutually exclusive and which harbor distinct biologies and therapeutic susceptibilities (14). An added layer of complexity arises due to the extensive metabolic rewiring observed in RAS-driven tumors (150), which can arise due to RAS-mutant dosage and alterations in signaling pathways downstream of mutated tumor suppressor genes (151). Increasingly, metabolic rewiring is known to be dependent on tissue-level dynamics within the tumor and the tumor microenvironment. Therefore, there is a need to develop rapid and powerful models of RAS-driven cancers that mimic the complex landscape of these tumors *in vivo*.

LKB1 is a master serine/threonine kinase that phosphorylates 13 downstream kinases of the AMP-activated protein kinase (AMPK) family to control cell growth and cell polarity (96). LKB1 activity is lost in a wide spectrum of human cancers and the gene that encodes LKB1 (*STK11*) is the third most frequently mutated tumor suppressor in human lung adenocarcinoma. Loss of LKB1 frequently occurs in KRAS-driven lung adenocarcinomas, and has been shown to promote metastasis, shorten overall survival, and confer resistance to targeted therapies and checkpoint inhibitors (149, 152-155). Altogether, these differences in survival and treatment outcomes

highlight the importance of *in vivo* models that recapitulate the innumerable levels of heterogeneity when developing and implementing cancer treatments.

Drosophila melanogaster is a powerful model system for studying cancer biology due to high conservation of human oncogene and tumor suppressor pathways (156, 157). Elegant genetic mosaic techniques in *Drosophila* allow tissue-specific overexpression of oncogenes and knockdown/knockout of tumor suppressors within distinct subpopulations of cells, which bestows the ability to build complex tumor landscapes *in vivo*. Seminal work using these methods in mice identified mutations in cell polarity proteins as sufficient to promote the metastasis of benign Kras-mutant tumors *in vivo* (134, 135). However, despite evidence that Lkb1 is sufficient to promote tumor progression and metastasis in Kras-mutant lung tumors in genetically engineered mouse models (94), to date no one has produced evidence of malignant synergy between Kras and Lkb1 using the rapid and genetically tractable *Drosophila* model.

Here, using a novel *Drosophila* model of Ras^{V12}/Lkb1-driven malignant progression, it was found that the relative levels of oncogenic Ras^{V12} determine clonal growth dynamics in Lkb1 mutant tissue. Low levels of oncogenic Ras^{V12} promote non-autonomous growth of surrounding wild-type tissue, while high-levels promote malignant progression and organismal lethality. To further characterize the metastatic capability of Ras^{V12}/Lkb1 malignant cells, simultaneous multiview light sheet microscopy was used to image live tumor-bearing larvae for up to 48hrs, and show that Ras^{V12}/Lkb1 cells exhibit single and multi-cellular dynamics during cell migration, and ultimately invade distant tissues. To further define the mechanism driving the progressive synergy between high oncogenic Ras^{V12} and loss of Lkb1 signaling networks in mosaic tissue were investigated.

Malignant Ras^{V12}/Lkb1 tumors concurrently activate mTOR and AMPK, the latter by a nucleotide-independent mechanism that depends on the CaMK cascade. Treatment of Ras^{V12}/Lkb1 tumor-bearing larvae with a CaMK inhibitor was shown to suppress whole-organism lethality. The translational potential of this work was validated by showing high level KRAS with concurrent mutation in LKB1 represents a unique subset of patients with worse overall survival and increased AMPK activation. This work uncovers a novel mechanism that may include oncogenic KRAS copy number gains or amplification as a novel synergistic mechanism that drives the aggressive nature of LKB1 mutant tumors. In addition, this work proves *Drosophila* as a powerful model for the rational design of targeted therapies for genetic subsets of RAS-driven cancers, and suggests that the LKB1 subset of KRAS-driven cancers may benefit from targeting of the CamK/AMPK circuit.

3.2 Materials and Methods

***Drosophila* stocks and maintenance:**

Flies were grown on a molasses-based food at 25°C.

The following *Drosophila* stocks were used: *FRT82B*, *w¹¹¹⁸;df(3R)Exel6169,P{XP-U}Exel6169/TM6B,Tb*, *UAS-Ras^{V12}*; *FRT82B (Ras^{L0}) (135)*, *UAS-Ras^{V12}*, *FRT82B (Ras^{Hi})* and *UAS-Ampk^{Trip20} (Ampk^{RNAi})* were provided by Bloomington *Drosophila* Stock Center. For Supplementary Figure 3.1, *UAS-P35* was provided by Bloomington *Drosophila* Stock Center. *w¹¹¹⁸* and *Viking-GFP (158)* were gifts from K. Moberg (Emory University). *Lkb1^{4A4-2}* and *Lkb1^{4B1-11}* were gifts from J. McDonald (Kansas State University). *Lkb1^{X5}* was a gift from W. Du (University of Chicago). Fluorescently labeled mitotic clones were induced in larval eye-imaginal discs using the following strain: *y,w, eyFLP1; Act >y+> Gal4, UAS-GFP (or RFP); FRT82B, Tub-Gal80*.

Generation of *Drosophila* Lkb1 antibody:

ProteinTech was used to generate a custom Lkb1 polyclonal antibody specific to *Drosophila* using the following peptide sequence: VEDEMTVLLANKNFHYDV-Cys. Guinea Pigs were immunized and supplemented with booster immunizations before final antibody production after 102 days. Antibodies were affinity purified with Elisa confirmation of purification, and final antibody concentrations were estimated by SDS-PAGE.

Western blotting:

Twenty 3rd instar larvae were dissected in 1X PBS and eye-imaginal discs were transferred to a 1.5ml microcentrifuge tube containing 1ml of fresh 1X PBS. Discs were spun down at 4°C for 1 min at 9,600g and supernatant was removed. 2X Laemmli Sample Buffer was added and discs were boiled for 10 minutes at 100°C, and spun down. Approximately 10µg of protein was loaded into a 12% polyacrylamide gel. Alternatively, 3rd instar larvae were dissected and 20µg of crude extract was loaded into a 10% polyacrylamide gel. Samples were run at 100V and separated by SDS-PAGE before transferring to a polyvinylidene difluoride (PVDF) membrane overnight at 0.07amps at 4°C. Membranes were blocked for 1 hour with 10% skim milk in 1X tris-buffered saline plus Tween 20 (TBST) and placed in primary antibody overnight in 1X TBST with 5% skim milk or BSA at 4°C. The following day, membranes were washed three times for 10 minutes each in 1X TBST and placed in secondary antibody in 1X TBST with 5% skim milk or BSA for 1 hour at RT. After three additional 10 minute washes in 1X TBST, ECL-reagent (Amersham, RPN2232) and X-ray film were used to detect signals. When necessary, membranes were stripped using GM Biosciences OneMinute Plus Western Blot Stripping Buffer (GM6011). Primary antibodies and dilution: affinity purified guinea pig anti-*Drosophila* Lkb1 (Protein Tech, 1:1000), rabbit anti-RAS (Cell Signaling 3965, 1:1000), rabbit anti-phospho AMPK (Thr 172) (40HP) (Cell Signaling, 1:1000), mouse anti-*Drosophila* AMPK1/2 (BioRad, 1:1000), rabbit anti-diphosphorylated ERK (Sigma, 1:1000), Rabbit anti-phospho MEK1 (Ser 217+221) (Invitrogen, 1:500), rabbit anti-*Drosophila* phospho p70 S6 Kinase (Thr 398) (Cell Signaling (1:1000), rabbit anti-phospho 4E-BP1 (Thr 37/46) (Cell Signaling, 1:1000), rabbit anti-phospho AKT (Ser 473) (Cell Signaling, 1:1000), mouse anti-phospho CaMKII (Thr 286) (22B1 Santa Cruz Biotechnology, 1:200), rabbit

anti-ATG8a (Creative Diagnostics, 0.2g/ml), and mouse anti-actin (JLA20) (Developmental studies Hybridoma Bank, 1:1000).

BrdU Staining:

3rd instar larval eye-imaginal discs were dissected in Grace's Insect Medium (ThermoFisher) then transferred into Grace's Insect Medium containing 0.25mg/ml BrdU (Invitrogen B23151) and incubated at 25°C for 90 minutes. Discs were then washed in Grace's Insect Medium for five minutes on ice followed by washing two times for five minutes each in 1X PBS on ice. Discs were fixed overnight (wrapped in foil) in 1% paraformaldehyde/0.05% Tween20. The following day discs were washed three times for five minutes each in 1X PBS and permeabilized for 20 minutes at RT in 0.3% PBST. To remove detergent, discs were washed five times for five minutes each in 1X PBS and DNase treated for 30 minutes at 37°C. Discs were then washed three times for 10 minutes each in 0.1% PBST and incubated overnight at 4°C in mouse anti-BrdU primary antibody (B44) (BD, 1:50). The next day, discs were washed 5 times for a total of 30 minutes with 0.1% PBST and incubated overnight in goat anti-mouse F(ab)'₂ AlexaFluor-555 secondary antibody (Cell Signaling, 1:500). Finally, discs were washed three times for 10 minutes each in 0.1% PBST and mounted in VectaShield anti-fade mounting medium.

Immunostaining:

3rd instar larval eye-imaginal discs were dissected in 1X phosphate-buffered saline (PBS) and fixed in 4% paraformaldehyde for 30 minutes on ice. Discs were then washed three times for 10 minutes each in ice cold 1X PBS, permeabilized in 0.3% Triton X100/1X PBS (PBST) for 20 minutes at RT, and washed again three times for 10 minutes each before blocking in 10% normal goat serum

in 0.1% PBST for 30 minutes at RT. Discs were incubated in primary antibodies (4°C overnight) in 10% normal goat serum (NGS)/0.1% PBST. The following day, discs were washed three times for five minutes each in 0.1% PBST before incubating in secondary antibodies (in the dark at RT for one hour) in 10% NGS/0.1% PBST. Finally, discs were washed three times for 10 minutes each in 1X PBS at RT and mounted using VectaShield anti-fade mounting medium. Primary antibodies and dilution: rabbit anti-cleaved *Drosophila* DCP-1 (Asp216) (Cell Signaling, 1:100), mouse anti-MMP1 (3A6B4/5H7B11/3B8D12 antibodies were mixed in equal amounts) (DSHB, 0.2µg/ml), Rabbit anti-pS6K (Cell Signaling 1:100), and Rabbit anti-pAMPK (T172) (Cell Signaling 1:100). Fluorescent secondary antibodies were from Life Technologies. DAPI was used to stain DNA.

Widefield and confocal imaging:

Brightfield adult images were taken using a Leica S6D dissecting microscope. Fluorescent images were taken on a Leica MZ10F ($\times 1$ 0.08899 NA) or Leica TCS SP8 inverted confocal microscope ($\times 10$ air HC PL Fluotar, 0.3 NA, $\times 20$ air HC PL APO, 0.75 NA, or $\times 40$ oil HC PL APO, 1.30 NA) using 0.88 µm z-stack intervals and sequential scanning (405 nm DMOD Flexible, 488 nm argon, 514 nm argon). All images were processed using ImageJ/FIJI and compiled in Adobe Photoshop.

Allografting:

Tissue allografting was performed as described previously (159). 3rd instar larvae were placed in a sterile petri dish containing 1X PBS and washed to remove residual fly food from the larval cuticle. Larval eye-imaginal discs were then dissected in 1X PBS. Sterile forceps were used to

mince tissue into small pieces in preparation for implantation. *W¹¹⁸* virgin female host flies were anesthetized with CO₂ and placed ventral-side up on double-sided sticky tape. Care was used to ensure that flies were well adhered to tape. A 10µl sterile Hamilton Syringe with a 34 gauge 1-inch needle (45° needle angle) was used to aspirate a single piece of eye disc tissue into the needle, loading as little 1X PBS as possible. Forceps were used to hold the host abdomen steady and the syringe needle was used to pierce the abdomen and inject the eye disc tissue. Host flies were then removed from the double-sided tape and moved to a fresh vial of food placed horizontally at all times. Between genotypes the needle was cleaned by pipetting in and out with 1X PBS several times. Flies were monitored daily for survival and GFP-positivity, with transfer to new vials every two days. Death observed during the first 7 days was deemed artefactual, due likely to the injection procedure and not malignant growth. Flies were monitored for a total of 32 days.

Cell-cycle analysis:

Cell-cycle analysis of live GFP-labelled 3rd instar eye-imaginal disc cells was performed as described previously (72). In short, larval eye-imaginal discs were dissected in 1X PBS and simultaneously dissociated with gentle agitation and stained (wrapped in foil) with Hoechst 33342 (Cell Signaling, 500 g/ml) for two hours using a solution of 450µl 10X Trypsin-EDTA (Sigma), 50µl 10X PBS, and 0.5µl Hoechst 33342. Cells were then passed through a 40µm cell strainer prior to FACS analysis. Hoechst 33342 expression was analyzed for a minimum of 10,000 GFP-positive cells by flow cytometry on a Becton Dickinson FACS Canto II cytometer using FACSDiva software. Elimination of dead cells and the distribution of cells within G1, S, and G2/M phases of the cell cycle was determined using FlowJo software.

SiMView Light Sheet Microscopy:

Prior to mounting, live wandering 3rd instar *Drosophila* larvae and giant larvae were selected for stage and proper expression then cooled in a petri dish placed on top of an ice bucket. After sufficiently cooled to minimize movement, the samples were attached posterior side up to a 3mm diameter stainless steel post using gel-control super glue (Ultra Gel Control, Loctite). When mounting, the sample's mouthparts were adhered in an extended state in order to improve image quality (i.e. reduce object depth) of the tumors. After allowing the adhesive to dry, the sample and post was loaded into an adapter that is magnetically attached to a multi-stage stack with degrees of freedom in the X-Y-Z and rotational directions. The sample chamber is sealed using custom-made rubber gaskets and filled with Schneider's Medium. The instrument is constructed as previously published with slight modification (160, 161). All data was collected using a Nikon 16x/0.8 NA LWD Plan Fluorite water-dipping objective and Hamamatsu Orca Flash 4.0 v2 sCMOS cameras. Exposure time for all experiments was 15ms per frame. Data was collected using a single camera view and two illumination arms, exciting with each arm in sequence for each color and timepoint. In our SiMView implementation for one-photon excitation, multiview image stacks are acquired by quickly moving the specimen over the desired z range and alternating light-sheet activation in the two illumination arms for each volume. This bidirectional illumination and detection captures recordings from two complementary views of each z plane in two illumination steps. Notably, no mechanical rotation of the specimen is required. The switching of laser shutters in the two illumination subsystems is performed within a few milliseconds. GFP and RFP fluorophores were excited using 488nm and 561nm Omicron Sole lasers, respectively. For the imaging session from Figure 4 and Supplemental Video 2 stacks were acquired 60s for 4 hours.

For the imaging session in Figure 3 and Supplemental Video 1 stacks were acquired every 60s for 48 hours.

Analysis of SiMView Data:

Following data acquisition, images were processed prior to analysis. All data had 90 counts subtracted to account for dark counts of the sCMOS cameras. Images from each illumination arm corresponding to the same Z slice were merged and corrected for intensity variation. Details on these algorithms are previously published (162). Collagen degradation over time from our tracheal region of interest in Fig. 3a was measured by using maximum intensity projections of 3D volumes from 11 different time points between 0 and 48 hours. The pixel intensity for the tracheal region of interest was measured for each time point using FIJI/Image J and graphed as the fold change compared to an internal control region (wing disc) using GraphPad Prism 8. 3D volumetric timelapse data were visualized using Bitplane IMARIS 9 (Fig. 3 a-d). Subsets of the entire 2000-3000 timepoint series (~3 - 5 TBs in size) were selected for 3D inspection and visualization from maximum intensity projection (MIP) images. 3D regions of interest (3D-ROI) for Fig. 3 b-d were created using IMARIS' intensity-based Surfaces function. For Fig. 4 cells were identified using IMARIS' Spots function and tracked over time. Snapshots and videos were directly exported from the IMARIS interface for chosen viewing angle.

Pharmacology:

Molasses-based food was melted and 10ml of food was aliquoted to vials. While warm, 10 μ l of H₂O or 10 μ l of 5mM KN-93 (Millipore Sigma, 422711) were added to vials, respectively. Food vials were cooled and allowed to solidify before use. Vials not immediately used were placed at

4°C. Adult *y,w, eyFLP1; Act>y+> Gal4, UAS-GFP; FRT82B, Tub-Gal80* virgin female flies were crossed to *FRT82B* or *Ras^{Hi}/Lkb1^{4A4-2}* males, respectively. Flies were moved to embryo “egg-laying cups” and allowed to egg-lay onto grape juice agar plates at 25°C. Flies were moved onto fresh agar plates every 24 hours. After each 24hr period, embryos were collected using forceps and placed onto a fresh vial of food. Embryos were placed at 25°C and allowed to hatch. Once of age, 2nd-instar larvae were collected and placed onto drug containing media at 25°C. Survival was quantified as the percentage of total embryos placed that survived to pupation and adulthood.

Survival analysis of patient data:

CBioPortal was used to obtain survival, copy number, mRNA expression, and RPPA expression data available through the Cancer Genome Atlas (TCGA). For survival analysis, specific studies used included: TCGA Pan-Lung Cancer study (163) and TCGA Lung Adenocarcinoma studies (PanCancer Atlas (164) and Provisional). Out of 1144 total samples, samples with specific KRAS G12C, G12D, or G12V mutations were selected for further analysis (115 samples for mRNA analysis and 76 samples for copy number analysis). Stratification as *RAS^{Lo}* or *RAS^{Hi}* was based on normalized (Log2) mRNA expression or relative copy number. Patients with KRAS normalized mRNA expression value less than 10.825 were designated as *RAS^{Lo}*, while patients with a normalized mRNA expression value greater than 10.825 were designated as *RAS^{Hi}*. For copy number analysis, diploid patients were designated as *RAS^{Diploid}*, while patients with RAS gains and amplifications were designated as *RAS^{Gain/Amp}*. Of these patients, secondary deletions or loss-of-function mutations in P53 or LKB1 were also obtained. For pAMPK correlation analysis, specific studies used included: TCGA Pan-Lung Cancer study (Nat Genet 2016) and TCGA Lung Adenocarcinoma study (PanCancer Atlas). Samples with specific KRAS G12C, G12D, or G12V

mutations as well as RPPA expression data for pAMPK (T172) were selected for further analysis (n = 71).

LysoTracker staining:

3rd instar larval eye-imaginal discs were dissected in Schneider's Insect Medium followed by incubation in 50 μ M LysoTracker Deep Red (1 mM stock, ThermoFisher) in 1X PBS for 10 minutes in the dark at RT. Discs were then washed three times in 1X PBS for 10 minutes each before being fixed in 4% paraformaldehyde for 20 minutes at RT. Samples were again washed three times for 10 minutes each in 1X PBS at RT before being mounted in VectaShield anti-fade mounting medium. Samples were imaged immediately due to photobleaching.

Canonical Circuit Activity Analysis:

The HiPathia method (<http://hipathia.babelomics.org>) was used to identify differentially expressed (activated or inhibited) pathways. The Genomic Data Commons (GDC) data portal (<https://portal.gdc.cancer.gov>) was used to obtain clinical, somatic variant, and KRAS RNA-sequencing expression raw read counts for TCGA lung adenocarcinoma (LUAD) patients. Patients without all data types were excluded. Patients were determined to be KRAS wild-type if concomitant somatic mutations in LKB1 were absent, and as mutant if secondary LKB1 mutations were present. For both wild-type and mutant groups, expression data was searched against all pathways available in the HiPathia database to identify up- or down-regulated pathways between the two groups, and their interactions. Genes with average counts per million (CPM) of greater than 0.1 across all samples were kept. Normalization was done using the median-ratios method in

DESeq2, and by log₂ transformation. Finally, differential gene fold change was estimated using the Limma R package.

Statistical Analysis:

GraphPad Prism 7 and 8 were used to generate *P* values using the two-tailed unpaired Student's *t*-test to analyze statistical significance between two conditions in an experiment, ordinary one-way ANOVA with a Tukey's multiple comparisons test for experiments with three or more comparisons, and Log-rank (Mantel-Cox) test for analysis of survival data. Significance was assigned to *P* values less than 0.05 unless otherwise indicated. For Figure 6e and f, statistical analysis was conducted using RStudio. Data was divided into two groups, LKB1 loss-of-function (*n* = 40) and LKB1 wild type (wt) (*n*= 31). A single outlier sample in the LKB1 mutation category was excluded and calculated z-score for pAMPK and KRAS expression data was used. The correlation between the AMPK and KRAS was conducted and a spearman's correlation test. Due to the relatively small sample size, a p-value of $\leq .1$ or 10% was considered significant. For Figure 6g, significant circuit activity was determined based on p- value (<0.05), false discovery rate (FDR), and differential gene fold change.

3.3 Results

Clonal loss of Lkb1 *in vivo* results in autonomous cell death

Recent work has highlighted effects of the dosage of oncogenic Ras on the progression of Ras-dependent cancers (165, 166). Previous work in *Drosophila* has identified myriad pathways that collaborate with mutant Ras^{V12} to promote tumor progression and metastasis (167). However, how the dosage of Ras^{V12} affects tumor progression in these multiple hit models is unknown. To address this question, oncogenic Ras^{V12} transgenes with differing expression levels were identified. One expresses oncogenic Ras^{V12} at levels similar to endogenous Ras (Ras^{Lo}). The other expresses Ras^{V12} at levels several fold higher (Ras^{Hi}) (Figure 3.1). To mimic the genetic landscape of human KRAS-driven cancers, LKB1 was co-mutated in Ras^{Lo} and Ras^{Hi} tissue. Most tumor specific LKB1 mutations are homozygous deletions or loss-of-heterozygosity with somatic mutation (80, 81, 168). Among the latter, nonsense or frameshift mutations leading to protein truncation are the most common (90). To identify the *Drosophila* Lkb1 loss-of-function allele with the strongest reduction in Lkb1 protein levels, an antibody to *Drosophila* Lkb1 was first generated. Lkb1 protein abundance in transheterozygous larvae was then assayed using three previously published Lkb1 loss-of-function alleles (X5, (169), 4B1-11, and 4A4-2 (170)) over a large deletion that removes the Lkb1 gene. The Lkb1^{X5} and Lkb1^{4B1-11} loss-of-function alleles reduced Lkb1 protein expression by 60% compared to control. However, the Lkb1^{4A4-2} allele reduced protein expression by 80% (Figure 3.1), which agrees with prior published genetic data suggesting Lkb1^{4B1-11} as having residual protein activity (171). The Lkb1^{4A4-2} allele was chosen for further study and will be referred to as Lkb1^{-/-}.

A GFP-labeled eye expression system (135) was used to express Ras^{Lo} in discreet patches or ‘clones’ of developing eye epithelial tissue. Expression of Ras^{Lo} resulted in ablation of eye tissue and benign outgrowths of eye cuticle similar to what has been previously reported using a *UAS-Ras^{V12}* transgene (135, 139) (Figure 3.1). The GFP-labeled eye expression system was then used to inactivate the Lkb1 tumor suppressor (Lkb1^{-/-}) in clones of cells in the developing eye. Inactivation of Lkb1 in clones resulted in adult flies with small, rough eyes (Figure 3.1), suggesting high levels of apoptosis. To test this, death caspase 1 (DCP-1) staining was assayed in mutant clones using immunofluorescence in wandering 3rd instar eye imaginal disc complexes. As expected, loss of Lkb1 (marked by GFP-positive tissue) resulted in a large increase in autonomous DCP-1 expression as compared to discs carrying control (*FRT82B*) clones (Figure 3.1). These data suggest that homozygous loss of Lkb1 within an otherwise wild-type epithelium can result in a high level of apoptosis *in vivo*.

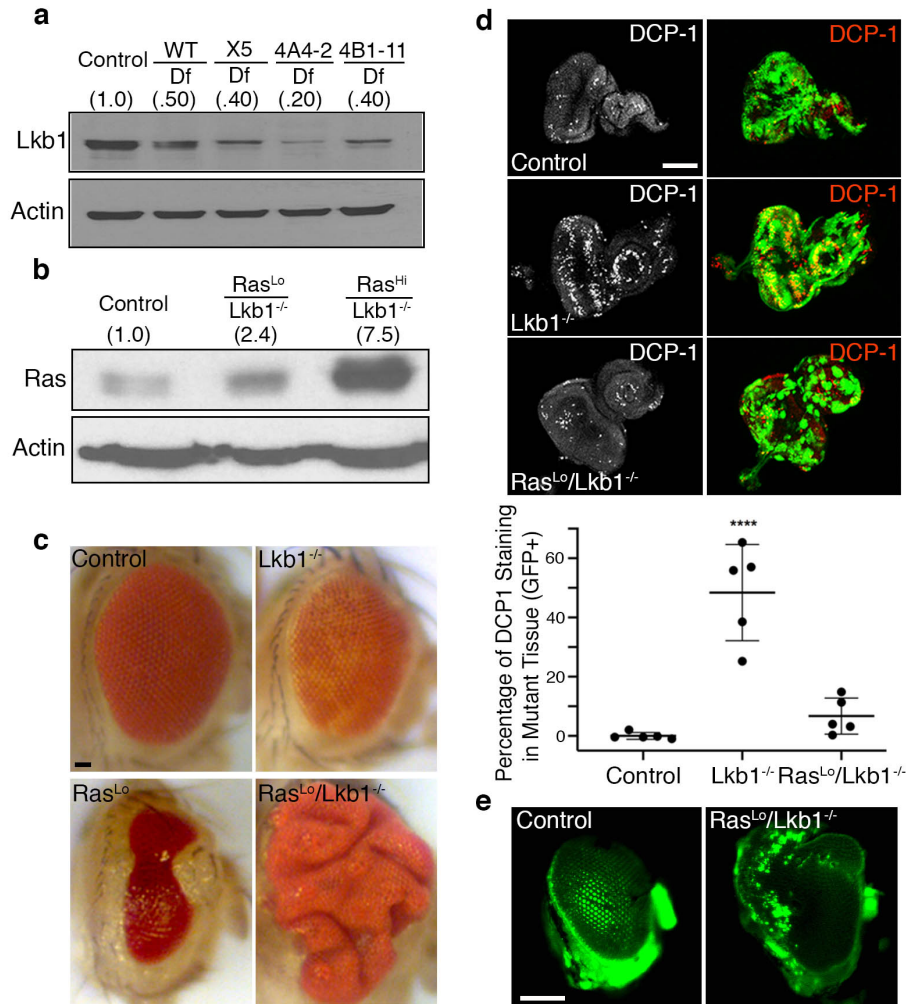


Figure 3.1. Clonal loss of Lkb1 in vivo results in autonomous cell death. (a) Western analysis of Lkb1 protein in transheterozygous larvae for a deletion (Df) that removes the Lkb1 gene, and either a wild-type third chromosome or three loss-of-function alleles of Lkb1 (X5, 4A4-2, 4B1-11). (b) Western analysis of Ras levels in mosaic eye imaginal discs from the indicated genotypes (control = FRT82B). Note the Ras antibody detects both endogenous and oncogenic Ras. (c) Representative brightfield images of mosaic adult eyes with clones of the indicated genotypes. Scale bar, 20 μ m. (d) (top) Confocal maximum intensity projections of third instar mosaic eye discs carrying GFP-tagged clones of the indicated genotypes, and stained for endogenous death caspase 1 (DCP-1). Scale bar, 100 μ m. (bottom) Percentage of DCP1 staining in GFP-positive mutant tissue was quantified from n=5 imaginal discs per condition using thresholding in FIJI (ImageJ). Data were collected as means \pm s.d. and plotted using Prism GraphPad. (****P<0.0001, one-way ANOVA with multiple comparisons). (e) Fluorescent images of adult eyes carrying GFP-labelled clones of the indicated genotypes. Images are representative of n=10 independent flies per genotype. Scale bar, 100 μ m.

Low-level Ras and loss of Lkb1 synergize to promote non-autonomous benign overgrowth

Data from genetically engineered mouse models (GEMMs) suggests loss of Lkb1 is sufficient to promote the progression and metastasis of nascent Kras mutant lung adenocarcinoma (94). Due to the redundancy of the vertebrate genome and paucity of rapid genetic mosaic analyses in GEMMs, the GFP-labeled *Drosophila* eye expression system was used to build a Ras^{V12}/Lkb1^{-/-} model of cooperative tumorigenesis. Ras^{L0} and depleted Lkb1 (Ras^{L0}/Lkb1^{-/-}) were simultaneously expressed in clones of developing eye epithelial tissue, and it was found that autonomous DCP-1 levels returned to those observed in control eye imaginal discs (Figure 3.1). These data suggest that low levels of oncogenic Ras^{V12} promote the survival of Lkb1^{-/-} mutant tissue *in vivo*. In addition, eye imaginal disc complexes carrying Ras^{L0}/Lkb1^{-/-} clones were larger than mosaic control discs but contained only a small amount of mutant GFP-positive tissue compared to the expression of Ras^{L0} alone (Figure 3.2). In agreement with these results, analysis of adult Ras^{L0}/Lkb1^{-/-} mosaic eyes revealed a large, overgrown eye phenotype composed of GFP-negative wild-type cells (Figure 3.1). To confirm the overgrown eye phenotype was due to synergy between Ras^{V12} and Lkb1 loss and not due to simply preventing cell death in Lkb1-mutant cells, the baculovirus caspase inhibitor p35 was expressed in Lkb1-mutant clones. Expressing p35 in Lkb1-mutant clones resulted in most flies having eyes that are phenotypically like expression of p35 alone (normal size eye), with 20% of flies exhibiting a more severe, smaller misformed eye (Supplementary Figure 3.1).

To investigate the mechanism that results in an increase in organ size in Ras^{L0}/Lkb1^{-/-} flies, BrdU incorporation was analyzed in mosaic Ras^{L0}/Lkb1^{-/-} eye imaginal disc tissue. Eye disc tissue carrying Ras^{L0}/Lkb1^{-/-} clones exhibits BrdU incorporation in GFP-negative wild-type cells

surrounding mutant clones (Supplementary Figure 3.2). Accordingly, Altogether, these data suggest that although $Ras^{Lo}/Lkb1^{-/-}$ mutant cells survive, they undergo G1 arrest while promoting the increased hyperplastic proliferation of surrounding wild-type tissue.

High level oncogenic Ras promotes the neoplastic transformation of Lkb1-mutant tissue

Previous studies have implicated the dose of mutant KRAS in tumor progression, cell motility, and metabolic reprogramming (149, 165, 166, 172), therefore the GFP-labeled eye expression system was again used to clonally express Ras^{Hi} and mutant Lkb1 in developing eye epithelia ($Ras^{Hi}/Lkb1^{-/-}$). When combined with Lkb1 loss-of-function, expression of Ras^{Hi} resulted in severely overgrown and disorganized 3rd instar larval eye-imaginal disc tumors composed of mostly GFP-positive mutant tissue (Figure 3.2). Fluorescence-activated cell sorting (FACS) analysis of mutant tissue revealed a shift in cell cycle phasing that favored G2/M, suggesting that mutant cells were precociously completing G1 (Supplementary Figure 3.2). Most larvae carrying $Ras^{Hi}/Lkb1^{-/-}$ mosaic discs did not pupate but continued to grow into ‘giant larvae’ while expression of Ras^{Hi} alone resulted in late pupal lethality (Figure 3.2). The giant larval phenotype is shared by loss-of-function mutations in the *Drosophila* neoplastic tumor suppressor genes (173) and suggests that $Ras^{Hi}/Lkb1^{-/-}$ tumors are malignant. To test this, an allograft assay was performed by implanting tumor tissue in the abdomens of wild-type hosts. Only transplanted $Ras^{Hi}/Lkb1^{-/-}$ tissue survived to grow into secondary tumors that significantly shortened host survival (Figure 3.2) thus confirming the malignancy of $Ras^{Hi}/Lkb1^{-/-}$ tumor tissue.

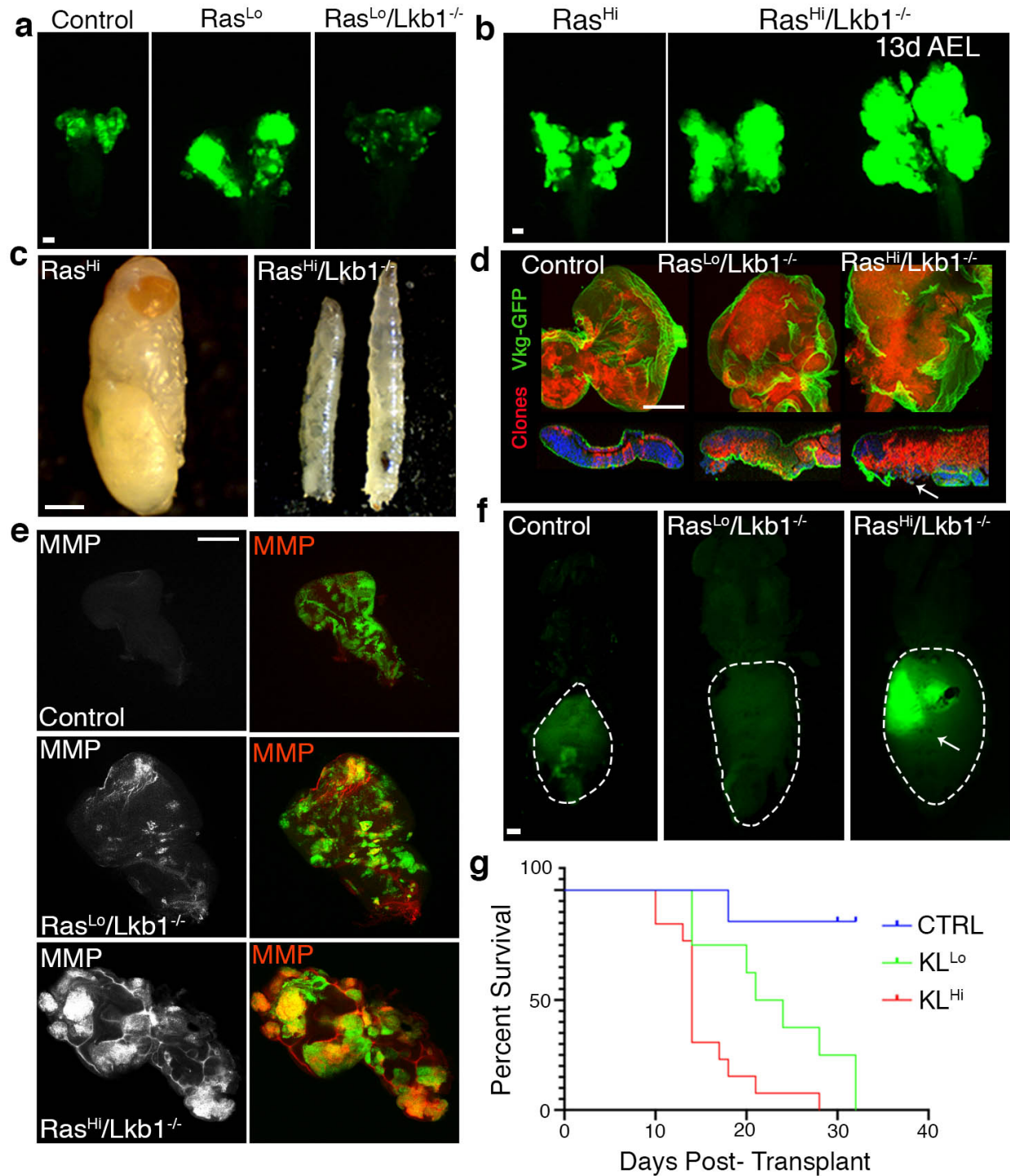


Figure 3.2. Oncogenic Ras^{Hi} promotes the malignant transformation of Lkb1 mutant tissue. (a-b) Fluorescent images of 3rd instar larval eye-imaginal discs carrying GFP-labelled clones of the indicated genotypes (control = FRT82B). Images are representative of n=10 independent eye-imaginal discs per genotype. Scale bar, 20 μ m. (c) Representative brightfield image of the lethal

stage of a fly carrying Ras^{Hi} clones (left) and Ras^{Hi}/Lkb1^{-/-} clones (right). Note that both age-matched third instar and giant larvae are shown. Scale bar, 100µm. (d) Confocal images of eye imaginal discs carrying RFP clones of the indicated genotypes and expressing type IV collagen-GFP (Vkg-GFP). Nuclei are labelled with DAPI (blue). White arrow indicates break in Vkg-GFP expression. Images are representative of n=5 independent eye-imaginal discs per genotype. Scale bar, 100µm. (e) Confocal images of third instar eye discs carrying GFP-tagged clones of the indicated genotypes and stained for matrix metalloproteinase 1 (MMP1). Images are representative of n=10 independent eye-imaginal discs per genotype. Scale bar, 100µm. (f) Fluorescent images of w¹¹¹⁸ adult virgin female hosts carrying transplanted allografts of 3rd instar eye-imaginal discs with GFP-labelled clones of the indicated genotypes. White arrow indicates Ras^{Hi}/Lkb1^{-/-} mutant tissue. Images are representative of n=5-10 independent hosts per genotype. Scale bar, 100µm. (g) Quantification of survival post-transplant in allograft assay. Survival was measured from n >5 independent adult hosts per genotype and graphed using a Kaplan-Meier survival plot. Survival post-transplant was measured from 7 days post-transplant to time of death. CTRL (Control), KL^{Lo} (Ras^{Lo}/Lkb1^{-/-}), and KL^{Hi} (Ras^{Hi}/Lkb1^{-/-}) (CTRL-KL^{Lo}, **P=0.0030, CTRL-KL^{Hi}, ***P=0.0001, KL^{Lo}-KL^{Hi}, *P=0.0129, Log-rank test).

High-level Ras promotes the invasion and metastasis of Lkb1-mutant tissue

Mutations in cell polarity proteins cooperate with oncogenic Kras to drive tumor cell invasion and metastasis (167). Previous studies have shown that Lkb1 regulates cell polarity and epithelial integrity across species (174, 175). Therefore, it was hypothesized that malignant Ras^{Hi}/Lkb1^{-/-} tumors would have invasive properties. To test this, it was first examined whether Ras^{V12}/Lkb1-mutant cells compromised basement membrane structure by examining the expression of GFP-tagged Collagen IV (Viking (Vkg)-GFP) using conventional fixation and confocal microscopy. Compared to control and Ras^{Lo}/Lkb1^{-/-} tissue which shows contiguous Vkg-GFP expression in epithelia, Ras^{Hi}/Lkb1^{-/-} tissue exhibits breaks in Vkg-GFP expression (Figure 3.2). Matrix metalloproteinase (MMP) expression was next assayed, as MMPs degrade basement membrane. Compared to control or Ras^{Lo}/Lkb1^{-/-} mutants, Ras^{Hi}/Lkb1^{-/-} mutant tissues express high-levels of MMPs in mutant clones (Figure 3.2). These data suggest Ras^{Hi}/Lkb1^{-/-} tumor cells invade through the basement membrane using an active proteolytic process.

Invasion and migration are difficult processes to visualize *in vivo*. Thus far, *Drosophila* tumor-bearing larvae have been precluded from fast, high resolution long-term intravital imaging techniques due to their size, degree of movement, and the significant amount of light scattering throughout the body because of the larval cuticle. To address this, a method to mount live tumor-bearing larvae for long-term intravital imaging was developed and simultaneous multiview (SiMView) light-sheet microscopy was used (see Methods and (160)) to visualize tumor cell and collagen IV dynamics for up to 48hrs. SiMView allowed imaging of rapid cellular processes over time with minimal photobleaching on an organismal scale. Over a period of 48hrs image stacks were collected in the *z* range every 60s on ‘giant’ tumor-bearing larvae with RFP-tagged

Ras^{Hi}/Lkb1^{-/-} mutant cells and Vkg-GFP expressed in the basement membrane of all epithelial tissues. Breakdown of Vkg-GFP was visible over time, especially in the overlying tracheal branch dorsal to the tumor surface. A region of interest was defined that encompassed the tracheal branch and collagen IV degradation over the 48hr imaging window was measured. Compared to an internal wing disc used as a control, the collagen IV GFP signal decreased over from 14 to 29hrs post imaging (Figure 3.3). 3D volume rendering and surface reconstruction of the tracheal branch revealed that tumor cells were found to contact trachea several hundred μm away from the primary tumor (Figure 3.3). On rare occasion, tumor cells were even found on the ‘interior’ surface of Vkg-GFP. These data suggest Ras^{Hi}/Lkb1^{-/-} mutant cells actively invade tracheal vascular cells to potentially spread to distant organs.

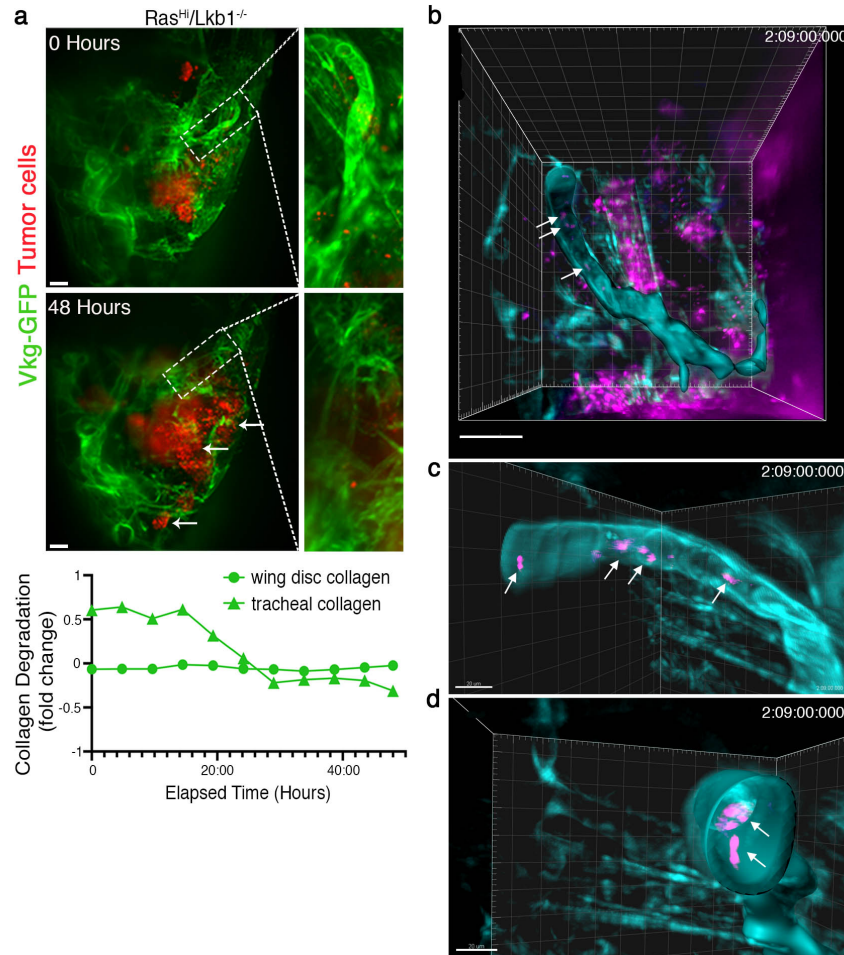


Figure 3.3. SiMView light sheet microscopy allows visualization of local and distant collagen IV degradation by tumor cells over time. (a, top) Maximum intensity projection (MIP) volume renders from a 48hr SiMView imaging session on the anterior end of a $Ras^{Hi}/Lkb1^{-/-}$ tumor bearing ‘giant’ larva. Mutant cells express RFP and Vkg-GFP (collagen IV) is expressed throughout the organism. White dashed box is our region of interest (ROI, tracheal branch) and is magnified in the panels on the right. White arrows indicate RFP-positive $Ras^{Hi}/Lkb1^{-/-}$ cells that have invaded dorsally. Scale bar, 20 μ m. (a, bottom) Fold change of collagen degradation from ROI compared to internal control region (wing disc) over the course of the 48hr SiMView imaging session. FIJI (ImageJ) was used to analyze degradation of fluorescent intensity. (b) An IMARIS Surface object of Vkg-GFP (teal) was generated from the ROI (above) using min and max thresholds of 250 and 385, respectively. White arrows indicate RFP positive tumor cells (magenta) that appear embedded within the tracheal collagen matrix. (c-d) Zoom and rotated data channels were duplicated with voxels outside the IMARIS object set to 0 in order to allow for better visualization with a maximum intensity projection view and clipping plane to show presence of RFP-positive cells within the tracheal matrix. Scale bar, 20 μ m.

Ras^{Hi}/Lkb1-mutant cells exhibit single and multicellular dynamics during cell migration *in vivo*

Traditional confocal microscopy on fixed tissues has revealed that Lkb1-mutant lung tumors exhibit collective migration strategies (93, 176). To visualize intravital cell migration strategies SiMView was used to image RFP-tagged Ras^{Hi}/Lkb1^{-/-} tumors in a live larva that was stage-matched to a control ‘wandering’ third instar larva. 3D volumes were collected every 60s over a period of 4hrs. 3D visualization of mutant cells over time and subsequent tracking analysis revealed two prominent cells that were observed to exit the primary tumor (Figure 3.4). Interestingly, both cells exited the tumor individually, but within 30min could be observed as a dynamic collective of two cells. 90min into the tracking analysis, a cell changing direction to migrate back to the primary tumor was observed. It was then once again observed as a two-cell collective before migrating away from the tumor. These data suggest that Lkb1-mutant cells may use both single and collective migration strategies *in vivo*.

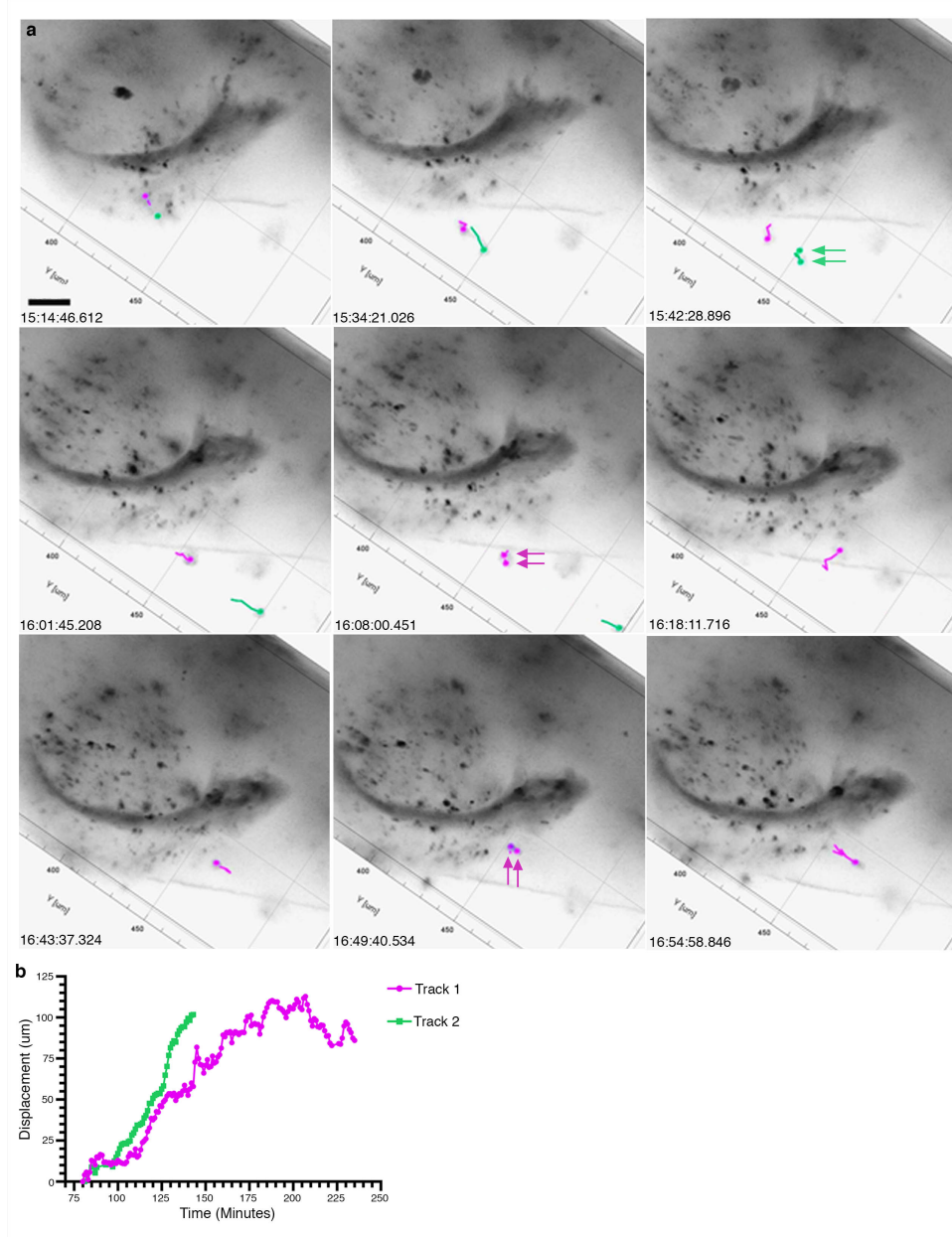


Figure 3.4. $Ras^{Hi}/Lkb1^{-/-}$ mutant cells exhibit single and multi-cell dynamics during cell migration in vivo. (a) MIPs from a 3D reconstructed simultaneous multiview in vivo recording of a third-instar $Ras^{Hi}/Lkb1^{-/-}$ tumor bearing larva. Fluorescence images visualized with an inverted lookup table for clarity; black = RFP tagged $Ras^{Hi}/Lkb1^{-/-}$ mutant cells. Mutant cells were tracked using IMARIS' Spots function, and the two longest contiguous tracks were analyzed (Track 1 = magenta and Track 2 = green). Time-points when dynamic 2-cell clusters are visualized are marked with double arrows. Scale bars, $20\mu m$. (b) Displacement of the two tracked cells over the indicated course of time.

Oncogenic Ras^{Hi} promotes co-activation of Ampk and mTOR in Lkb1-mutant tumors *in vivo*

Targeting effector signaling in KRAS-driven non-small cell lung cancer has resulted in limited efficacy in the clinic. In addition, previous studies have highlighted the complex transcriptional and signaling network changes in KRAS tumors co-mutated with the tumor suppressor LKB1 (96). Therefore, rapid and genetically tractable models of KRAS/LKB1 tumors may shed light on the complex rewiring of signaling pathways and highlight novel targeting approaches. To probe effector pathways in this tumor model, western analysis on a panel of *Drosophila* epithelia harboring mutant clones for Ras^{Lo}, Ras^{Lo}/Lkb1^{-/-}, Ras^{Hi}, and Ras^{Hi}/Lkb1^{-/-} was used. Increases in the activation of the Ras effector circuit Erk/Mek were observed along with S6K and 4EBP1, suggesting increased mTOR pathway activity (Figure 3.5). Compared to all other genotypes, Akt is not active in Ras^{Hi}/Lkb1^{-/-} cells most likely owing to sustained pS6K signaling resulting in a negative feedback loop by ribosomal protein S6. Previous studies have attributed increased TOR pathway activity in LKB1 mutant tissue to loss of mTOR pathway inhibition by AMPK (177). Therefore, loss of Ampk activity in our panel of Lkb1^{-/-} mutant *Drosophila* tissue was tested. Basal activation of Ampk in control tissue was observed, followed by minimal activation in Ras^{Lo}/Lkb1^{-/-} mutants, most likely resulting from the overgrowth of surrounding wild-type epithelial tissue (Figure 3.5). However, in Ras^{Hi}/Lkb1^{-/-} tissue, sustained pAmpk levels were observed. These data suggest that that autochthonous Ras^{Hi}/Lkb1^{-/-} tumors are re-wired to activate Ampk in the absence of Lkb1. To test whether Ras^{Hi}/Lkb1^{-/-} tumors are dependent on Ampk, an RNAi transgene to Ampk was expressed in developing GFP-positive Ras^{Hi}/Lkb1^{-/-} tissue. Inhibition of Ampk via RNAi in Ras^{Hi}/Lkb1^{-/-} mutants resulted in flies surviving into adulthood with small, rounded GFP-positive Ras^{Hi}/Lkb1^{-/-} cells scattered throughout the adult eye (Figure 3.5). These data confirm that Ras^{Hi}/Lkb1^{-/-} tumors are dependent on Ampk for malignant progression.

A recent study from the Guo group found that autophagy may sustain AMPK activity upon LKB1 loss to support tumor growth (178). Increased lipidated ATG8a was found in Ras^{Hi}/Lkb1^{-/-} tumors, even in the presence of active TOR signaling, a known negative regulator of autophagy (179) (Figure 3.5). LysoTracker staining confirmed an increase in cell autonomous acidic vesicle formation in Ras^{Hi}/Lkb1^{-/-} tissues compared to other genotypes (Supplementary Figure 3.3). These data suggest increased autophagic flux in Ras^{Hi}/Lkb1^{-/-} tumors, and indicate that Ras^{Hi}/Lkb1^{-/-} tumors have adapted metabolically to survive energetic stress.

The Ca²⁺/calmodulin-dependent protein kinase kinase (CaMKK2) is a nucleotide-independent activator of AMPK (180). Therefore, activation of the *Drosophila* ortholog CamkIIB (48% identical/63% similar to CaMKK) was assayed in this panel of mutant tissue. Activation of CamkIIB was elevated in Ras^{Hi}/Lkb1^{-/-} tumors (Figure 3.5). To test whether Ras^{Hi}/Lkb1^{-/-} tumors are dependent on CamkIIB activity, pharmacologic inhibition of the CaMKK cascade was used by feeding developing Ras^{Hi}/Lkb1^{-/-} larvae with the inhibitor KN-93 (181). Treatment of Ras^{Hi}/Lkb1^{-/-} larvae resulted in a significant rescue of whole-organism lethality, with an increase in the number of flies surviving to the pupal and adult stage (6.5% adult survival for KN-93 vs. 0% adult survival for vehicle control) (Figure 3.5). Taken together, these data indicate that in the context of loss of Lkb1, high levels of oncogenic Ras^{V12} drive co-activation of both mTOR and the Ampk pathway to promote the growth and survival of malignant tumor tissue. Moreover, targeting the upstream AMPK activator CaMKK may offer therapeutic benefit to KRAS/LKB1-mutant lung adenocarcinoma patients.

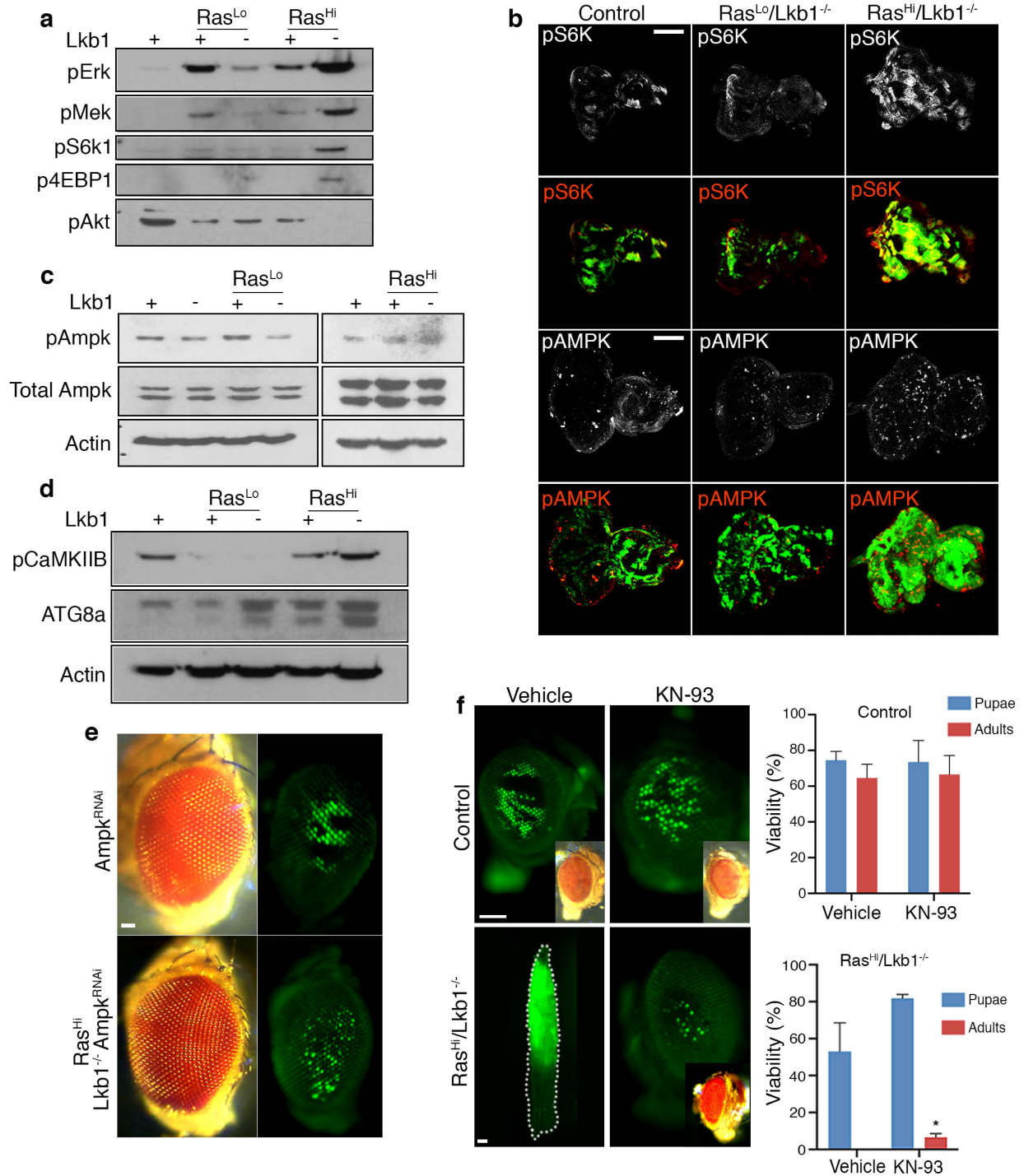


Figure 3.5. Oncogenic Ras^{Hi} promotes co-activation of AMPK and mTOR in Lkb1-mutant malignant tumors in vivo. (a) Western analysis to assay activation of the Mek/Erk, Tor, and PI3K/Akt pathways in mosaic larval eye-imaginal discs of the indicated genotypes. (b) Confocal images of eye imaginal discs carrying GFP⁺ clones of the indicated genotypes (control =

FRT82B), and stained for phosphorylated S6 Kinase (pS6K) (top) or phosphorylated Ampk (bottom). Images are representative of n=10 independent eye-imaginal discs per genotype. Scale bar, 100 μ m. (c) Western analysis of Ampk activation from mosaic larval eye imaginal discs of the indicated genotypes. (d) Western analysis of mosaic eye imaginal discs of the indicated genotypes. Immunoblots show expression of pathway components upstream and downstream of Ampk. (e) Representative brightfield (left) and fluorescent (right) images of adult eyes expressing GFP-labelled clones of the indicated genotypes. Scale bar, 20 μ m. (f) Representative fluorescent and brightfield (inset) images of either control (FRT82B) or GFP-labelled Ras^{Hi}/Lkb1^{-/-} clones that were pharmacologically treated with vehicle or the pan CaMKK inhibitor KN-93 (5 μ M) as 1st instar larvae. The percent survival to pupal and adult stages was quantified (right). Data were plotted as percentages of total, with two separate experiments for a total of n=50 larvae per condition. *p-value = .0493). Scale bars, 100 μ m.

High levels of oncogenic KRAS and loss of LKB1 result in decreased patient survival and AMPK signaling circuit activation in lung adenocarcinoma patients

To test the translational relevance of our findings in *Drosophila*, human lung adenocarcinoma genomic and clinical data was analyzed using cBioPortal (182, 183) to study how differences in levels of oncogenic KRAS affect tumor progression in LKB1 mutant patients. The TCGA Lung Adenocarcinoma PanCancer Atlas and TCGA Provisional Lung Adenocarcinoma datasets were used to select the proportion of patients with KRAS mutations (G12C, G12D, or G12V) for further study. Available RNA sequencing data was then used to stratify patients as either RAS^{Lo} or RAS^{Hi}. Next, overall patient survival was investigated by comparing cohorts of RAS^{Lo} or RAS^{Hi} alone, to those that contained deletions and/or loss-of-function mutations in LKB1. No difference in overall survival in RAS^{Lo} vs. RAS^{Lo}/LKB1^{Mut} patients was observed, but strikingly RAS^{Hi}/LKB1^{Mut} patients exhibited significantly worse overall survival when compared with RAS^{Hi} patients (Figure 3.6). KRAS copy number was next studied to determine whether changes in copy number could account for the changes in overall survival. Similar results were obtained when patients were stratified into either oncogenic RAS^{Diploid} or RAS^{Gain/Amp} (Figure 3.6). Interestingly, the ability of high level vs. low level KRAS to drive survival differences did not extend to patients with TP53 mutations (Supplementary Figure 3.4).

A recent study reported that Ampk has a pro-tumorigenic role in Lkb1 wild-type lung cancer GEMMs (100). Moreover, data from this *Drosophila* Lkb1-mutant tumor model indicate that genetic ablation of Ampk is sufficient to shrink tumors and reverse whole-organism lethality. To test whether AMPK signaling may be involved in human KRAS/LKB1-mutant lung adenocarcinoma, a correlation analysis between pAMPK and oncogenic KRAS mRNA for LKB1

loss-of-function and LKB1 wild-type patients was conducted. A positive correlation trend between pAMPK and oncogenic KRAS levels was detected, but only in LKB1-mutant patients (spearman's correlation coefficient = 0.3, $p = 0.068$ for loss-of-function vs coefficient = -0.076, $p = 0.683$ for wild-type) (Figure 3.6). To further test this hypothesis, bioinformatic canonical circuit activity analysis (CCAA) (184) which recodes gene expression data into measurements of changes in the activity of signaling circuits was used, ultimately providing high-throughput estimations of cell function. CCAA was performed to estimate activity of the AMPK pathway in $KRAS^{Hi}/LKB1^{Mut}$ lung adenocarcinoma patients compared to $KRAS^{Hi}$ patients. Three sub-circuits of the AMPK pathway that are significantly upregulated in $KRAS^{Hi}/LKB1^{Mut}$ patients were found. The three upregulated circuits are predicted to result in functional changes in the UniProt functions fatty acid metabolism, translational regulation, and the circadian control of gluconeogenesis (biological rhythms) (Figure 3.6). These data confirm the translational relevance of this *Drosophila* model for the identification of targetable pathway vulnerabilities in human lung cancer, and suggest that high oncogenic KRAS levels, perhaps through copy number gains, determine an aggressive subset of LKB1-mutant lung adenocarcinomas that require rewiring of specific sub-circuits of the AMPK signaling pathway to promote malignant progression.

Figure 3.6. High level oncogenic KRAS drives decreased patient survival and is associated with AMPK activation in LKB1 mutant patients. (a-b) Analysis of patient survival using the TCGA Pan Lung Cancer study. Kaplan Meier plots stratified by RAS^{Lo} or RAS^{Hi} using KRAS mRNA expression and further stratified based on LKB1 deletion and loss-of-function mutation status. LKB1 deletion with loss-of-function is associated with poor survival (log rank p=0.0426). (c-d) Analysis of patient survival using the TCGA Pan Lung Cancer study. Kaplan Meier plots stratified by RAS^{Lo} or RAS^{Hi} using KRAS copy number data and further stratified based on LKB1 deletion and loss-of-function mutation status. LKB1 deletion and loss-of-function mutation status is associated with significantly poor survival (log rank p = 0.0137). (e-f) Analysis of phosphorylated AMPK (T172) expression as it correlates with KRAS mRNA expression and LKB1 mutation status. KRAS appears to be weakly positively correlated with AMPK expression (spearman correlation coefficient = 0.296, p = 0.068) in those with loss-of-function but not in wild type (p = 0.683). (g) Canonical circuit activity analysis (CCAA) (<http://hipathia.babelomics.org>) was used to estimate the activity of AMPK effector circuits that result in functional cell activities. Genes in red represent genes upregulated in RAS^{Hi}/LKB1^{Mut} lung adenocarcinoma tumors with respect to RAS^{Hi} tumors; genes in blue represent downregulated genes and genes with no color were not differentially expressed. The activity of three effector circuits are upregulated, one ending in the node that contains the protein PPARGC1A (p = 0.0049; FDR = 0.0377 Uniprot function Biological rhythms), the second one ending in the node with the MYLCD protein (p = 0.0064; FDR = 0.0450 Uniprot function Fatty acid metabolism), and the third ending in the node containing EIF4EBP1 (p = 0.0010; FDR = 0.0138 Uniprot function Translation regulation).

3.4 Discussion

Co-occurring genomic alterations in oncogene-driven lung adenocarcinoma are emerging as critical determinants of tumor-autonomous and non-autonomous phenotypes (14). Here, we have generated the first *Drosophila* model of Ras^{V12}/Lkb1 co-mutation, a major subgroup of KRAS-driven lung adenocarcinomas. These results indicate that the levels of oncogenic Ras^{V12} determine key autonomous vs. non-autonomous phenotypes in Lkb1-mutant tissue. Low-level oncogenic Ras^{V12} expression (Ras^{L0}) combined with Lkb1 co-mutation results in autonomous G1 arrest and overgrowth of the surrounding wild-type epithelium. Conversely, high-level oncogenic Ras^{V12} (Ras^{Hi}) combined with Lkb1 co-mutation leads to autonomous transformation, invasion, and metastasis.

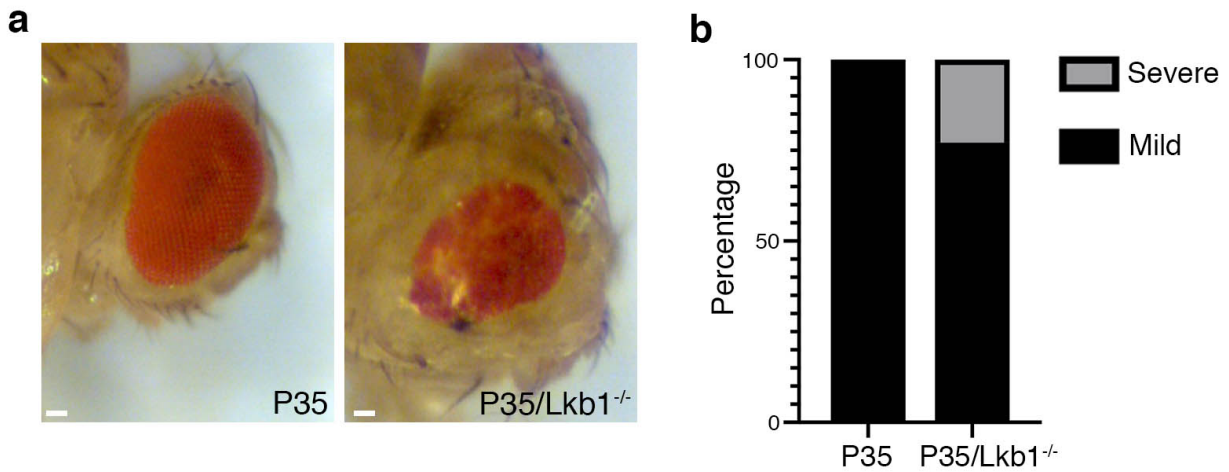
It has been proposed that RAS-induced senescence functions as a tumor suppressive mechanism (185). More recent data have built upon these studies to show that high levels of Hras are required to activate tumor suppressor pathways *in vivo* (165), and that doubling the levels of oncogenic Kras is sufficient to cause metabolic rewiring leading to differences in therapeutic susceptibilities (166). Mutant Kras copy gains are positively selected for during tumor progression in a p53-mutant background (186). However, results analyzing survival in patients indicate that unlike KRAS/LKB1, high levels of KRAS in TP53-mutant lung adenocarcinoma patients may not be a key factor in determining overall survival. In contrast, high-level KRAS and loss of LKB1 leads to significantly decreased overall survival in lung cancer. Interestingly, LKB1 has been shown to control genome integrity downstream of DNA damaging agents and cellular accumulation of ROS. Moreover, alterations in the gene that encodes LKB1 (*STK11*) occur more frequently in patients

with no known mitogenic driver (187). Future work should uncover whether KRAS copy number gains and amplifications are positively selected for due to the role of LKB1 as a gatekeeper of genome integrity.

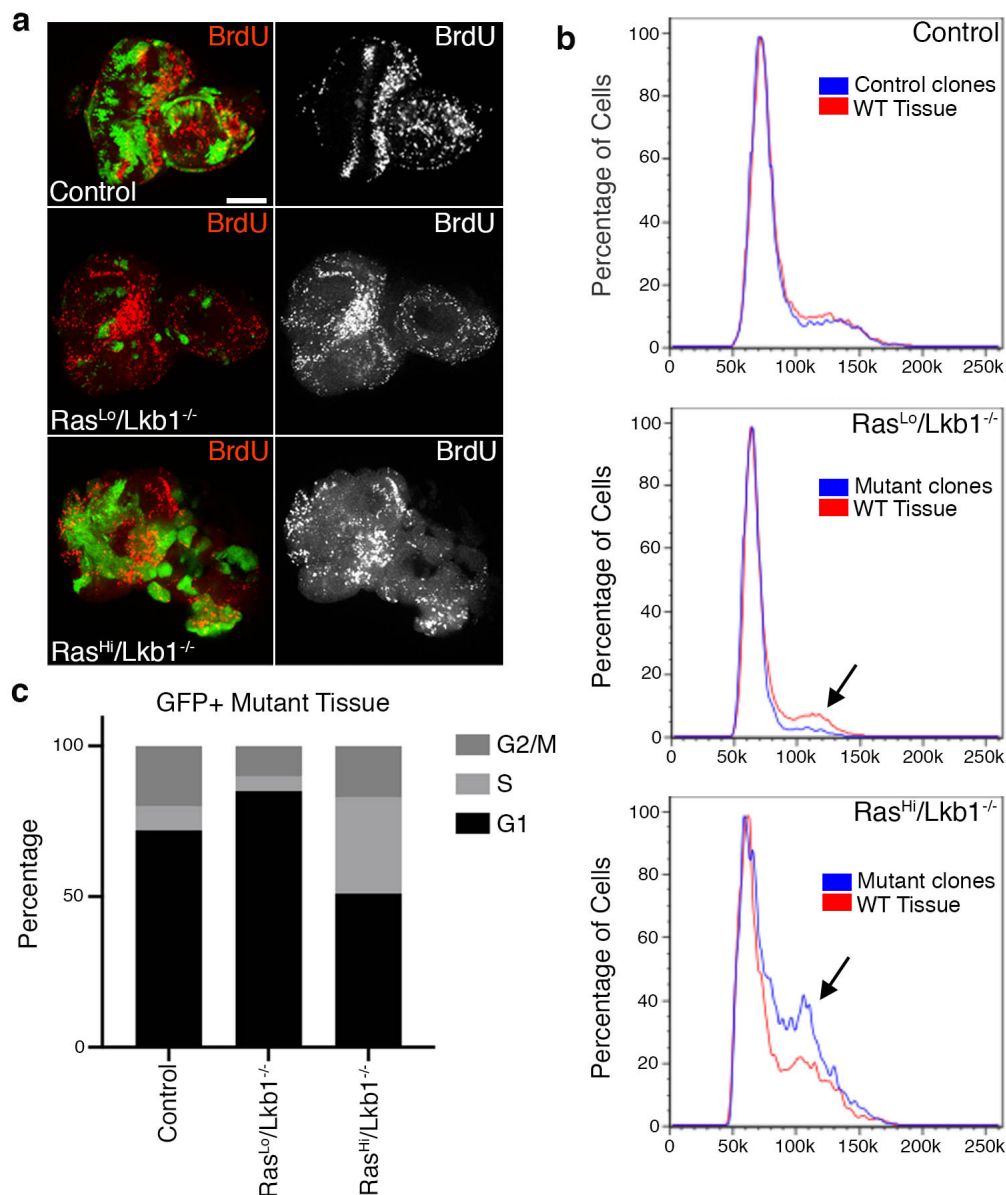
Seminal work in *Drosophila* identified the loss of epithelial polarity genes as key cooperating events in Kras-driven tumors *in vivo* (134, 135). In addition to its role in regulating cell growth, the Lkb1 protein is required to establish and maintain cell polarity across eukaryotes. However, alleles of Lkb1 were not reported to synergize with oncogenic Kras in these previous studies. These results suggest this may have been the result of insufficient oncogenic Kras levels. The fact that loss of Lkb1 behaves differently than other known polarity mutants suggests that an alternate function underlies the aggressive nature of Lkb1-mutant cancer. This work shows that functional Ampk activity is required for the progression of Ras^{Hi}/Lkb1-mutant tumors. These findings are also supported by patient data, as expression of phosphorylated AMPK correlates with increased oncogenic KRAS expression in patients with loss of LKB1. Data suggest that the CamkIIB signaling pathway activates Ampk in the absence of Lkb1 to induce autophagy, which allows tumor progression to proceed. In support of this, autophagy has been recently reported to confer metabolic flexibility upon KRAS/LKB1 tumor cells (178). Pharmacologic inhibition of CaMKK using the compound KN-93 resulted in partial suppression of larval/pupal lethality to adulthood, supporting the proposed hypothesis and opening avenues for further studies investigating the use of CaMKK/AMPK targeting agents as a treatment for the LKB1 genetic subset of RAS-driven cancers.

Lastly, we have discovered concurrent activation of both mTOR and Ampk in Ras^{Hi}/Lkb1^{-/-} tumor tissue, results that are supported by our bioinformatics approach using publically available lung adenocarcinoma patient data. The mTOR and AMPK pathways have previously been shown to be antagonistic in times of energy stress (177), but a recent study using a systems-level approach identified concurrent activation of mTOR and AMPK by amino acids, the latter in a CaMKK-dependent manner, during times of nutrient sufficiency (179). Recent studies have postulated amino acid deprivation as a potential therapeutic strategy for cancer therapy (188). Future studies should focus on the precise amino acids required to inhibit both mTOR and AMPK as a combination therapeutic strategy for KRAS/LKB1-mutant cancers.

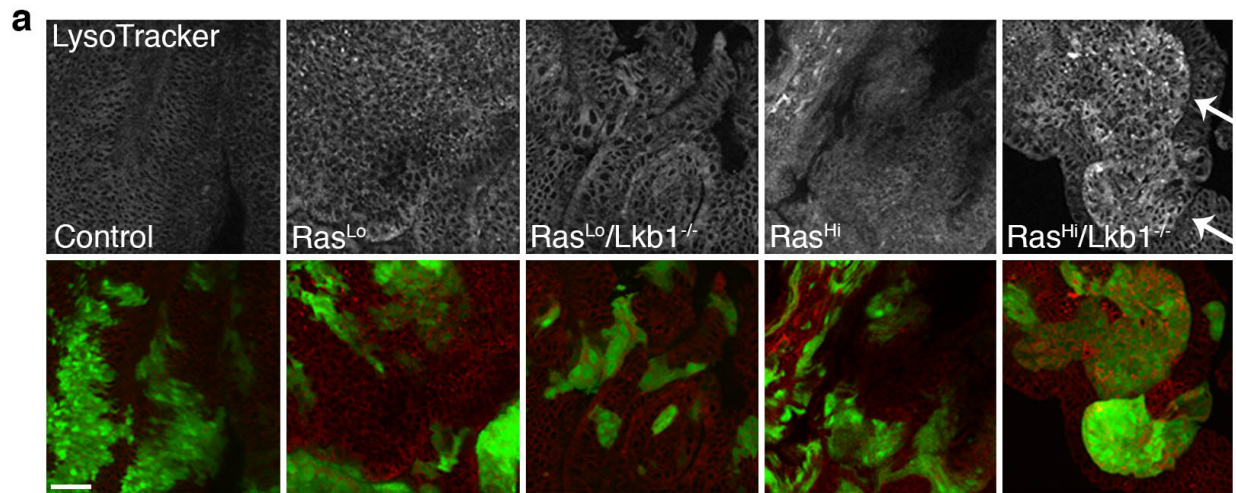
Supplemental Information



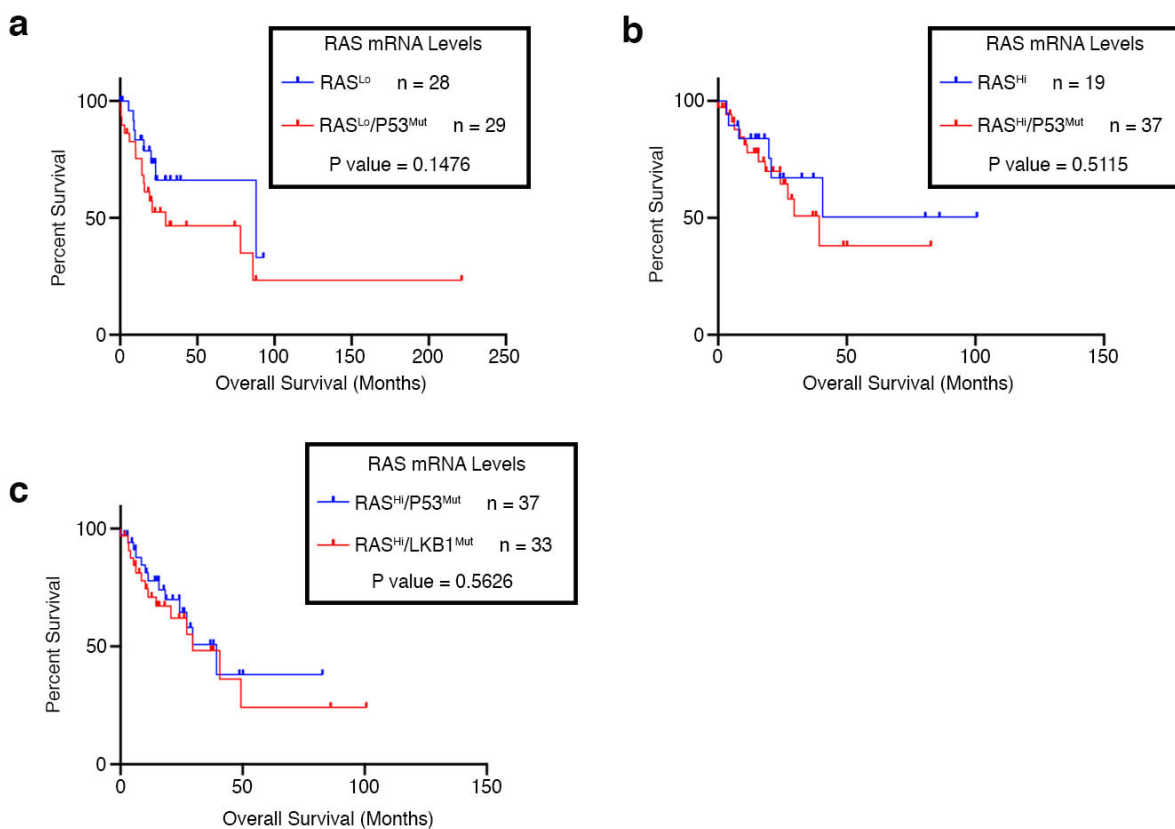
Supplementary Figure 3.1. Blocking cell death with P35 in Lkb1 mutant clones does not phenocopy Ras^{L0}/Lkb1^{-/-}. (a) Brightfield images of mosaic adult eyes expressing P35 (left) or P35/Lkb1^{-/-} (right). Scale bar, 20 μ m. (b) Percentage of P35 or P35/Lkb1^{-/-} mosaic eyes with either a mild or severe phenotype (severe phenotype is pictured in (a) for P35/Lkb1^{-/-}).



Supplementary Figure 3.2. High level oncogenic Ras promotes proliferation and S-phase progression of Lkb1-mutant tissue. (a) Confocal images of mosaic eye imaginal discs carrying GFP⁺ clones of the indicated genotypes (control = FRT82B), and stained for BrdU incorporation. Images are representative of n=10 independent eye-imaginal discs per genotype. Scale bar, 100 μ m. (b) Fluorescence-activated cell sorting (FACS) analysis of mosaic eye imaginal discs with GFP-labelled clones of the indicated genotypes. Black arrows point to shifts in relative cell cycle phasing. Analysis is representative of n=3 independent experiments of 20-40 imaginal discs/genotype. (c) Histogram showing percentage of GFP-labelled control or mutant cells in each phase of the cell cycle.



Supplementary Figure 3.3. Acidic vesicle accumulation in $Ras^{Hi}/Lkb1^{-/-}$ tissue. (a) Confocal images of mosaic eye imaginal discs of the indicated genotypes (control = FRT82B) stained with LysoTracker (red). Mutant tissue expresses GFP. Images are representative of n=3 independent eye-imaginal discs per genotype. Scale bars, 20 μ m.



Supplementary Figure 3.4. High level KRAS does not result in survival differences in TP53 mutant lung cancer patients. (a-b) Survival analysis using the TCGA Pan Lung Cancer study. Patients were stratified as RAS^{Lo} or RAS^{Hi} using KRAS mRNA expression and further stratified based on P53 deletion and loss-of-function mutation status. Data were graphed using a Kaplan-Meier survival plot. (c) Survival analysis comparing KRAS^{Hi}/P53^{Mut} and KRAS^{Hi}/LKB1^{Mut} patients.

Chapter 4: Summary and Future Directions

4.1 Discussion of Dissertation

Efforts to understand LKB1 and the role it plays in progression of disease has been extensive over the past several decades. After being identified as the major cause of the autosomal dominant disorder PJS, LKB1 was determined to also be a frequently mutated tumor suppressor with lost function in sporadic lung adenocarcinomas. From there, focus has shifted to learning about the role this serine/threonine kinase plays in tumor development and progression. For example, a prominent study using a clinically relevant mouse model of lung cancer determined that Lkb1 loss-of-function in combination with expression of oncogenic Kras significantly increased tumor progression and metastasis in comparison to inactivation of other tumor suppressors, such as p53 (94). In addition to mouse work, genomic analysis using lung adenocarcinoma patients has uncovered that activating mutations in KRAS frequently co-occur with inactivating mutations in LKB1 (9). The data presented in this dissertation aim to further explore the role of the prevalent oncogene KRAS, in LKB1-mutant tumor progression. While research has shown that KRAS and LKB1 loss-of-function cooperate to drive tumor progression and metastasis in patients and mouse models, a gap remains in understanding HOW these mutations drive tumor progression. Thus, further studies on co-mutant KRAS/LKB1 tumor tissues is warranted to understand the mechanisms by which these two mutations work together to drive tumor development, progression, and metastasis. Initial findings, presented in chapter 2, develop a *Drosophila* Ras^{V12}/Lkb1-mutant tumor model and use this model to propose that Ras^{V12}/Lkb1-mutant tumor progression is driven via autonomous cell proliferation with attempted, but ineffective, compensatory cell death. Determining differences in mechanisms driving tumor progression in Ras^{V12}/Lkb1-mutant tissues was the catalyst for investigating whether levels of oncogenic Ras^{V12} play a role in driving neoplastic transformation *in vivo*. These results, presented in chapter 3,

identified that high levels of oncogenic Ras^{V12} are necessary for neoplastic transformation and tumor cell invasion of *Lkb1*-null tissues. Additionally, this chapter uncovered mechanisms by which high levels of Ras^{V12} act to drive this transformation. Taken together, these data demonstrate that not only does Ras^{V12} act synergistically to drive *Lkb1*-mutant tumor progression, but more specifically, high levels of oncogenic Ras^{V12} are required for neoplastic transformation and progression of the metastatic cascade.

4.2 Oncogenic Ras^{V12} drives *Lkb1*-mutant tissue overgrowth

4.2.1 Summary of findings

Mutations in KRAS have been repeatedly shown to drive tumor formation and metastatic progression, especially when combined with inactivating mutations in the tumor suppressor LKB1 (94, 105). The work presented in this dissertation builds upon several seminal papers in the RAS field that demonstrate LKB1 is necessary to promote more severe disease progression in addition to decreased treatment responses (59, 64, 65, 104). Our work uses *Drosophila* as a model organism and identifies that knockdown of *Lkb1* drives tissue overgrowth in developing Ras^{V12}-mutant tissues. Additionally, we determined that this tissue overgrowth extends beyond developing larval tissues and drives phenotypic abnormalities in both adult eye and wing structures, suggesting that this combination of mutations is not just relevant in the developing larvae, but persists through adulthood. Using IMARIS 3D rendering software, it was found that co-mutant Ras^{V12}/*Lkb1* knockdown tissue overgrowth is driven by autonomous cell proliferation combined with attempted compensatory autonomous cell death. Additionally, cell size was found to play no role in overgrowth phenotypes observed, as loss of *Lkb1* rescued increased cell size seen with expression

of oncogenic Ras^{V12} alone. Taken together, this work provided insight into how Ras^{V12} and Lkb1 loss work together to drive tumor development and progression, and suggests that knockdown of Lkb1 function works together with expression of oncogenic Ras^{V12} to drive tissue overgrowth in *Drosophila* imaginal discs and adult structures by means of autonomous cell proliferation and death. Further, this work led to the development of subsequent *in vivo* and translational projects to advance understanding of the mechanisms and pathways required for Ras^{V12} and *Lkb1*-null synergistic cooperation.

In addition to the effects of LKB1 mutations and oncogenic RAS on tumor development and progression, research has shown that LKB1 plays a key role in polarity regulation via *cdc42*, cell motility, and cell adhesion via inhibition of focal adhesion kinase (FAK) (91-93). Other studies have shown that oncogenic Ras^{V12} and Lkb1 loss-of-function promote tumor cell metastasis, especially in the context of murine models and lung adenocarcinoma patient tissue samples (94, 189). However, given some ambiguity in molecular details, central questions remain as to how these mutations work together (190). Given these roles, it was assumed that loss of Lkb1 function would promote Ras^{V12}-mutant tumor invasion and metastasis. To explore this in the context of a *Drosophila in vivo* model, we began exploring how Lkb1 knockdown via RNAi work with activating mutations in Ras^{V12} to drive this metastatic cascade. As hypothesized, combined mutations in Ras^{V12} with knockdown of Lkb1 drove autonomous MMP expression indicative of basement membrane degradation. Furthermore, notable F-actin filament disorganization was observed with co-expression of Ras^{V12} with knockdown of Lkb1. These data suggest that loss of Lkb1 is important for early invasive steps of the metastatic cascade in Ras^{V12}-mutant tumor tissues.

4.2.2 Future directions

Overall, our developed *Drosophila* model is consistent with KRAS/LKB1 data observed in both patients and mice. In lung adenocarcinoma, LKB1 is inactivated or deleted in up to 30% of KRAS-mutant non-small cell lung cancers, potentially identifying a source contributing to KRAS-mutant tumors' poor response to therapy. In mice, loss of *Lkb1* was shown to promote tumors resistant to chemotherapeutics and combination therapies with co-mutation of *Kras*. Additionally, *Lkb1* inactivation in mouse models demonstrate shorter latency to tumor formation, and promote more frequent, aggressive, metastatic spread. While work presented in this chapter only begins to demonstrate processes necessary for tumor formation, progression, and dissemination to secondary sites, they represent a strong foundation for which to continue further investigation into the mechanisms by which these mutations work together to drive cancer progression and invasion. Additionally, this model offers opportunities from which to begin these investigations with the goal of better targeted therapeutics for better treatment of patients with these subsets of mutations.

On the molecular level, there are several areas of LKB1 biology that have yet to be fully studied, but that may play a role in phenotypes observed, especially with co-mutation of KRAS. It has been established that loss of LKB1 does not appear to correlate with a specific KRAS mutation, but how different LKB1 mutations may impact KRAS-mutant tumor progression remains an area for study. Patients harboring LKB1 mutations do not show a clear mutational pattern, especially in the context of lung adenocarcinoma. Mutations occur across the whole gene body and are most frequently nonsense, truncating, mutations. Research into how C-terminal domain (CTD) truncations affect LKB1 function has shown that the CTD, specifically farnesylation of this domain, is required for aspects of LKB1 function such as cellular polarity and directional

persistence (191). Patients also present with missense mutations that most likely have differing repercussions on the cell biology of the tumor. Therefore, continuing to study the impact of clinically relevant mutations and whether they confer differing sensitivities to tumor formation, progression, and metastasis, with respect to oncogenic KRAS, would be invaluable for understanding these subsets of mutations. Additionally, understanding more about these differing mutations may offer insight into downstream pathways that are differentially active in each of these cases. Ultimately, delving into this area of study could positively impact treatment strategies utilized for patients with different LKB1 mutations in combination with activating oncogenic mutations in KRAS. In pursuit of answering this question, CRISPR-Cas9 genome editing has been used to introduce a commonly observed LKB1 truncating mutation (Y183*) into our model organism *Drosophila*. Future studies will aim to combine this mutation, and eventually others, with activating mutations in Ras^{V12} to begin determining what effects, if any, they have on Ras^{V12}-mutant tumor progression, metastasis, and treatment efficacy.

4.3 High levels of oncogenic Ras^{V12} are required for neoplastic transformation and metastatic spread

4.3.1 Summary of findings

It has been proposed that RAS-induced senescence functions as a tumor suppressive mechanism (185). More recent data have built upon these studies to show that high levels of Hras are required to activate tumor suppressor pathways *in vivo* (165), and that doubling the levels of oncogenic Kras is sufficient to cause metabolic rewiring leading to differences in therapeutic susceptibilities (166). Furthermore, mutant Kras copy gains are positively selected for during tumor progression

in a p53 mutant background (186). Work in this chapter uses *Drosophila* as a model organism to expound upon data showing differing levels of Ras^{V12} have different effects on tumor transformation. Using tissue allografting techniques, we uncover that high levels of oncogenic Ras^{V12} are required in combination with Lkb1 loss-of-function for neoplastic transformation. As established in chapter 2, oncogenic Ras^{V12} drives tumor cell proliferation. This chapter extends that knowledge and shows that cell proliferation is significantly higher in high level Ras^{V12} tissues. Interestingly, it was determined that clonal expression of high level Ras^{V12} with loss-of-function alleles drives progression into S-phase of the cell cycle, while expression of low level Ras^{V12} drives G1 arrest. Together, this work provided insight into how levels of oncogenic Ras^{V12} combine with loss of Lkb1 to promote neoplasia, and suggest that high levels of Ras^{V12} are in fact required for tumor progression.

Influential work in *Drosophila* identified the loss of epithelial polarity genes as key cooperating events in Kras-driven tumors *in vivo* (134, 135). In addition to its role in regulating cell growth, Lkb1 protein is required to establish and maintain cell polarity across eukaryotes. Furthermore, data obtained from chapter 2 show that Ras^{V12} and knockdown of Lkb1 work together to promote metastatic progression via F-actin disorganization and basement membrane degradation. Therefore, we naturally postulated that high levels of oncogenic Ras^{V12} would further exacerbate invasive phenotypes observed with knockdown of Lkb1. We not only confirmed that expression of high level Ras^{V12} drove autonomous MMP1 expression in Lkb1-null tissues, but we also used SIMView light sheet microscopy to study tumor cell invasion in real time in living *Drosophila* 3rd instar larvae. Fascinatingly, we show tumor cells breaking down, and apparently invading into collagen-rich tracheal structures in the developing fly. Beyond this, we also show cells utilizing

cell-to-cell communication to migrate in a single cell capacity, as well as collectively in a possible leader/follower-like fashion. To our knowledge, this is the first time such cooperativity has been observed in real time and *in vivo*. In sum, we show that high level Ras^{V12} drives both single, and cooperative tumor cell invasion strategies *in vivo*, ultimately promoting tumor cell invasion and metastasis.

To test the translational relevance of findings in *Drosophila*, human lung adenocarcinoma genomic and clinical data was analyzed using cBioPortal (182, 183). As TCGA data previously showed, KRAS and LKB1 are frequently co-mutated in patients, but how differences in levels of oncogenic KRAS affect tumor progression in LKB1 mutant patients had yet to be investigated. (9). We determined that high-level KRAS and loss of LKB1 leads to significantly decreased overall survival in lung cancer. Conversely however, high levels of KRAS in TP53-mutant lung adenocarcinoma patients may not be a key factor in determining the overall survival. Therefore, we determined that phenotypes observed in *Drosophila* are also supported by findings in patient data.

Finally, work presented in this dissertation sought to begin parsing apart mechanisms by which co-mutations in Ras^{V12} and Lkb1 work together to drive tumor progression. Again, our findings are supported by patient data, as expression of phosphorylated AMPK correlates with increased oncogenic KRAS expression in patients with loss of LKB1 as well as in our *Drosophila* model system. Our data suggest that the CamKIIB signaling pathway activates Ampk in the absence of Lkb1 to induce autophagy, which allows tumor progression to proceed. In support of this, autophagy has been recently reported to confer metabolic flexibility upon KRAS/LKB1 tumor

cells (178). We found that pharmacologic inhibition of CaMKK using the compound KN-93 resulted in partial suppression of larval/pupal lethality to adulthood, supporting our proposed hypothesis and opening avenues for further studies. Finally, our findings also show concurrent activation of both mTOR and Ampk in Ras^{V12} and Lkb1-null tumor tissue, results that are supported by bioinformatics approaches using publically available lung adenocarcinoma patient data.

4.3.2 Future directions

Data presented in this chapter expand KRAS/LKB1 data observed in patients and mice and not only suggests mechanisms by which levels of Ras^{V12} may contribute to poor treatment responses, but also identifies downstream pathway components that could be contributing to ineffective therapies. While this chapter begins to suggest mechanisms that may be involved in Ras^{V12}/Lkb1 tumor progression and represents a strong foundation for which to continue investigating implications of these findings, it also presents numerous questions that remain to be explored, as well as many new directions in which this research can be taken. These questions scope from understanding whether RAS expression levels behave to drive LKB1-null tumorigenesis in human cancer cell lines and murine models in the same manner as the fly, to the translational implications of pathway components identified as relevant to these mutations, to understanding how levels of oncogenic RAS drive metabolic differences that can be potentially exploited therapeutically.

As our model predicts, high levels of oncogenic Ras^{V12} are required for neoplastic transformation of LKB1-null tissues. This conclusion is supported by patient data suggesting that high levels of RAS drive decreased overall survival in patients with loss-of-function mutations in LKB1.

However, whether RAS expression levels are driving forces of LKB1-null tumorigenesis in human cell lines and murine models remains to be explored further. One possible method to take these studies a step further would involve identifying and isolating differential KRAS expression patterns in LKB1-null cell lines and labeling them as high or low regarding KRAS expression level. CDK4/hTERT-immortalized normal human bronchial epithelial cells (HBECs), when virally transformed with KRAS, have already demonstrated how high levels of KRAS are important for tumorigenesis (192). Therefore, HBECs with secondary loss-of-function mutations in LKB1 can be isolated based on KRAS expression level (high vs. low), and phenotypic changes observed. Additionally, secondary studies could include studying tumor formation and metastasis of these HBEC-mutants *in vivo*. These studies may help further confirm phenotypes observed in *Drosophila*, and present a second model for further study of novel sensitivities that may make these mutations more susceptible to treatment.

The mTOR and AMPK pathways have previously been shown to be antagonistic in times of energy stress (177), but a recent study using a systems-level approach identified concurrent activation of mTOR and AMPK by amino acids, the latter in a CaMKK-dependent manner, during times of nutrient sufficiency (179). Recent studies have postulated amino acid deprivation as a potential therapeutic strategy for cancer therapy (188). Future studies should focus on the precise amino acids required to inhibit both mTOR and AMPK as a combination therapeutic strategy for KRAS/LKB1-mutant cancers. Investigation into this area of study can begin with use of our *Drosophila* model and can be combined with single and combinatorial amino acid deprivation in fly food to determine which amino acids are necessary for driving Ras^{V12}/Lkb1-mutant phenotypes observed (193).

Lastly, the main goal in attempting to better understand Ras^{V12} biology and how expression levels drive tumor progression, is to extend these findings to better treatment of patients. One question that was basally addressed in this chapter involves downstream pathway components that can be targeted for better treatment of high level Ras^{V12}/Lkb1-null patients. An obvious progression to this data involves investigating the use of CaMKK/AMPK targeting agents as a treatment for the LKB1 genetic subset of RAS-driven cancers. As shown in this chapter, treatment with the CaMKK inhibitor KN-93, helps to rescue tumor severity. Further studies should aim to study the effects of KN-93 treatment on KRAS/LKB1 mutant murine tumors, using either xenograft models with injection of previously described KRAS/LKB1-mutant HBECs, or possibly even using KRAS/LKB1 GEMMs. One additional positive to extending these studies into mouse models, is the ability to further study tumor formation and metastasis and what effects drug treatments have on preventing disease progression. Furthermore, additional opportunities for investigating downstream pathway components are limited in *Drosophila* due to availability of resources, and these barriers to investigation can be overcome using mouse models. Overall, these data could help precision medicine efforts to learn more about the subsets of mutations that exist within tumors, and assist with improving treatment options for patients that need it most.

References

1. Siegel RL, Miller KD, Jemal A. Cancer statistics. *CA Cancer J. Clin* **70**, 7-30 (2020).
2. Chaffer CL, Weinberg RA. A Perspective on Cancer Cell Metastasis. *Science* **331**, 1559-1564 (2011).
3. Popper HH. Progression and metastasis of lung cancer. *Cancer Metastasis Rev* **35**, 75-91 (2016).
4. Inamura K. Lung Cancer: Understanding Its Molecular Pathology and the 2015 WHO Classification. *Front Oncol* **7** (2017).
5. Planchard D, Besse B. Lung cancer in never-smokers. *Eur Respir J* **45**, 1214-1217 (2015).
6. Parkin DM, Bray F, Ferlay J, Pisani P. Global Cancer Statistics. *CA Cancer J. Clin* **55**, 74-108 (2005).
7. Sun S, Schiller JH, Gazdar AF. Lung cancer in never smokers — a different disease. *Nat Rev Cancer* **7**, 778-790 (2007).
8. Hirsch FR, Spreafico A, Novello S, Wood MD, Simms L, Papotti M. The Prognostic and Predictive Role of Histology in Advanced Non-Small Cell Lung Cancer: A Literature Review. *J Thorac Oncol* **3**, 1468-1481 (2008).
9. Cancer Genome Atlas Research N. Comprehensive molecular profiling of lung adenocarcinoma. *Nature* **511**, 543-550 (2014).
10. Chan BA, Hughes BG. Targeted therapy for non-small cell lung cancer: current standards and the promise of the future. *Transl Lung Cancer Res* **4**, 36-54 (2015).
11. Pao W, Hutchinson KE. Chipping away at the lung cancer genome. *Nat Med* **18**, 349-351 (2012).
12. Pao W, Girard N. New driver mutations in non-small-cell lung cancer. *Lancet Oncol* **12**, 175-180 (2011).
13. Ding L, *et al.* Somatic mutations affect key pathways in lung adenocarcinoma. *Nature* **455**, 1069-1075 (2008).
14. Skoulidis F, Heymach JV. Co-occurring genomic alterations in non-small-cell lung cancer biology and therapy. *Nat Rev Cancer* **19**, 495-509 (2019).
15. Neal JW. The SATURN trial: the value of maintenance erlotinib in patients with non-small-cell lung cancer. *Future Oncol* **6**, 1827-1832 (2010).

16. Rossi A, Di Maio M. Platinum-based chemotherapy in advanced non-small-cell lung cancer: optimal number of treatment cycles. *Expert Rev Anticancer Ther* **16**, 653-660 (2016).
17. Tsao AS, *et al.* Scientific Advances in Lung Cancer. *J Thorac Oncol* **11**, 613-638 (2016).
18. Albain KS, *et al.* Radiotherapy plus chemotherapy with or without surgical resection for stage III non-small-cell lung cancer: a phase III randomised controlled trial. *Lancet Oncol* **374**, 379-386 (2009).
19. Zhang C, Leighl NB, Wu Y-L, Zhong W-Z. Emerging therapies for non-small cell lung cancer. *J Hematol Oncol* **12**, 45 (2019).
20. Yu HA, *et al.* Analysis of Tumor Specimens at the Time of Acquired Resistance to EGFR-TKI Therapy in 155 Patients with EGFR-Mutant Lung Cancers. *Clin Cancer Res* **19**, 2240-2247 (2013).
21. Zhou C, *et al.* Erlotinib versus chemotherapy as first-line treatment for patients with advanced EGFR mutation-positive non-small-cell lung cancer (OPTIMAL, CTONG-0802): a multicentre, open-label, randomised, phase 3 study. *Lancet Oncol* **12**, 35-42 (2011).
22. Maemondo M, *et al.* Gefitinib or Chemotherapy for Non-Small-Cell Lung Cancer with Mutated EGFR. *N Engl J Med* **362**, 2380-2388 (2010).
23. Oxnard GR, *et al.* Acquired Resistance to EGFR Tyrosine Kinase Inhibitors in EGFR-Mutant Lung Cancer: Distinct Natural History of Patients with Tumors Harboring the T790M Mutation. *Clin Cancer Res* **17**, 1616-1622 (2011).
24. Mitsudomi T, Yatabe Y. Mutations of the epidermal growth factor receptor gene and related genes as determinants of epidermal growth factor receptor tyrosine kinase inhibitors sensitivity in lung cancer. *Cancer Res* **98**, 1817-1824 (2007).
25. Wang Y, *et al.* HER2 exon 20 insertions in non-small-cell lung cancer are sensitive to the irreversible pan-HER receptor tyrosine kinase inhibitor pyrotinib. *Ann Oncol* **30**, 447-455 (2019).
26. Ahn M-J, *et al.* Activity and safety of AZD3759 in EGFR-mutant non-small-cell lung cancer with CNS metastases (BLOOM): a phase 1, open-label, dose-escalation and dose-expansion study. *Lancet Respir Med* **5**, 891-902 (2017).
27. Yang JC-H, *et al.* Osimertinib in Pretreated T790M-Positive Advanced Non-Small-Cell Lung Cancer: AURA Study Phase II Extension Component. *J Clin Oncol* **35**, 1288-1296 (2017).

28. Katayama R, *et al.* Mechanisms of Acquired Crizotinib Resistance in ALK-Rearranged Lung Cancers. *Sci Transl Med* **4**, 120ra17-ra17 (2012).
29. Huang W-S, *et al.* Discovery of Brigatinib (AP26113), a Phosphine Oxide-Containing, Potent, Orally Active Inhibitor of Anaplastic Lymphoma Kinase. *J Med Chem* **59**, 4948-4964 (2016).
30. Gainor JF, *et al.* Molecular Mechanisms of Resistance to First- and Second-Generation ALK Inhibitors in ALK-Rearranged Lung Cancer. *Cancer Discov* **6**, 1118-1133 (2016).
31. Shaw AT, *et al.* Lorlatinib in non-small-cell lung cancer with ALK or ROS1 rearrangement: an international, multicentre, open-label, single-arm first-in-man phase 1 trial. *Lancet Oncol* **18**, 1590-1599 (2017).
32. PDQ Adult Treatment Editorial Board. *Non-Small Cell Lung Cancer Treatment (PDQ®): Health Professional Version.* (2002-2020).
33. Murray S, *et al.* Somatic mutations of the tyrosine kinase domain of epidermal growth factor receptor and tyrosine kinase inhibitor response to TKIs in non-small cell lung cancer: an analytical database. *J Thorac Oncol* **3**, 832-839 (2008).
34. Liu F, Yang X, Geng M, Huang M. Targeting ERK, an Achilles' Heel of the MAPK pathway, in cancer therapy. *Acta Pharm Sin B* **8**, 552-562 (2018).
35. Ostrem JM, Peters U, Sos ML, Wells JA, Shokat KM. K-Ras(G12C) inhibitors allosterically control GTP affinity and effector interactions. *Nature* **503**, 548-551 (2013).
36. Ostrem JML, Shokat KM. Direct small-molecule inhibitors of KRAS: from structural insights to mechanism-based design. *Nat Rev Drug Discov* **15**, 771-785 (2016).
37. Cox AD, Der CJ, Philips MR. Targeting RAS Membrane Association: Back to the Future for Anti-RAS Drug Discovery? *Clin Cancer Res* **21**, 1819 (2015).
38. Yang H, Liang S-Q, Schmid RA, Peng R-W. New Horizons in KRAS-Mutant Lung Cancer: Dawn After Darkness. *Front Oncol* **9**, 953 (2019).
39. Canon J, *et al.* The clinical KRAS(G12C) inhibitor AMG 510 drives anti-tumour immunity. *Nature* **575**, 217-223 (2019).
40. Li J, Li W, Huang K, Zhang Y, Kupfer G, Zhao Q. Chimeric antigen receptor T cell (CAR-T) immunotherapy for solid tumors: lessons learned and strategies for moving forward. *J Hematol Oncol* **11**, 22 (2018).
41. Turtle CJ, *et al.* CD19 CAR-T cells of defined CD4+:CD8+ composition in adult B cell ALL patients. *J Clin Invest* **126**, 2123-2138 (2016).

42. Park K, *et al.* A First-in-Human Phase 1 Trial of the EGFR-cMET Bispecific Antibody JNJ-61186372 in Patients with Advanced Non-Small Cell Lung Cancer (NSCLC). *J Thorac Oncol* **13**, S344-S345 (2018).
43. Moores SL, *et al.* A Novel Bispecific Antibody Targeting EGFR and cMet Is Effective against EGFR Inhibitor–Resistant Lung Tumors. *Cancer Res* **76**, 3942-3953 (2016).
44. Desantis CE, Miller KD, Goding Sauer A, Jemal A, Siegel RL. Cancer statistics for African Americans, 2019. *CA Cancer J. Clin* **69**, 211-233 (2019).
45. Wolf A, *et al.* Persistence of racial disparities in early-stage lung cancer treatment. *J Thorac Cardiovasc Surg* **157**, 1670-1679 (2019).
46. Liu P, Wang Y, Li X. Targeting the untargetable KRAS in cancer therapy. *Acta Pharm Sin B* **9**, 871-879 (2019).
47. Bos JL, Rehmann H, Wittinghofer A. GEFs and GAPs: Critical Elements in the Control of Small G Proteins. *Cell* **129**, 865-877 (2007).
48. Scheffzek K, *et al.* The Ras-RasGAP Complex: Structural Basis for GTPase Activation and Its Loss in Oncogenic Ras Mutants. *Science* **277**, 333-338 (1997).
49. Pylayeva-Gupta Y, Grabocka E, Bar-Sagi D. RAS oncogenes: weaving a tumorigenic web. *Nat Rev Cancer* **11**, 761-774 (2011).
50. Mascoux C, *et al.* The role of RAS oncogene in survival of patients with lung cancer: a systematic review of the literature with meta-analysis. *Br J Cancer* **92**, 131-139 (2005).
51. Shepherd FA, *et al.* Pooled analysis of the prognostic and predictive effects of KRAS mutation status and KRAS mutation subtype in early-stage resected non–small-cell lung cancer in four trials of adjuvant chemotherapy. *J Clin Oncol* **31**, 2173-2181 (2013).
52. De Roock W, *et al.* Association of KRAS p.G13D Mutation With Outcome in Patients With Chemotherapy-Refractory Metastatic Colorectal Cancer Treated With Cetuximab. *JAMA* **304**, 1812-1820 (2010).
53. Andreyev HJ, *et al.* Kirsten ras Mutations in Patients With Colorectal Cancer: the Multicenter “RASCAL” Study. *Br J Cancer* **85**, 692-696 (2001).
54. Young A, Lou D, McCormick F. Oncogenic and Wild-type Ras Play Divergent Roles in the Regulation of Mitogen-Activated Protein Kinase Signaling. *Cancer Discov* **3**, 112-123 (2013).
55. di Magliano MP, Logsdon CD. Roles for KRAS in Pancreatic Tumor Development and Progression. *Gastroenterology* **144**, 1220-1229 (2013).

56. Dearden S, Stevens J, Wu Y-L, Blowers D. Mutation incidence and coincidence in non small-cell lung cancer: meta-analyses by ethnicity and histology (mutMap). *Ann Oncol* **24**, 2371-2376 (2013).
57. Balbin OA, *et al.* Reconstructing targetable pathways in lung cancer by integrating diverse omics data. *Nat Commun* **4**, 2617 (2013).
58. Singh A, *et al.* A gene expression signature associated with “K-Ras addiction” reveals regulators of EMT and tumor cell survival. *Cancer Cell* **15**, 489-500 (2009).
59. Skoulidis F, *et al.* Co-occurring genomic alterations define major subsets of KRAS-mutant lung adenocarcinoma with distinct biology, immune profiles, and therapeutic vulnerabilities. *Cancer Discov* **5**, 860-877 (2015).
60. Schabath MB, *et al.* Differential association of STK11 and TP53 with KRAS mutation-associated gene expression, proliferation and immune surveillance in lung adenocarcinoma. *Oncogene* **35**, 3209-3216 (2016).
61. Kottakis F, *et al.* LKB1 loss links serine metabolism to DNA methylation and tumorigenesis. *Nature* **539**, 390-395 (2016).
62. Krall EB, *et al.* KEAP1 loss modulates sensitivity to kinase targeted therapy in lung cancer. *Elife* **6**:e18970 (2017).
63. Romero R, *et al.* Keap1 loss promotes Kras-driven lung cancer and results in dependence on glutaminolysis. *Nat Med* **23**, 1362-1368 (2017).
64. Skoulidis F, *et al.* STK11/LKB1 Mutations and PD-1 Inhibitor Resistance in KRAS-Mutant Lung Adenocarcinoma. *Cancer Discov* **8**, 822-835 (2018).
65. Shepherd FA, *et al.* Pooled analysis of the prognostic and predictive effects of TP53 comutation status combined with KRAS or EGFR mutation in early-stage resected non-small-cell lung cancer in four trials of adjuvant chemotherapy. *J Clin Oncol* **35**, 2018-2027 (2017).
66. Forbes SA, *et al.* COSMIC: mining complete cancer genomes in the Catalogue of Somatic Mutations in Cancer. *Nucleic Acids Res* **39**, D945-D950 (2011).
67. Garassino MC, *et al.* Different types of K-Ras mutations could affect drug sensitivity and tumour behaviour in non-small-cell lung cancer. *Ann Oncol* **22**, 235-237 (2011).
68. Svaton M, *et al.* The prognostic role of KRAS mutation in patients with advanced NSCLC treated with second-or third-line chemotherapy. *Anticancer Res* **36**, 1077-1082 (2016).

69. Nadal E, *et al.* KRAS-G12C mutation is associated with poor outcome in surgically resected lung adenocarcinoma. *J Thorac Oncol* **9**, 1513-1522 (2014).
70. Ihle NT, *et al.* Effect of KRAS oncogene substitutions on protein behavior: implications for signaling and clinical outcome. *J Natl Cancer Inst* **104**, 228-239 (2012).
71. Jia Y, *et al.* Characterization of distinct types of KRAS mutation and its impact on first-line platinum-based chemotherapy in Chinese patients with advanced non-small cell lung cancer. *Oncol Lett* **14**, 6525-6532 (2017).
72. Saxton RA, Sabatini DM. mTOR Signaling in Growth, Metabolism, and Disease. *Cell* **168**, 960-976 (2017).
73. Ruder D, *et al.* Concomitant targeting of the mTOR/MAPK pathways: novel therapeutic strategy in subsets of RICTOR/KRAS-altered non-small cell lung cancer. *Oncotarget* **9**, 3995-4008 (2018).
74. Liang S-Q, *et al.* mTOR mediates a mechanism of resistance to chemotherapy and defines a rational combination strategy to treat KRAS-mutant lung cancer. *Oncogene* **38**, 622-636 (2019).
75. Jenne DE, *et al.* Peutz-Jeghers syndrome is caused by mutations in a novel serine threonine kinase. *Nat Genet* **18**, 38-43 (1998).
76. Hemminki A, *et al.* A serine/threonine kinase gene defective in Peutz–Jeghers syndrome. *Nature* **391**, 184-187 (1998).
77. Schumacher V, *et al.* STK11 genotyping and cancer risk in Peutz-Jeghers syndrome. *J Med Genet* **42**, 428-435 (2005).
78. Chae H-D, Jeon C-H. Peutz-Jeghers syndrome with germline mutation of STK11. *Ann Surg Treat Res* **86**, 325-330 (2014).
79. Lim W, *et al.* Relative frequency and morphology of cancers in STK11 mutation carriers. *Gastroenterology* **126**, 1788-1794 (2004).
80. Sanchez-Cespedes M, *et al.* Inactivation of LKB1/STK11 is a common event in adenocarcinomas of the lung. *Cancer Res* **62**, 3659-3662 (2002).
81. Wingo SN, *et al.* Somatic LKB1 Mutations Promote Cervical Cancer Progression. *PLoS One* **4**, e5137 (2009).
82. Forster L, Defres S, Goudie D, Baty D, Carey F. An Investigation of the Peutz-Jeghers Gene (LKB1) in Sporadic Breast and Colon Cancers. *J Clin Pathol* **53**, 791-793 (2000).

83. Guldberg P, *et al.* Somatic mutation of the Peutz-Jeghers syndrome gene, LKB1/STK11, in malignant melanoma. *Oncogene* **18**, 1777-1780 (1999).
84. Zhou W, Zhang J, Marcus AI. LKB1 tumor suppressor: Therapeutic opportunities knock when LKB1 is inactivated. *Genes Dis* **1**, 64-74 (2014).
85. Gan R-Y, Li H-B. Recent progress on liver kinase B1 (LKB1): expression, regulation, downstream signaling and cancer suppressive function. *Int J Mol Sci* **15**, 16698-16718 (2014).
86. Hardie DG, Alessi DR. LKB1 and AMPK and the cancer-metabolism link - ten years after. *BMC Biology* **11**, 36 (2013).
87. Jaleel M, *et al.* Identification of the sucrose non-fermenting related kinase SNRK, as a novel LKB1 substrate. *FEBS Letters* **579**, 1417-1423 (2005).
88. Lizcano JM, *et al.* LKB1 is a master kinase that activates 13 kinases of the AMPK subfamily, including MARK/PAR-1. *EMBO J* **23**, 833-843 (2004).
89. Hawley SA, *et al.* Complexes between the LKB1 tumor suppressor, STRAD α/β and MO25 α/β are upstream kinases in the AMP-activated protein kinase cascade. *J Biol* **2**, 28 (2003).
90. Shaw RJ, *et al.* The tumor suppressor LKB1 kinase directly activates AMP-activated kinase and regulates apoptosis in response to energy stress. *Proc Natl Acad Sci U S A* **101**, 3329-3335 (2004).
91. Zhang S, *et al.* The Tumor Suppressor LKB1 Regulates Lung Cancer Cell Polarity by Mediating cdc42 Recruitment and Activity. *Cancer Res* **68**, 740-748 (2008).
92. Kline ER, Shupe J, Gilbert-Ross M, Zhou W, Marcus AI. LKB1 represses focal adhesion kinase (FAK) signaling via a FAK-LKB1 complex to regulate FAK site maturation and directional persistence. *J Biol Chem* **288**, 17663-17674 (2013).
93. Gilbert-Ross M, *et al.* Targeting adhesion signaling in KRAS, LKB1 mutant lung adenocarcinoma. *JCI Insight* **2**, e90487 (2017).
94. Ji H, *et al.* LKB1 modulates lung cancer differentiation and metastasis. *Nature* **448**, 807-810 (2007).
95. Yao Y-H, *et al.* Attenuated LKB1-SIK1 signaling promotes epithelial-mesenchymal transition and radioresistance of non-small cell lung cancer cells. *Chin J Cancer* **35**, 50 (2016).
96. Momcilovic M, Shackelford DB. Targeting LKB1 in cancer – exposing and exploiting vulnerabilities. *Br J Cancer* **113**, 574-584 (2015).

97. Jeon S-M. Regulation and function of AMPK in physiology and diseases. *Exp Mol Med* **48**, e245 (2016).
98. Dasgupta B, Chhipa RR. Evolving Lessons on the Complex Role of AMPK in Normal Physiology and Cancer. *Trends Pharmacol Sci* **37**, 192-206 (2016).
99. Shaw RJ. LKB1 and AMP-activated protein kinase control of mTOR signalling and growth. *Acta Physiol (Oxf)* **196**, 65-80 (2009).
100. Eichner LJ, *et al.* Genetic Analysis Reveals AMPK Is Required to Support Tumor Growth in Murine Kras-Dependent Lung Cancer Models. *Cell Metab* **29**, 285-302 (2019).
101. Vara-Ciruelos D, Russell FM, Hardie DG. The strange case of AMPK and cancer: Dr Jekyll or Mr Hyde? *Open Biol* **9**, 190099 (2019).
102. Jeon S-M, Hay N. The double-edged sword of AMPK signaling in cancer and its therapeutic implications. *Arch Pharm Res* **38**, 346-357 (2015).
103. Penfold L, *et al.* CAMKK2 Promotes Prostate Cancer Independently of AMPK via Increased Lipogenesis. *Cancer Res* **78**, 6747-6761 (2018).
104. Chen Z, *et al.* A murine lung cancer co-clinical trial identifies genetic modifiers of therapeutic response. *Nature* **483**, 613-617 (2012).
105. Carretero J, *et al.* Integrative Genomic and Proteomic Analyses Identify Targets for Lkb1-Deficient Metastatic Lung Tumors. *Cancer Cell* **17**, 547-559 (2010).
106. Kim J, *et al.* CPS1 maintains pyrimidine pools and DNA synthesis in KRAS/LKB1-mutant lung cancer cells. *Nature* **546**, 168-172 (2017).
107. Lazebnik Y. What are the hallmarks of cancer? *Nat Rev Cancer* **10**, 232-233 (2010).
108. Seyfried TN, Huysentruyt LC. On the origin of cancer metastasis. *Crit Rev Oncog* **18**, 43-73 (2014).
109. Lintz M, Muñoz A, Reinhart-King CA. The Mechanics of Single Cell and Collective Migration of Tumor Cells. *J Biomech Eng* **139**, 0210051-0210059 (2017).
110. Nieto MA, Huang RY-J, Jackson RA, Thiery JP. EMT: 2016. *Cell* **166**, 21-45 (2016).
111. Thiery JP, Acloque H, Huang RY, Nieto MA. Epithelial-mesenchymal transitions in development and disease. *Cell* **139**, 871-990 (2017).
112. Serrano-Gomez SJ, Maziveyi M, Alahari SK. Regulation of epithelial-mesenchymal transition through epigenetic and post-translational modifications. *Mol Cancer* **15**, 18 (2016).

113. Chaffer CL, San Juan BP, Lim E, Weinberg RA. EMT, cell plasticity and metastasis. *Cancer Metastasis Rev* **35**, 645-654 (2016).
114. Yao D, Dai C, Peng S. Mechanism of the Mesenchymal–Epithelial Transition and Its Relationship with Metastatic Tumor Formation. *Mol Cancer Res* **9**, 1608-1620 (2011).
115. Gialeli C, Theocharis AD, Karamanos NK. Roles of matrix metalloproteinases in cancer progression and their pharmacological targeting. *FEBS J* **278**, 16-27 (2011).
116. Cheung KJ, Ewald AJ. A collective route to metastasis: Seeding by tumor cell clusters. *Science* **352**, 167-169 (2016).
117. Friedl P, Locker J, Sahai E, Segall JE. Classifying collective cancer cell invasion. *Nat Cell Biol* **14**, 777-783 (2012).
118. Khalil AA, Friedl P. Determinants of leader cells in collective cell migration. *Integr Biol (Camb)* **2**, 568-574 (2010).
119. Konen J, *et al.* Image-guided genomics of phenotypically heterogeneous populations reveals vascular signaling during symbiotic collective cancer invasion. *Nat Commun* **8**, 15078 (2017).
120. Popper HH. Progression and metastasis of lung cancer. *Cancer Metastasis Rev* **35**, 75-91 (2016).
121. Gabor S, *et al.* Invasion of blood vessels as significant prognostic factor in radically resected T1-3N0M0 non-small-cell lung cancer. *Eur J Cardiothorac Surg* **25**, 439-442 (2004).
122. Hendriks LEL, *et al.* EGFR mutated non-small cell lung cancer patients: More prone to development of bone and brain metastases? *Lung Cancer* **84**, 86-91 (2014).
123. Miles WO, Dyson NJ, Walker JA. Modeling tumor invasion and metastasis in *Drosophila*. *Dis Model Mech* **4**, 753-761 (2011).
124. Jennings BH. *Drosophila* – a versatile model in biology & medicine. *Materials Today* **14**, 190-195 (2011).
125. Pandey UB, Nichols CD. Human disease models in *Drosophila melanogaster* and the role of the fly in therapeutic drug discovery. *Pharmacol Rev* **63**, 411-436 (2011).
126. Hales KG, Korey CA, Larracuente AM, Roberts DM. Genetics on the Fly: A Primer on the *Drosophila* Model System. *Genetics* **201**, 815-842 (2015).
127. Consortium M, *et al.* Identification of functional elements and regulatory circuits by *Drosophila* modENCODE. *Science* **330**, 1787-1797 (2010).

128. Rubin GM, Kidwell MG, Bingham PM. The molecular basis of PM hybrid dysgenesis: the nature of induced mutations. *Cell* **29**, 987-994 (1982).
129. Brand AH, Perrimon N. Targeted gene expression as a means of altering cell fates and generating dominant phenotypes. *Development* **118**, 401-415 (1993).
130. Golic KG, Lindquist S. The FLP recombinase of yeast catalyzes site-specific recombination in the *Drosophila* genome. *Cell* **59**, 499-509 (1989).
131. Gateff E. Cancer, Genes, and Development: The *Drosophila* Case. *Adv Cancer Res* **37**, 33-74 (1982).
132. Hariharan IK, Bilder D. Regulation of Imaginal Disc Growth by Tumor-Suppressor Genes in *Drosophila*. *Annu Rev Genet* **40**, 335-361 (2006).
133. Woodhouse E, Hersperger E, Shearn A. Growth, metastasis, and invasiveness of *Drosophila* tumors caused by mutations in specific tumor suppressor genes. *Dev Genes Evol* **207**, 542-550 (1998).
134. Brumby AM, Richardson HE. Scribble mutants cooperate with oncogenic Ras or Notch to cause neoplastic overgrowth in *Drosophila*. *EMBO J* **22**, 5769-5779 (2003).
135. Pagliarini RA, Xu T. A Genetic Screen in *Drosophila* for Metastatic Behavior. *Science* **302**, 1227 (1998).
136. Read RD, Cavenee WK, Furnari FB, Thomas JB. A *drosophila* model for EGFR-Ras and PI3K-dependent human glioma. *PLoS Genet* **5**, e1000374 (2009).
137. Ryan MB, Corcoran RB. Therapeutic strategies to target RAS-mutant cancers. *Nat Rev Clin Oncol* **15**, 709-720 (2019).
138. Caiola E, *et al.* Co-occurring KRAS mutation/LKB1 loss in non-small cell lung cancer cells results in enhanced metabolic activity susceptible to caloric restriction: an in vitro integrated multilevel approach. *J Exp Clin Cancer Res* **37**, 302 (2018).
139. Karim FD, Rubin GM. Ectopic expression of activated Ras1 induces hyperplastic growth and increased cell death in *Drosophila* imaginal tissues. *Development* **125**, 1 (1998).
140. Perkins LA, *et al.* The Transgenic RNAi Project at Harvard Medical School: Resources and Validation. *Genetics* **201**, 843-852 (2015).
141. Dietzl G, *et al.* A genome-wide transgenic RNAi library for conditional gene inactivation in *Drosophila*. *Nature* **448**, 151-156 (2007).

142. Sopko R, *et al.* Combining genetic perturbations and proteomics to examine kinase-phosphatase networks in Drosophila embryos. *Dev Cell* **31**, 114-127 (2014).
143. Hu Y, *et al.* UP-TORR: online tool for accurate and Up-to-Date annotation of RNAi Reagents. *Genetics* **195**, 37-45 (2013).
144. Katajisto P, *et al.* LKB1 signaling in mesenchymal cells required for suppression of gastrointestinal polyposis. *Nat Genet* **40**, 455-459 (2008).
145. Tanwar PS, *et al.* Stromal Liver Kinase B1 [STK11] Signaling Loss Induces Oviductal Adenomas and Endometrial Cancer by Activating Mammalian Target of Rapamycin Complex 1. *PLoS Genet* **8**, e1002906 (2012).
146. Ollila S, *et al.* Stromal Lkb1 deficiency leads to gastrointestinal tumorigenesis involving the IL-11-JAK/STAT3 pathway. *J Clin Invest* **128**, 402-414 (2018).
147. Raabe T. The Sevenless signaling pathway: variations of a common theme. *Biochim Biophys Acta* **1496**, 151-163 (2000).
148. Ray M, Lakhotia SC. The commonly used eye-specific sev-GAL4 and GMR-GAL4 drivers in Drosophila melanogaster are expressed in tissues other than eyes also. *J Genet* **94**, 407-416 (2015).
149. Haigis KM. KRAS Alleles: The Devil Is in the Detail. *Trends Cancer* **3**, 686-697 (2017).
150. Kerr EM, Martins CP. Metabolic rewiring in mutant Kras lung cancer. *FEBS J* **285**, 28-41 (2018).
151. Cairns RA, Harris IS, Mak TW. Regulation of cancer cell metabolism. *Nat Rev Cancer* **11**, 85-95 (2011).
152. Downward J. Targeting RAS signalling pathways in cancer therapy. *Nat Rev Cancer* **3**, 11-22 (2003).
153. Downward J. RAS Synthetic Lethal Screens Revisited: Still Seeking the Elusive Prize? *Clin Cancer Res* **21**, 1802-1809 (2015).
154. Dong Z-Y, *et al.* Potential Predictive Value of TP53 and KRAS Mutation Status for Response to PD-1 Blockade Immunotherapy in Lung Adenocarcinoma. *Clin Cancer Res* **23**, 3012-3024 (2017).
155. Koyama S, *et al.* STK11/LKB1 Deficiency Promotes Neutrophil Recruitment and Proinflammatory Cytokine Production to Suppress T-cell Activity in the Lung Tumor Microenvironment. *Cancer Res* **76**, 999-1008 (2016).

156. Mirzoyan Z, *et al.* *Drosophila melanogaster*: A Model Organism to Study Cancer. *Front Genet* **10**, 51 (2019).
157. Sonoshita M, Cagan RL. Modeling Human Cancers in *Drosophila*. *Current Topics in Developmental Biology: Academic Press*, 287-309 (2017).
158. Morin X, Daneman R, Zavortink M, Chia W. A protein trap strategy to detect GFP-tagged proteins expressed from their endogenous loci in *Drosophila*. *Proc Natl Acad of Sci U S A* **98**, 15050-15055 (2001).
159. Neufeld TP, de la Cruz AFA, Johnston LA, Edgar BA. Coordination of Growth and Cell Division in the *Drosophila* Wing. *Cell* **93**, 1183-1193 (1998).
160. Tomer R, Khairy K, Amat F, Keller PJ. Quantitative high-speed imaging of entire developing embryos with simultaneous multiview light-sheet microscopy. *Nat Methods* **9**, 755-763 (2012).
161. Royer LA, *et al.* Adaptive light-sheet microscopy for long-term, high-resolution imaging in living organisms. *Nat Biotechnol* **34**, 1267-1278 (2016).
162. Amat F, *et al.* Efficient processing and analysis of large-scale light-sheet microscopy data. *Nat Protoc* **10**, 1679-1696 (2015).
163. Campbell JD, *et al.* Distinct patterns of somatic genome alterations in lung adenocarcinomas and squamous cell carcinomas. *Nat Genet* **48**, 607-616 (2016).
164. Hoadley KA, *et al.* Cell-of-Origin Patterns Dominate the Molecular Classification of 10,000 Tumors from 33 Types of Cancer. *Cell* **173**, 291-304 (2018).
165. Sarkisian CJ, *et al.* Dose-dependent oncogene-induced senescence in vivo and its evasion during mammary tumorigenesis. *Nat Cell Biol* **9**, 493-505 (2007).
166. Kerr EM, Gaude E, Turrell FK, Frezza C, Martins CP. Mutant Kras copy number defines metabolic reprogramming and therapeutic susceptibilities. *Nature* **531**, 110-113 (2016).
167. Richardson HE, Portela M. Modelling Cooperative Tumorigenesis in *Drosophila*. *BioMed Res Internat* **2018**, 1-29 (2018).
168. Matsumoto S, *et al.* Prevalence and specificity of LKB1 genetic alterations in lung cancers. *Oncogene* **26**, 5911-5918 (2007).
169. Lee JH, *et al.* JNK pathway mediates apoptotic cell death induced by tumor suppressor LKB1 in *Drosophila*. *Cell Death Differ* **13**, 1110-1122 (2006).
170. Martin SG, St Johnston D. A role for *Drosophila* LKB1 in anterior–posterior axis formation and epithelial polarity. *Nature* **421**, 379-384 (2003).

171. Amin N, *et al.* LKB1 regulates polarity remodeling and adherens junction formation in the *Drosophila* eye. *Proc Natl Acad of Sci U S A* **106**, 8941-8946 (2009).
172. Schäfer C, *et al.* Differential KrasV12 protein levels control a switch regulating lung cancer cell morphology and motility. *Converg Sci Phys Oncol* **2**, 035004 (2016).
173. Bilder D. Epithelial polarity and proliferation control: links from the *Drosophila* neoplastic tumor suppressors. *Genes Dev* **18**, 1909-1925 (2004).
174. Spicer J, Ashworth A. LKB1 Kinase: Master and Commander of Metabolism and Polarity. *Curr Biol* **14**, R383-R385 (2004).
175. Partanen JI, Tervonen TA, Klefstrom J. Breaking the epithelial polarity barrier in cancer: the strange case of LKB1/PAR-4. *Philos Trans R Soc Lond B Biol Sci* **368**, 20130111 (2013).
176. Richardson AM, *et al.* Vimentin Is Required for Lung Adenocarcinoma Metastasis via Heterotypic Tumor Cell–Cancer-Associated Fibroblast Interactions during Collective Invasion. *Clin Cancer Res* **24**, 420-432 (2018).
177. Hindupur SK, González A, Hall MN. The Opposing Actions of Target of Rapamycin and AMP-Activated Protein Kinase in Cell Growth Control. *Cold Spring Harb Perspect Biol* **7**, a019141 (2015).
178. Bhatt V, *et al.* Autophagy modulates lipid metabolism to maintain metabolic flexibility for Lkb1-deficient Kras-driven lung tumorigenesis. *Genes Dev* **33**, 150-165 (2019).
179. Dalle Pezze P, *et al.* A systems study reveals concurrent activation of AMPK and mTOR by amino acids. *Nat Commun* **7**, 13254 (2016).
180. Garcia D, Shaw RJ. AMPK: Mechanisms of Cellular Energy Sensing and Restoration of Metabolic Balance. *Mol Cell* **66**, 789-800 (2017).
181. Sumi M, *et al.* The newly synthesized selective Ca²⁺-calmodulin dependent protein kinase II inhibitor KN-93 reduces dopamine contents in PC12h cells. *Biochem Biophys Res Commun* **181**, 968-975 (1991).
182. Cerami E, *et al.* The cBio Cancer Genomics Portal: An Open Platform for Exploring Multidimensional Cancer Genomics Data. *Cancer Discov* **2**, 401-404 (2012).
183. Gao J, *et al.* Integrative Analysis of Complex Cancer Genomics and Clinical Profiles Using the cBioPortal. *Sci Signal* **6**, p11 (2013).
184. Hidalgo MR, *et al.* High throughput estimation of functional cell activities reveals disease mechanisms and predicts relevant clinical outcomes. *Oncotarget* **8**, 5160-5178 (2017).

185. Ben-Porath I, Weinberg RA. When cells get stressed: an integrative view of cellular senescence. *J Clin Invest* **113**, 8-13 (2004).
186. Junttila MR, *et al.* Selective activation of p53-mediated tumour suppression in high-grade tumours. *Nature* **468**, 567-571 (2010).
187. Jordan EJ, *et al.* Prospective Comprehensive Molecular Characterization of Lung Adenocarcinomas for Efficient Patient Matching to Approved and Emerging Therapies. *Cancer Discov* **7**, 596-609 (2017).
188. Fung MKL, Chan GC-F. Drug-induced amino acid deprivation as strategy for cancer therapy. *J Hematol Oncol* **10**, 144 (2017).
189. Calles A, *et al.* Immunohistochemical Loss of LKB1 Is a Biomarker for More Aggressive Biology in KRAS-Mutant Lung Adenocarcinoma. *Clin Cancer Res* **21**, 2851-2860 (2015).
190. Marcus AI, Zhou W. LKB1 Regulated Pathways in Lung Cancer Invasion and Metastasis. *J Thorac Oncol* **5**, 1883-1886 (2010).
191. Konen J, *et al.* LKB1 kinase-dependent and -independent defects disrupt polarity and adhesion signaling to drive collagen remodeling during invasion. *Mol Biol Cell* **27**, 1069-1084 (2016).
192. Sato M, *et al.* Human lung epithelial cells progressed to malignancy through specific oncogenic manipulations. *Mol Cancer Res* **11**, 638-650 (2013).
193. Colombani J, *et al.* A Nutrient Sensor Mechanism Controls Drosophila Growth. *Cell* **114**, 739-749 (2003).